Bohmian Mechanics: Towards Illuminating The Quantum Potential

by

Matthew Brown

A thesis
presented to the University of Waterloo
in fulfillment of the
thesis requirement for the degree of
Master of Science
in
Physics

Waterloo, Ontario, Canada, 2018

I hereby declare that I am the sole author of this thesis. This is a true copy of the thesis, including any required final revisions, as accepted by my examiners.

I understand that my thesis may be made electronically available to the public.

Abstract

This thesis deals with the theoretical and experimental details of trying to understand and infer the quantum potential from Bohmian mechanics using Bohmian trajectories. In this work, some of the key components of the history of Bohmian mechanics is given, a theoretical explanation of how to measure the Bohmian potential, followed by an overview of the experimental apparatus and its components. Some tests of the experimental apparatus are then presented followed by a discussion of the results. Lastly, some interesting follow up experiments are defined and discussed.

Bohmian mechanics, while completely agreeing with quantum mechanics could not be more different from the standard notions such as the fact that particles retain their classical identity of a point like object that have definite and causal trajectories. In this realm, first developed by de Broglie, these particles move and are guided by a wave, which turns out to be the wave function itself. Typically, the velocity of the particles anywhere in space is given by spatial derivatives of the phase of this wave and the energy content of the particles is given by the temporal derivative. The trajectories can bend even when there are no outside (classical) forces that are acting on the objects. This is due to the fact that these observations of Bohmian mechanics must conform to the standard measurements in quantum mechanics.

One detail that has gone unmeasured (in the sense of inference) in a laboratory setting, is the quantum potential (the mysterious force that moves particle to make sure they reproduce the measurements of quantum mechanics). Using the technique of measuring the trajectories of photons, the question was asked, can the quantum potential for single photons in the double slit be inferred? A setup has been built in order to try and answer this question using a single photon detecting camera and a heralding spontaneous parametric down conversion source. Unfortunately, the quantum potential still goes unmeasured due to noise in the camera pictures destroying the integrity of the signal and an interesting problem of trying to stitch together the quantum potential at the varying z-planes.

Acknowledgements

I would first like to thank Professor Dr. Kevin Resch for the opportunity and the privilege to learn and grow under his direction and for his support these past two and a half years. I would also like to acknowledge that it was his conception of the project that made it all possible. I would also like to thank my committee members Dr.'s Eduardo Martin-Martinez (Assistant Professor) and Roger Melko (Associate Professor) for being on my committee and for their interesting discussions. Finally, I would like to thank Professor Dr. Norbert Lütkenhaus for being able to sit on my defense committee.

I would also like to thank all of the previous and current members of the QOQI group for not only their continued friendship, but also for their guidance and wisdom, for continually challenging me to better myself, and for passing down all of the knowledge of optics that our group has obtained over the years. I would particularly like to thank Dr. Kent Bonsma-Fisher for having the patience to teach me the basics of optics lab work and to help me begin my experiment. I would also like to thank Dr. John Donohue, Dr. Mike Mazurek, Jean-Philippe MacLean, Jeff Salvail, Morgan Mastrovich, and Patrick Daley for all of the many and useful conversations about this work. I would also like to thank our summer student Austin Bradley who contributed with many measurements of the system (the pinhole waist measurements, the pin magnification measurements, the first weak momentum measurements and trajectories, and helping develop the labview software that was used to interact with the PI-MAX 4 camera) and for the great time and memories.

I would be remiss, if I did not thank the many of friends that I have made throughout my time at the IQC and to those that came before. All of whom have helped in some way or another to get me where I am today. A few in my mind have stood out in particular and in no particular order: Chris Pugh, Aimee Gunther and Sebastian Salaman for being the fun office, but also a place of great wisdom; to the hammer wielding goons, Connor Fry-Sykora and Rhyse Maryanuik, for being there and offering anything from support to uncontrollable laughter; Chris Warren for the many wonderful discussions and memories -best of luck in Spain; Helen Percival for being an amazing friend and a lovely person; to Ramy Tannous for being my rock, putting up with my antics, and being an amazing friend; Sebastian Verschoor for being much more than just tech support; to Guillaume and Sascha Agne for putting up with my dumb questions; and, to Gillian Seymour for being there for me and making me smile. And, thanks to all for putting up with my terrible jokes.

I would like to thank, the IQC for setting up such a wonderful environment that I got to meet the many of my friends that I have made. And, finally, I would like to thank the Ontario Government for contributing financially through the Queen Elizabeth II Scholarship.

Dedication

This is dedicated to my friends and family.

Table of Contents

List of Figures

Chapter 1

Background & Theory

1.1 de Broglie

Before one can talk about Bohm and his Bohmian mechanics, it is probably best to start from the beginning of the subject. The reason for this distraction is partially because the story of Bohmian mechanics is much older and much more interesting than is usually thought. There is a significant amount of interesting history to the subject that no longer is common knowledge on how quantum mechanics was developed; and, also, because the beginning gives a lot of physicality and meaning to the picture that is not typically found in the current literature (though it has made its way to the public in some ways). Furthermore, there are some technical details that should be discussed to understand the environment of quantum mechanics at the time that Bohmian mechanics was developed. The roots of Bohmian mechanics spread all the way back to de Broglie's 1925 PhD thesis (and before in his papers) titled, "Recherches Sur La Théorie Des Quanta." Most modern day physicists remember this work solely through his seminal "de Broglie Hypothesis," which was the idea that not only does light exhibit a particle and wave duality, but also electrons (and later shown to be all matter). However, what is interesting to the Bohmian is how de Broglie developed his hypothesis as it will become clear that the machinery created by de Broglie was essentially taken and reformatted by David Bohm for his Bohmian mechanics. In this way, most people attribute the contribution of de Broglie by naming it de Broglie-Bohm theory; however, due to the fact that de Broglie's main thesis on this mechanics diverges from modern Bohmian mechanics, this moniker will be dropped in favor of the name Bohmian mechanics to make the distinction more clear (the distinction will be discussed further in 1.2).

As stated earlier, most physicists recognize de Broglies thesis as the first widely-known description (he had several other papers earlier where he discussed the possibility of using Einstein's equations for quanta other than light [7]) of matter waves and, in as much, we only really remember the pair of equations $E = h\nu$ and $\lambda = \frac{h}{p}$ [25]. Interestingly, his discussion starts by assuming that all types of objects have this type of quanta association and develops the discussion in his thesis stating these ideas in a relativistic reference frame while discussing the dynamics of waves (matter or not) which de Broglie dubbed as "phase waves." He noted that the existence of these waves are not necessarily limited to the extent of the particle and, in fact, are functions over all of space. In this construction, he does not ask what causes these waves nor does he claim to understand where they come from, but he does attempt to build a physical picture out of these waves. Using a purely classical approach (including special relativity), he derives relations for the phase and group velocities of the phase waves and more surprisingly relates these to the least time approaches of Fermat and Maupertuis as well as physical properties of particles. Thus, the typical description of optics, that the rays where "corpuscles" of light travel on are described by the Eikonal equations (i.e. normals to the surface of constant phase or $|\nabla S|^2 = n^2$ where S is the phase surface function and n is the index of refraction) can also be attributed to matter waves as well (since the normals to the surface of constant phase will be shown to be related to the velocity of any particle see section 1.2) and will be the backbone of de Broglie's theory of particle movement [7]. Interestingly, this concludes that Newton's first law is no longer holds as waves will interfere causing the particles trajectory line to change direction even though there are no external "forces" on the object in the classical sense. de Broigle even noticed this and stated as much in his thesis; however, he even goes on to state that there exists such a potential function so that trajectories bend in the correct way in order to reproduce quantum mechanical effects, but he did not prefer this approach and thought that these trajectories should be the most basic element and not guided by these equations [2]. From this approach, de Broglie reproduces the Bohr-Sommerfeld quantization condition for the hydrogen atoms' electron radius, which is the usual way to teach this quantization (meaning that the orbits must have the condition of being an integer number of the de Broglie wavelength). However, as pointed out in [2], de Broigle realized that this kind of quantization did not work for every situation and had come up with a quasiperiodic description, but it was ultimately found to be flawed. While there is more to consider in his thesis, the majority is not within the scope of this work.

Contrary to popular belief, de Broglie's thesis (and the works that it was based off of) did not take off and was relatively unnoticed (in fact being a shadow to his brother). However, in a communication from Einstein to Lorentz [22], Einstein talks about de Broglie's thesis and claims to have found some support of de Broglie's idea in his discovery of two

terms in his Bose-Einstein statistics which was reminiscent of a wave part and a particle part [11]. It was this work of Einstein that cited de Broglie's thesis that allowed de Broglie's ideas to move outside of France. While there are more examples given in [2], the most shocking was that Schrödinger's wave equation was a direct result of Schrödinger (only after reading Einstein's paper above) taking de Broglie's idea on the quantization of the hydrogen atom and making a nonrelativistic approximation resulting in the correct energy levels, which had proven difficult for de Broglie. This shows that de Broglie's ideas were the inspiration for wave mechanics and not the reverse which is typically assumed by the physics community [2].

Now that scientists had access to the extremely powerful tool of Schrödinger's equation, the community was full of new ideas and they have resulted in a dynasty of thought. Use of this equation is one of the most common approaches to teaching quantum mechanics in undergraduate and graduate texts. It has resulted in an explosion of experimental and theoretical ground work from particle colliders to computers. With this powerful new tool though, comes interpretation in the real world and Erwin Madelung in the mid 1920's proposed an abstracted hydrodynamic form of the equation where one chooses the solution for the equation to be given in the polar form $\psi = R(x,t)e^{iS(x,t)}$. Once the solution is passed through the Schrödinger equation, the result gives back a form which governs the energy of the wave and also a conservation equation just like how one might think of a wave in the classical sense [20]. de Broglie, while independent from Madelung, took his plane wave solutions (note that this is essentially what Madelung did, but without a complex phase) and substituted them in the relativistic version of Schrödinger's equation (now known as the Klein-Gordon equation). de Broglie reused his idea where the particles are real objects that exist in the real world where they are represented in the mathematics as some singular part of the wave and this singularity is guided by the wave (hence the pilot-wave theory). By the time of the 1927 Solvay conference de Broglie presented his, "La Nouvelle Dynamique Des Quanta." In this work, he took the sum of his ideas with the exception of his double solution (explained later) and brought it to the table for consideration (since much of the math is going to be presented in the next section on Bohmian mechanics, we shall discuss the ideas from these conference proceedings). To paraphrase, there exists simultaneously a point and an associated wave [17]. Combining this with the Klein-Gordon equation, he was able to find a solution of the equation so that the final form of the solution yields the same dynamics as expected in the trajectories (see section 1.2). He even gave a formula for multipartite systems, something that is widely attributed to Bohm. However, after all of this, the new dynamics of de Broglie was harshly criticized and was dropped by de Broglie in favor of the more common Copenhagen interpretation [2]. The defeated de Broglie would not pick up this reasoning again until after Bohm would expose his interpretation

(Bohmian mechanics) to the world. Thus, the quantum orthodoxy came to rise.

1.2 Bohmian Mechanics

In 1952, David Bohm submitted his two part work on what is now called Bohmian mechanics [3, 4]. In these works, Bohm rediscovered the work of de Broglie and Madelung and improved upon them. However, there were some significant differences. First, de Broglie believed that the particle was a (mathematically) singular region of the wave function (as will be seen the magnitude of the solution does not affect the trajectories of the particles). The particles in some way were a separate solution. This is where de Broigle's double solution program came in the late 50's (de Broglie became emboldened after Bohm went against the orthodoxy). The double solution, essentially, was two waves where one solutions was the typical solution to the Schrödinger equation and the second was the solution that carried the particle singularity. In Madelung's solution, the interpretation is left rather void of interpretation; however, some components have been extrapolated. In this case, the velocity that both Bohm and de Broglie associated with a particle velocity is thought of as a flow of probability in the quantum hydrodynamical view point. Finally, both Bohm and Madelung prescribe there to be a fundamental force on particles that causes them to organize in a way that quantum mechanics requires, whereas de Broglie decided to remove Newton's first law and believed that the particle trajectories were the more fundamental since these trajectories were the same ones that minimized the Hamiltonian [7]. In this way, Bohmian mechanics differs from both of his predecessors, de Broglie and Madelung.

1.2.1 Single Particles

The classic derivation of the properties of Bohmian mechanics was done by both Madelung [20] and de Broglie [17] is done by assuming the wave function is written in the polar form (just as Madelung and de Broglie did in 1927) and using this ansatz to reformulate the solution of Schrödinger's equation yielding a set of complex solutions. So, letting $\psi(x_i,t) = R(x_i,t)e^{\frac{i}{\hbar}S(x_i,t)}$,

$$\begin{aligned} i\hbar\frac{\partial\psi}{\partial t} &= -\frac{\hbar^2}{2m}\nabla^2\psi + V\psi \\ i\hbar\frac{\partial R(x_i,t)e^{\frac{i}{\hbar}S(x_i,t)}}{\partial t} &= -\frac{\hbar^2}{2m}\nabla^2 R(x_i,t)e^{\frac{i}{\hbar}S(x_i,t)} + VR(x_i,t)e^{\frac{i}{\hbar}S(x_i,t)} \end{aligned}$$

Now, since both $R(x_i,t)$ and $S(x_i,t)$ are both explicitly dependent on the spatial and temporal coordinates, this nomenclature will be dropped just to clean the derivation; thus, $\psi = Re^{\frac{i}{\hbar}S}$. Now, expanding the derivatives yields:

$$\begin{aligned} i\hbar\frac{\partial Re^{\frac{i}{\hbar}S}}{\partial t} &= -\frac{\hbar^2}{2m}\nabla^2 Re^{\frac{i}{\hbar}S} + VRe^{\frac{i}{\hbar}S} \\ i\hbar\frac{\partial R}{\partial t} - R\frac{\partial S}{\partial t} &= \frac{-\hbar^2}{2m}\left(\nabla^2 R + \frac{i}{\hbar}2\nabla R\cdot\nabla S - \frac{1}{\hbar^2}R(\nabla S)^2 + \frac{i}{\hbar}R\nabla^2 S\right) + VR \end{aligned}$$

Choosing the real part and imaginary parts of the equation to be satisfied simultaneously, we find

$$\begin{aligned} \text{Real: } -R\frac{\partial S}{\partial t} &= \frac{-\hbar^2}{2m}\left(\nabla^2 R - \frac{R}{\hbar^2}(\nabla S)^2\right) + VR \\ -\frac{\partial S}{\partial t} &= \frac{-\hbar^2}{2m}\left(\frac{\nabla^2 R}{R} - \frac{1}{\hbar^2}(\nabla S)^2\right) + V \\ -\frac{\partial S(x_i,t)}{\partial t} &= Q(x_i,t) + \frac{1}{2m}\left[\nabla S(x_i,t)\right]^2 + V(x_i,t) \end{aligned} \tag{1.1}$$

where the final form of the real part like the Hamilton-Jacobi equation for a classical system where ∇S reminds us of the momentum of the object and Q is the so called Quantum Potential.

$$\begin{aligned} \text{Imaginary: } \hbar\frac{\partial R}{\partial t} &= \frac{-\hbar^2}{2m}\left(\frac{2\nabla R\cdot\nabla S}{\hbar} + \frac{R\nabla^2 S}{\hbar}\right) \\ -\frac{R}{R}\frac{\partial R}{\partial t} &= \frac{1}{2m}\left(\frac{2R\nabla R\cdot\nabla S}{R} + \frac{R^2\nabla^2 S}{R}\right) \\ \frac{\partial R^2}{\partial t} &= \frac{\nabla R^2\cdot\nabla S}{m} + \frac{R^2}{m}\nabla^2 S \\ \frac{\partial \rho(x_i,t)}{\partial t} &= \nabla\cdot\left[\rho(x_i,t)\frac{\nabla S(x_i,t)}{m}\right] \end{aligned} \tag{1.2}$$

Looking at the imaginary solution, we find that the imaginary part looks similar to a continuity equation where the quantity ρ is conserved. Now,

$$\rho = R(x_i,t)^2 = R(x_i,t)e^{\frac{i}{\hbar}S(x_i,t)}R(x_i,t)e^{\frac{-i}{\hbar}S(x_i,t)} = |\psi(x_i,t)|^2 \tag{1.3}$$

we see that ρ is in fact the probability density; therefore, equation 1.2 is really a conservation of probability density for the system.

It is good to note that in the case of the system, that the particle –just like in de Broglie's interpretation– must follow a singular path. So, if knowledge about the location and the velocity of the particle (and technically all others in the universe) is known at one location then, it is known for all others. For example, if we assume a single particle universe and that a photon is found at a camera pixel with a specific velocity, we could follow the trajectory of that photon from that pixel either backwards or forwards in time. For N particles, the above equations get transformed into the following:

$$\text{Real:} \quad -\partial_t S = \sum_{k=1}^{N} \frac{(\nabla_k S)^2}{2m_k} - \sum_{k=1}^{N} \frac{\hbar^2}{2m_k} \frac{\nabla_k^2 R}{R}$$

$$\text{Imaginary:} \quad -\partial_t \rho = \sum_{k=1}^{N} \nabla_k \cdot (\rho \frac{\nabla_k S}{m_k})$$

where the quantum potential is given as $Q = -\sum_{k}^{N} \frac{\hbar^2}{2m_k} \frac{\nabla_k^2 R}{R}$, k indexes over the different particle numbers; and, R and S are functions of every particle assumed to exist (i.e. $R = R(x_1, x_2, ..., x_k, ..., x_N)$ and similar for S). So, now the quantum potential is dependent on the state of every particle at the same time since each particle contributes to a global wave function. Here global means that it contains information about every particle. In this way, the trajectories of a particle are immediately changed upon the measurement of one of the constituents. To put it simply, the ψ that was governing the system has now been changed such that the wave function of the particle in that was measured is now in an eigenstate of that measurement operator. Thus, the overall wave function has been changed to a new state ψ'. The new wave function now acts as the coordinator for the configuration of the system. In the case of an entangled state, this change in the system will affect the trajectory of the unmeasured particle instantaneously; however, because the transmission of this change cannot in any way send information from one party to another this is allowed [3, 4].

1.2.2 Bohmian Trajectories

Within the last 60 years, there has been an extensive amount of work ranging on understanding the equilibrium condition (the statement that particles must already be distributed by $|\psi(x_i, 0)|^2$ before being able to propagate them) [9], building a working quantum field theory [15], to trying to describe trajectories [13, 30, 9, 19, 21, 31] and the quantum potential for physical systems [24]. Of current interest in the community has been the

experimental determination of Bohmian trajectories by both Kocsis, Mahler, and Xiao [19, 21, 31]. These works are based off of a proposal done by Wiseman [30], where the use of weak values allow for the determination of trajectories.

In essence, Kocsis, Mahler and Xiao used relatively identical measurement apparatuses to measure the weak velocity in the x-direction at a point in space [19, 21, 31]. This should seem unsettling to those coming out of an undergraduate or perhaps graduate course in quantum mechanics. The reason to be unsettled is due to Heisenberg's uncertainty principle, which should also be true for Bohmian mechanics if it is to reproduce the same results of quantum mechanics. Bohm's argument for where the uncertainty principle arises in Bohmian mechanics states that the uncertainty in the, ironically, deterministic view of Bohmian mechanics comes from the fact that there is always a disturbance introduced via the measurement apparatus [3, 4]. In fact, the proof is much the same in Bohmian mechanics as it is in regular quantum mechanics since the wave function is identical in both. Thus, as we measure in one basis, the wave function becomes sharply peaked in that representation, but in the opposing basis the wave function must be broad. Now, while particles do have well defined positions and momenta, any measurement on the state of the wave function (as, for example, the velocity of the particles is a measurement of the wave function) will cause violent fluctuations of particle trajectories in the canonically opposite basis to the one that is to be measured. This the cause of the uncertainty principle. However, the caveat here is that the measurement device is now seen as an interaction with the state and not thought of as a typical quantum measurement [4]. Furthermore, the question of absolute uncertainty arises, as [10] explains and as discussed earlier, the state of the system must be fully deterministic since the Bohmian interpretation requires that particles obey the laws of motion that arise from the Schrödinger equation. Ultimately, the true wave function of the system is one that takes into account every particle in the universe and their interactions including (but not limited to) ourselves, the measurement apparatus, etc. The given probability distribution for just the system under test is a good approximation, but it is an approximation nonetheless. Thus, one would have to know the exact state of the entire universe in order to effectively make use of this deterministic property.

However, in this case, how then could Kocsis, Mahler and Xiao find trajectories? The determination of trajectories is given by use of weak measurements. The major problem as pointed out above, is that under typical measurements, the wave function of the particle(s) in question will always be disturbed, but if we could make sure to disturb the wave function in a relatively small fashion, then in principle we could measure both properties simultaneously. This is called a weak measurement [1], and this type of measurement has a few interesting properties as well as a track record for being known to cause controversy.

The weak measurement is defined as $\langle \hat{A}_w \rangle = \frac{\langle \psi_f | \hat{A} | \psi_i \rangle}{\langle \psi_f | \psi_i \rangle}$ where $|\psi_f\rangle$ and $|\psi_i\rangle$ are the post-selected and initial state of the system and $\hat{A}$ is the operator under test. In this case, the most natural selection for the operator is the momentum operator (see derivation below). Where, we shall post-select at different positions on the camera. However, since we are only disturbing the state a little in these weak measurements, the measurements must be repeated many times in order to create an average for the weak value at that particular location. This average, under some approximations, can be shown to be give the same results to the standard measurement of the weak operator on the system. This way as long as enough particles are measured in the setup, the true value of the operator can be found. To explain in more detail, Kocsis et al. describes the theory for the experiment in more detail and a transcription follows in the following section [19].

1.2.3 Finding the Weak Momentum

This section is an overview of the calculations that have been done in previous sources; however, to be consistent this will be presented again with more commentary than is typically presented the calculation of the interaction of light in the weak measurement crystal from first principles will be given in the next section. To begin, the state of the photons as they leave the source is given as $\frac{1}{\sqrt{2}}|\psi(x,t)\rangle|\phi(x,t)\rangle \otimes (|HH\rangle + |VV\rangle)$ where $|\psi(x,t)\rangle$ is the spatial extent of Alice's photon and $|\phi(x,t)\rangle$ is the spatial extent of Bob's photon leaving the rest of the state to be the polarization state $|HH\rangle + |VV\rangle$. Now, why is the state just of a single spatial dimension? Well the simple answer is that the z-dimension represents time in this case and the y-dimension will be integrated over. Put in more words, the phase that will be introduced by the weak measurement will only be acted in the x-dimension meaning that the y-dimension does not hold new information. Thus, by integrating over all of pixels at a specific x-position, we remove all of the y information and strengthen the information that is gained at that x position. In this way, we simplify the calculation to only include the x-direction and, with out loss of generality, since the state is only measured in specific z-planes the time is always set which allows us to reduce our state to one only talking about the x-dimension. A full treatment with the y-dimension is possible; however, for the purposes here it suffices to just reduce to the one dimensional case.

Bob's photon (as labeled as the second Hilbert space above for clarification) is measured (or just measured as seen in [31]) purely in the polarization state [19, 21]. First, dealing with the case where the photon is measured to be in some polarization state given by $\cos(\theta)|H\rangle + e^{i\phi}\sin(\theta)|V\rangle$; however, there are no specific measurements on the spatial state

of the photon. Thus, the state of Alice's photon is given by

$$
\begin{aligned}
& I \otimes \langle \phi(x)| \left(I \otimes \left[\cos(\theta)\langle H| + e^{i\phi}\sin(\theta)\langle V| \right] \right) \left(\frac{1}{\sqrt{2}} |\psi(x)\rangle |\phi(x)\rangle \otimes (|HH\rangle + |VV\rangle) \right) \\
=& \frac{1}{\sqrt{2}} \langle \phi(x)|\phi(x)\rangle |\psi(x)\rangle \otimes \left(I \otimes (\cos(\theta)\langle H| + e^{i\phi}\sin(\theta)\langle V|)(|HH\rangle + |VV\rangle) \right) \\
=& \frac{1}{\sqrt{2}} |\psi(x)\rangle \otimes \left(\cos(\theta)\langle H|(|HH\rangle + |VV\rangle) + e^{i\phi}\sin(\theta)\langle V|(|HH\rangle + |VV\rangle) \right) \\
=& \frac{1}{\sqrt{2}} |\psi(x)\rangle \otimes \left(\cos(\theta)|H\rangle + e^{i\phi}\sin(\theta)|V\rangle \right)
\end{aligned}
$$

Next, the remaining photon passes through a long piece of calcite which is used to create the separate paths of the double slit experiment. A naive way to write this mathematically, is as the operator $I \otimes |H\rangle\langle H| + |\psi(x+2a)\rangle\langle\psi(x)| \otimes |V\rangle\langle V|$, where a is half of the spatial distance the beams move away from each other. Acting on the state, this finds

$$
\begin{aligned}
& (I \otimes |H\rangle\langle H| + |\psi(x+2a)\rangle\langle\psi(x)| \otimes |V\rangle\langle V|) \left(\frac{1}{\sqrt{2}} |\psi(x)\rangle \otimes (\cos(\theta)|H\rangle + e^{i\phi}\sin(\theta)|V\rangle) \right) \\
=& \frac{1}{\sqrt{2}} \left(|\psi(x)\rangle \otimes \cos(\theta)|H\rangle + |\psi(x+2a)\rangle \otimes e^{i\phi}\sin(\theta)|V\rangle \right)
\end{aligned}
$$

Further, since the zero is arbitrary on this scale in the x-direction we can rewrite the state without loss of generality as:

$$
\frac{1}{\sqrt{2}} (|\psi(x-a)\rangle \otimes \cos(\theta)|H\rangle + |\psi(x+a)\rangle \otimes e^{i\phi}\sin(\theta)|V\rangle)
$$

Each beam then experiences a polarization rotation so that each beam has the same polarization, $|D\rangle$. This leaves the state as

$$
\begin{aligned}
& \frac{1}{\sqrt{2}} (|\psi(x-a)\rangle \otimes \cos(\theta)|D\rangle + |\psi(x+a)\rangle \otimes e^{i\phi}\sin(\theta)|D\rangle) \\
&= \frac{1}{\sqrt{2}} (|\psi(x-a)\rangle \cos(\theta) + |\psi(x+a)\rangle e^{i\phi}\sin(\theta)) \otimes |D\rangle \\
&= |\psi(x)\rangle \otimes |D\rangle
\end{aligned}
$$

Where another simplification was made by assuming that the spatial part of the wave function is conglomerated into a singular state given by $|\psi(x)\rangle$. Thus the state is given as $|\psi(x)\rangle \otimes |D\rangle$. The beams next pass through the weak measurement crystal. In this case, the interaction Hamiltonian is given as $H_I = g\hat{k}_x \otimes \hat{S}_z$. The evolution of the state is then determined by the time evolution operator for this interaction Hamiltonian and is given by $e^{\frac{-igt}{\hbar}\hat{k}_x \otimes \hat{S}_z}$, where g is the strength of the interaction in the material and t is the time that the light is in the material. The time and the interaction strength are then combined into an effective parameter, ζ with units of m. To make for n easier comparison later, we create a unit-less parameter η (the interaction parameter) by pulling out a factor of $\frac{1}{|k|}$.

$$
\begin{aligned}
& e^{\frac{-igt}{\hbar}\hat{k}_x \otimes \hat{S}_z}|\psi(x)\rangle \otimes |D\rangle && (1.4)\\
&= e^{\frac{-i\eta}{|k|\hbar}\hat{k_x} \otimes \hat{S}_z}|\psi(x)\rangle \otimes |D\rangle \\
&\approx (\mathbb{1} \otimes \mathbb{1} - i\frac{\eta}{\hbar}\frac{\hat{k}_x}{|k|} \otimes \frac{\hbar}{2}\hat{\sigma}_z)|\psi(x)\rangle \otimes |D\rangle \\
&= (|\psi(x)\rangle \otimes |D\rangle - i\frac{\eta}{2}\frac{\hat{k}_x}{|k|} \otimes \hat{\sigma}_z|\psi(x)\rangle \otimes |D\rangle) && (1.5)\\
&= (|\psi(x)\rangle \otimes |D\rangle - i\frac{\eta}{2}\frac{\hat{k}_x}{|k|}|\psi(x)\rangle \otimes |A\rangle)
\end{aligned}
$$

Finally, the beams are measured in the position and the polarization basis. To make the calculations easier, the position measurement will be made first and then the polarization; however, it does not matter which measurement happens first in principal, but the experiment must take place in the reverse order as most position measurements cannot allow a subsequent polarization measurement. The polarization measurement in this case is done in the $|R\rangle$ and $|L\rangle$ basis.

$$
\begin{aligned}
& \langle x| \left(|\psi(x)\rangle \otimes |D\rangle - i\frac{\eta}{2}\frac{\hat{k}_x}{|k|}|\psi(x)\rangle \otimes |A\rangle \right) \\
&= \langle x|\psi(x)\rangle \otimes |D\rangle - i\frac{\eta}{2}\langle x|\frac{\hat{k}_x}{|k|}|\psi(x)\rangle \otimes |A\rangle \\
&= \langle x|\psi(x)\rangle \left(|D\rangle - i\frac{\eta}{2|k|}\frac{\langle x|\hat{k}_x|\psi(x)\rangle}{\langle x|\psi(x)\rangle}|A\rangle \right)
\end{aligned}
$$

Which, by definition of the weak value in the previous section, it can be written as

$$
\begin{aligned}
&= \langle x|\psi(x)\rangle \left(|D\rangle + i\frac{\eta}{|k|2}\langle k_x\rangle_w |A\rangle \right) \\
&= \langle x|\psi(x)\rangle \left(\frac{1}{\sqrt{2}}(|H\rangle + |V\rangle) + i\frac{\eta}{2|k|}\langle k_x\rangle_w \frac{1}{\sqrt{2}}(|H\rangle - |V\rangle) \right) \\
&= \frac{\langle x|\psi(x)\rangle}{\sqrt{2}} \left((|H\rangle + |V\rangle) + i\frac{\eta}{2|k|}\langle k_x\rangle_w (|H\rangle - |V\rangle) \right) \\
&= \frac{\langle x|\psi(x)\rangle}{\sqrt{2}} \left((1 + i\frac{\eta}{2|k|}\langle k_x\rangle_w)|H\rangle + (1 - i\frac{\eta}{2|k|}\langle k_x\rangle_w)|V\rangle \right) \\
&\approx \frac{\langle x|\psi(x)\rangle}{\sqrt{2}} \left(e^{i\frac{\eta}{2|k|}\langle k_x\rangle_w}|H\rangle + e^{-i\frac{\eta}{2|k|}\langle k_x\rangle_w}|V\rangle \right) \\
&= \frac{\langle x|\psi(x)\rangle}{\sqrt{2}} \left(e^{i\frac{\eta}{2|k|}\langle k_x\rangle_w}\frac{1}{\sqrt{2}}(|R\rangle + |L\rangle) + e^{-i\frac{\eta}{2|k|}\langle k_x\rangle_w}\frac{-i}{\sqrt{2}}(|R\rangle - |L\rangle) \right) \\
&= \frac{\langle x|\psi(x)\rangle}{2} \left((e^{i\frac{\eta}{2|k|}\langle k_x\rangle_w} - ie^{-i\frac{\eta}{2|k|}\langle k_x\rangle_w})|R\rangle) + (e^{i\frac{\eta}{2|k|}\langle k_x\rangle_w} + ie^{-i\frac{\eta}{2|k|}\langle k_x\rangle_w})|L\rangle \right)
\end{aligned}
$$

Finally, measuring the polarization yields

$$
\begin{aligned}
|\langle R|\langle x|\Psi\rangle|^2 &= \left| \frac{\langle x|\psi(x)\rangle}{2} \left(e^{i\frac{\eta}{2|k|}\langle k_x\rangle_w} - ie^{-i\frac{\eta}{2|k|}\langle k_x\rangle_w} \right) \right|^2 \\
|\langle R|\langle x|\Psi\rangle|^2 &= \frac{|\psi(x)|^2}{2} \left| \left(e^{i\frac{\eta}{2|k|}\langle k_x\rangle_w} - ie^{-i\frac{\eta}{2|k|}\langle k_x\rangle_w} \right) \right|^2 \\
|\langle R|\langle x|\Psi\rangle|^2 &= \frac{|\psi(x)|^2}{4} \left(2 - i(e^{-i\frac{\eta}{|k|}\langle k_x\rangle_w} - e^{i\frac{\eta}{|k|}\langle k_x\rangle_w}) \right) \\
|\langle R|\langle x|\Psi\rangle|^2 &= \frac{|\psi(x)|^2}{4} \left(2 + 2\sin\left(\frac{\eta}{|k|}\langle k_x\rangle_w \right) \right) \\
|\langle R|\langle x|\Psi\rangle|^2 &= \frac{|\psi(x)|^2}{2} \left(1 + \sin\left(\frac{\eta}{|k|}\langle k_x\rangle_w \right) \right)
\end{aligned}
$$

&

$$|\langle L|\langle x|\Psi\rangle|^2 = |\frac{\langle x|\psi(x)\rangle}{2}(e^{i\frac{\eta}{2|k|}\langle k_x\rangle_w} + ie^{-i\frac{\eta}{2|k|}\langle k_x\rangle_w})|^2$$
$$|\langle L|\langle x|\Psi\rangle|^2 = \frac{|\psi(x)|^2}{4}|(e^{i\frac{\eta}{2|k|}\langle k_x\rangle_w} + ie^{-i\frac{\eta}{2|k|}\langle k_x\rangle_w})|^2$$
$$|\langle L|\langle x|\Psi\rangle|^2 = \frac{|\psi(x)|^2}{4}(2 + i(e^{-i\frac{\eta}{|k|}\langle k_x\rangle_w} - e^{i\frac{\eta}{|k|}\langle k_x\rangle_w}))$$
$$|\langle L|\langle x|\Psi\rangle|^2 = \frac{|\psi(x)|^2}{4}(2 - 2\sin\left(\frac{\eta}{|k|}\langle k_x\rangle_w\right))$$
$$|\langle L|\langle x|\Psi\rangle|^2 = \frac{|\psi(x)|^2}{2}(1 - \sin\left(\frac{\eta}{|k|}\langle k_x\rangle_w\right))$$

Noticing these measurements, it is possible to recover $\langle k_x\rangle_w$ by realizing

$$\frac{|\langle R|\langle x|\psi\rangle|^2 - |\langle L|\langle x|\psi\rangle|^2}{|\langle R|\langle x|\psi\rangle|^2 + |\langle L|\langle x|\psi\rangle|^2} = \sin\left(\frac{\eta}{|k|}\langle k_x\rangle_w\right)$$

which implies

$$\frac{\langle k_x\rangle_w}{|k|} = \frac{1}{\eta}\sin^{-1}(\frac{|\langle R|\langle x|\psi\rangle|^2 - |\langle L|\langle x|\psi\rangle|^2}{|\langle R|\langle x|\psi\rangle|^2 + |\langle L|\langle x|\psi\rangle|^2}). \tag{1.6}$$

Thus, now that the weak measurement of the momentum in the x-direction is known at a specific location at a specific z-plane. The next question is how to take the information of this velocity field and transform into particle trajectories. The trajectories are created by taking some selection of initial points and, then, assuming that the speed in the z-direction for the photons is given by the speed of light (since $\frac{k_x}{|k|} << \frac{k_z}{|k|}$ as prescribed by the paraxial-Helmholtz equation for any directional beam). It is then further assumed that since the photons should be traveling at the speed of light, the velocity of the particles in the x-direction is then defined to be $v_x = c\frac{\langle k_x\rangle^w(x,z)}{|k|}$. By taking each of the initial points (which we chose), we can find the update of the state/positions of the particles by using an Euler approximation to solve for the path that the particle takes:

$$x_{new} = x_{old} + v_x(x_{old}, z_{old}) \times (\frac{z_{new} - z_{old}}{c}) \tag{1.7}$$

where z_{new} and z_{old} are taken to be the planes where each of the different measurements take place and x_{old} and x_{new} are the positions of the particles at the planes z_{old} and z_{new}

respectfully. By then connecting the points for every z-plane, the trajectories have been constructed. In the limit where there are many planes, the trajectories will converge to the trajectories. Now, there is a certain question about how to choose the initial points, but the discussion will be left to the next section 1.2.4.

1.2.4 Technical Considerations for the Trajectories

This section is devoted to a few topics that have been glossed over when defining Bohmian trajectories in the previous section. These issues are about the definition of the trajectories, the connection between light and Bohmian photons, seed points for the trajectories, and how to create a weak measurement using optical components. There are a few theoretical debates in some of the areas as well that have not been fully resolved. I will try to acknowledge them while pressing further as they are beyond the scope of this project.

Theoretical Issues

The first theoretical issue is a question about the identity of the trajectories. This is only one of many such trajectory configurations that could be deemed to be the correct configuration. This is due to the fact that there are any number of velocity fields will give rise to the same statistics as defined above (since adding the curl of any field will automatically satisfy equation 1.2 since the divergence of any curl is 0) and, thus, technically there are then infinitely many solutions for the trajectory configurations. However, as Wiseman argues, this is the only configuration of trajectories that matter, because it is the only solution of trajectories that are experimentally realizable [30]. This solution is then the one we define as the Bohmian trajectories.

Next, there is a subtle incompatibility that we have over looked. In the above analysis, we used the time dependent Schödinger equation to talk about the quantum state of light. Formally, though, light typically needs the full power of a field theory to be described since photons are the very essence of a relativistic particle and are solutions of Maxwells equations. However, there are certain configurations of light that are known to follow what is known as the paraxial-Helmholtz equation and is the typical way of describing a lasers output. Effectively, these solutions of the Helmholtz equation are for any beam such that the angle that the wave vector makes with the axis of propagation is much smaller than one. The equation is given by $\nabla_\perp^2\psi + 2i|k|\frac{\partial}{\partial z}\psi = 0$ where $\nabla_\perp^2 = \frac{\partial^2}{\partial x^2} + \frac{\partial^2}{\partial y^2}$ [26]. Let us now compare this equation to Schrödinger's equation -with no outside potential:

$$
\begin{aligned}
i\hbar\frac{\partial}{\partial t}\psi + \frac{\hbar^2\nabla^2}{2m}\psi = 0 \\
2i|k|\frac{\partial}{\partial z}\psi + \nabla_\perp^2\psi = 0
\end{aligned}
\tag{1.8}
$$

If we choose that our Schrödinger equation is confined to the two dimensions perpendicular to the direction of beam propagation and that the z direction is related to time under the approximation that $z = tc$, then we see that the equations are a perfect analog of one another. This means that without needing to move to a quantum field theoretic formulation, we should be able to approximate our more complicated relativistic particles using the Schrödinger equation! In fact, by comparing the two equations and by constant matching, we can attach a mass to our equivalent Schrödinger system:

$$
\begin{aligned}
\nabla_\perp^2\psi + 2i|k|\frac{\partial}{\partial z}\psi = 0 \\
\frac{1}{2|k|}\nabla_\perp^2\psi + i\frac{\partial}{\partial z}\psi = 0 \\
\frac{1}{2|k|}\nabla_\perp^2\psi + i\frac{\partial}{\partial (ct)}\psi = 0 \\
\frac{c}{2|k|}\nabla_\perp^2\psi + i\frac{\partial}{\partial t}\psi = 0 \\
\frac{\hbar\nabla_\perp^2}{2m}\psi + i\frac{\partial}{\partial t}\psi = 0
\end{aligned}
\tag{1.9}
$$

Thus, we see the old naive approximation for the mass of the photon ($m_p = \frac{\hbar|k|}{c}$). It should be noted that the solution found and described here relies heavily on the approximation that the beam is moving with small angles to the direction of propagation. Without this, this mass definition would not hold in the general case. Furthermore, it should be noted that when we measure in the experiment, we measure the paraxial Helmholtz not the Schrödinger equation. Thus, we need to take our measurements and convert them into the Schrödinger basis by changing z to t and factoring in the effective mass. This allows us to describe the Bohmian particles. By then switching back to the measurement basis we can report the Bohmian trajectories in physical space.

There is, however, a problem that some have with the above analysis. The main issue is that this analysis rests on the fact that a mass-less field can be localized or have a first quantized representation. The reason for this discrepancy is from a few proofs that state that position operators are impossible to define for a photon making the construction of

a probability density impossible [18, 23, 29]. Without a suitable first quantized field, the idea of a Bohmian particle and trajectory are difficult to define as Bohmian mechanics requires such a notion in order to define these constructions. Hence there is a fundamental incompatible with the notion of quantum field theory. Furthermore, there have been some attempts to try to quantize the electromagnetic field in the paraxial regime to give rise to a local quantum field theory where localization and the ability to define a first quantization are possible (see [8, 6]). The major issue with this realization is that by assuming a paraxial equation, the covariance of the theory is lost meaning that by looking in different frames may cause the outcome of the measurements to be different. So, with this all said, what would the experiment actually measure if not for photon trajectories? Using this analysis, there are claims that the more appropriate way to identify the measurement outcome is the momentum components of the stress-energy tensor and are in some way measuring energy flow of the system [12]. However, I am not in a position to dispute or confirm either of the views that are presented here. So, I will assume that there is some truth to the first quantization procedure as that is the impetus for this project and as well as choose to follow along with the current claims of [19, 21, 31] in order to be cohesive and follow the current narrative of experiments.

Further, there is an issue with how to choose the initial points. Kocsis, et al. argue that the only seed points should be the ones allowed where the k_x value is measured (i.e. only at the center of the pixels on the camera) [19]. However, there is no basis that other points could not be allowed. After all, just because the average momentum was measured over some width, does not mean that there is no interpolating curve between the various points. In fact, intuitively we would expect this curve to match the theoretical curve even though we are averaging in the x-direction. We know this because the number of pixels should be smaller than our major features and except for points at or near the minima and maxima where the average would be slightly smaller than the true value, everywhere else each pixel will only be linear in terms of the weak momentum as a function of the x-direction. This means that the average value over the pixel should be the value given exactly at the center of the pixel. Therefore, we can interpolate for the velocity in between the middle pixel measurements that we would be taking.

Finally, while de Broglie would be proud to see his trajectories in such high esteem, it is not enough for the Bohmian. To the Bohmian, remember, what is sacred above all else is the quantum potential. For it is this potential that drives the photons into their configurations even though there are no forces that act upon them in the classical sense. The purpose of my experiment was to investigate if there was a method that could derive the quantum potential from the trajectories of photons as was done by [19, 21, 31].

Realizing the Weak Measurement

The physical realization of the weak measurement starts by assuming that there is a birefringent material that has two indices of refraction (n_o and n_e), an optical axis given at some angle to the normal of the surface –θ_{opt},– and a material length given by L. The photon then enters the material at some angle, $\theta = \frac{k_x}{|k|}$. The photon then gains a phase given by the formula

$$\phi = nL|k| \tag{1.10}$$

However, it should be noted that the length and the index of refraction are dependent on the polarization and the angle of the incoming light. Effectively, this gives two phases (and two paths for the light). The important part is then to look at the phase difference between the two paths. Remembering that there are two operators going on: the polarization projection due to the birefringence and the momentum of the photon. We will right away start with the polarization degree of freedom as an operator and then uplift the momentum when we need to. We also assign, without loss of generality (or at least up to a minus sign), that the $|H\rangle$ polarized light takes the path defined using n_o and $|V\rangle$ polarized light will take the other path defined with the index of refraction $n_e(\theta'') = \frac{1}{\sqrt{\frac{\cos^2(\theta''+\theta_{opt})}{n_o^2}+\frac{\sin^2(\theta''+\theta_{opt})}{n_e^2}}}$.

$$\phi_{|H\rangle} = \frac{n_o L|k|}{\cos\theta'}|H\rangle\langle H| \tag{1.11}$$

$$\phi_{|V\rangle} = \frac{n_e(\theta'')L|k|}{\cos\theta''}|V\rangle\langle V| \tag{1.12}$$

The distinction here is that $\theta'(\theta)$ and $\theta''(\theta)$ are the internal angles that the beam takes as it goes through the material which are functions of the incident angle θ and are calculated by applying Snells law. Calculating the difference in the phase, we find

$$\begin{aligned}
\delta\phi =& \phi_{|H\rangle} - \phi_{|V\rangle} && (1.13)\\
=& \frac{n_o L|k|}{\cos\theta'}|H\rangle\langle H| - \frac{n_e(\theta'')L|k|}{\cos\theta''}|V\rangle\langle V| && (1.14)\\
=& L|k| \begin{pmatrix} \frac{n_o}{\cos\theta'} & 0 \\ 0 & -\frac{n_e(\theta'')}{\cos\theta''(\theta)} \end{pmatrix} && (1.15)\\
=& \frac{L|k|\alpha'(\theta)}{2} I + \frac{L|k|\beta'(\theta)}{2}\sigma_z && (1.16)
\end{aligned}$$

$$=\frac{\alpha(\theta)}{2}I + \frac{\beta(\theta)}{2}\sigma_z \tag{1.17}$$

where $\alpha(\theta) = L|k|(\frac{n_o}{\cos\theta'} - \frac{n_e(\theta'')}{\cos\theta''})$ and $\beta(\theta) = L|k|(\frac{n_o}{\cos\theta'} + \frac{n_e(\theta'')}{\cos\theta''})$. Now, remembering that a crystal with its optic axis in the x-z plane acts like a a wave retarder, the rotation on the polarization goes as

$$e^{-i\delta\phi} = e^{-i(\frac{\alpha(\theta)}{2}\hat{I} + \frac{\beta(\theta)}{2}\hat{\sigma}_z)} \tag{1.18}$$

We now note that both $\alpha(\theta)$ and $\beta(\theta)$ can be expressed as a Taylor series. Using this fact, we find

$$[\alpha(\hat{\theta})\otimes\hat{I}, \beta(\hat{\theta})\otimes\hat{\sigma}_z] = \frac{1}{2}\Big([\alpha(\hat{\theta}), \beta(\hat{\theta})]\otimes\{\hat{I}, \hat{\sigma}_z\} + \{\alpha(\hat{\theta}), \beta(\hat{\theta})\}\otimes[\hat{I}, \hat{\sigma}_z]\Big) \tag{1.19}$$

$$= \frac{1}{2}\Big([\alpha(\hat{\theta}), \beta(\hat{\theta})]\otimes\{\hat{I}, \hat{\sigma}_z\} + \{\alpha(\hat{\theta}), \beta(\hat{\theta})\}\otimes 0\Big) \tag{1.20}$$

$$= \frac{1}{2}[\alpha(\hat{\theta}), \beta(\hat{\theta})]\otimes\{\hat{I}, \hat{\sigma}_z\} \tag{1.21}$$

$$= \frac{1}{2}[\alpha(\hat{\theta}), \beta(\hat{\theta})]\otimes 2\hat{\sigma}_z \tag{1.22}$$

$$= [\alpha(\hat{\theta}), \beta(\hat{\theta})]\otimes\hat{\sigma}_z \tag{1.23}$$

$$= [\sum_n \alpha^{(n)}(0)\hat{\theta}^n, \sum_m \beta^{(m)}(0)\hat{\theta}^m]\otimes\hat{\sigma}_z \tag{1.24}$$

$$= \sum_n\sum_m [\alpha^{(n)}(0)\hat{\theta}^n, \beta^{(m)}(0)\hat{\theta}^m]\otimes\hat{\sigma}_z \tag{1.25}$$

focusing on the terms of $\hat{\theta}$ we see the above commutator reduces to sums of the commutator below

$$[\beta^{(m)}(0)\hat{\theta}^m, \alpha^{(n)}(0)\hat{\theta}^n] = \beta^{(m)}(0)\alpha^{(n)}(0)[\hat{\theta}^m, \hat{\theta}^n] \tag{1.26}$$

$$= 0 \tag{1.27}$$

Thus,

$$[\alpha(\hat{\theta})\otimes\hat{I}, \beta(\hat{\theta})\otimes\hat{\sigma}_z] = \sum_n\sum_m [\alpha^{(n)}(0)\hat{\theta}^n, \beta^{(m)}(0)\hat{\theta}^m]\otimes\hat{\sigma}_z \tag{1.28}$$

$$= \sum_n \sum_m 0 \otimes \hat{\sigma}_z \tag{1.29}$$

$$= 0 \tag{1.30}$$

Hence, we find that we can rewrite the solution of above (1.18) as

$$e^{-i\left(\frac{\alpha(\hat{\theta})}{2}\hat{I}+\frac{\beta(\hat{\theta})}{2}\hat{\sigma}_z\right)} = e^{-i\frac{\alpha(\hat{\theta})}{2}\hat{I}}e^{-i\frac{\beta(\hat{\theta})}{2}\hat{\sigma}_z} \tag{1.31}$$

$$\tag{1.32}$$

Now, acting that unitary on the state $|\psi\rangle \otimes |D\rangle$ and realizing that both $\alpha(\hat{\theta})$ and $\beta(\hat{\theta})$ can be expanded as a Taylor series around $\theta = 0$, we press on with the calculation

$$e^{-i\frac{\alpha(\hat{\theta})}{2}\hat{I}}e^{-i\frac{\beta(\hat{\theta})}{2}\hat{\sigma}_z}|\psi\rangle \otimes |D\rangle = e^{-i(\frac{\mu+\upsilon\hat{\theta}}{2}+\frac{\sum_{m>1}^{\infty}\alpha^{(m)}(0)\hat{\theta}}{2m!})\hat{I}}e^{-i(\frac{\gamma+\eta\hat{\theta}}{2}+\frac{\sum_{n>1}^{\infty}\beta^{(n)}(0)\hat{\theta}^n}{2n!})\hat{\sigma}_z}|\psi\rangle \otimes |D\rangle \tag{1.33}$$

which can be reduced by using analogs of the commutator (see equation 1.27) to the following

$$e^{-i\frac{\alpha(\hat{\theta})}{2}\hat{I}}e^{-i\frac{\beta(\hat{\theta})}{2}\hat{\sigma}_z}|\psi\rangle \otimes |D\rangle = \tag{1.34}$$

$$= e^{-i(\frac{\mu}{2})}e^{-i(\frac{\upsilon\hat{\theta}}{2})\otimes\hat{I}}e^{-i(\frac{\sum_{m>1}^{\infty}\alpha^{(m)}(0)\hat{\theta}}{2m!})\otimes\hat{I}}e^{-i(\frac{\gamma}{2})\otimes\hat{\sigma}_z}e^{-i(\frac{\eta\hat{\theta}}{2})\otimes\hat{\sigma}_z}e^{-i(\frac{\sum_{n>1}^{\infty}\beta^{(n)}(0)\hat{\theta}^n}{2n!})\otimes\hat{\sigma}_z}|\psi\rangle \otimes |D\rangle \tag{1.35}$$

$$= e^{-i(\frac{\mu}{2})}e^{-i(\frac{\upsilon\hat{\theta}}{2})\otimes\hat{I}}\prod_{m>1}^{\infty}e^{-i(\frac{\alpha^{(m)}(0)\hat{\theta}}{2m!})\otimes\hat{I}}e^{-i(\frac{\gamma}{2})\otimes\hat{\sigma}_z}e^{-i(\frac{\eta\hat{\theta}}{2})\otimes\hat{\sigma}_z}\prod_{n>1}^{\infty}e^{-i(\frac{\beta^{(n)}(0)\hat{\theta}^n}{2n!})\otimes\hat{\sigma}_z}|\psi\rangle \otimes |D\rangle \tag{1.36}$$

$$= e^{-i(\frac{\mu}{2})}e^{-i(\frac{\upsilon\hat{\theta}}{2})\otimes\hat{I}}\prod_{m>1}^{\infty}e^{-i(\frac{\alpha^{(m)}(0)\hat{\theta}}{2m!})\otimes\hat{I}}e^{-i(\frac{\gamma}{2})\otimes\hat{\sigma}_z}e^{-i(\frac{\eta\hat{\theta}}{2})\otimes\hat{\sigma}_z}\prod_{n>1}^{\infty}\sum_{j=0}^{\infty}\frac{(-i(\frac{\beta^{(n)}(0)\hat{\theta}^n}{2n!})\otimes\hat{\sigma}_z)^j}{j!}|\psi\rangle \otimes |D\rangle \tag{1.37}$$

$$= e^{-i(\frac{\mu}{2})}e^{-i(\frac{\upsilon\hat{\theta}}{2})\otimes\hat{I}}\prod_{m>1}^{\infty}e^{-i(\frac{\alpha^{(m)}(0)\hat{\theta}}{2m!})\otimes\hat{I}}e^{-i(\frac{\gamma}{2})\otimes\hat{\sigma}_z}e^{-i(\frac{\eta\hat{\theta}}{2})\otimes\hat{\sigma}_z}\ldots$$

$$\prod_{n>1}^{\infty}(\hat{I}\otimes\hat{I}-i(\frac{\beta^{(n)}(0)\hat{\theta}^n}{2n!})\otimes\hat{\sigma}_z+\ldots)|\psi\rangle\otimes|D\rangle \tag{1.38}$$

Further, for $p>1$, due to the paraxial approximation the $\theta\ll 1$ which means that we can make the approximation that $\theta^p\approx 0$, we can act our $\hat{\theta}$ operator on our state yielding

$$\begin{aligned}
\hat{\theta}^p\otimes\hat{I}|\psi\rangle|D\rangle &= \hat{\theta}^p|\psi\rangle\otimes|D\rangle && (1.39)\\
&= \frac{\hat{k}_x^p}{|k|^p}|\psi\rangle\otimes|D\rangle && (1.40)\\
&= \int_{-\infty}^{\infty}\frac{\hat{k}_x^p}{|k|^p}|k_x\rangle\langle k_x|\psi\rangle\otimes|D\rangle dk_x && (1.41)\\
&= \int_{-\infty}^{\infty}\left(\frac{k_x}{|k|}\right)^p|k_x\rangle\langle k_x|\psi\rangle\otimes|D\rangle dk_x && (1.42)\\
&= \int_{-\infty}^{\infty}\theta^p|k_x\rangle\langle k_x|\psi\rangle\otimes|D\rangle dk_x && (1.43)\\
&\approx \int_{-\infty}^{\infty}0|k_x\rangle\langle k_x|\psi\rangle\otimes|D\rangle dk_x && (1.44)\\
&\approx 0 && (1.45)
\end{aligned}$$

Thus, continuing the main calculation on the state from equation 1.38

$$\begin{aligned}
&= e^{-i(\frac{\mu}{2})}e^{-i(\frac{\upsilon\hat{\theta}}{2})\otimes\hat{I}}\prod_{m>1}^{\infty}e^{-i(\frac{\alpha^{(m)}(0)\hat{\theta}}{2m!})\otimes\hat{I}}e^{-i(\frac{\gamma}{2})\otimes\hat{\sigma}_z}e^{-i(\frac{\eta\hat{\theta}}{2})\otimes\hat{\sigma}_z}\ldots\\
&\qquad\prod_{n>1}^{\infty}(\hat{I}\otimes\hat{I}-i(\frac{\beta^{(n)}(0)\hat{\theta}^n}{2n!})\otimes\hat{\sigma}_z+\ldots)|\psi\rangle\otimes|D\rangle && (1.46)\\
&= e^{-i(\frac{\mu}{2})}e^{-i(\frac{\upsilon\hat{\theta}}{2})\otimes\hat{I}}\prod_{m>1}^{\infty}e^{-i(\frac{\alpha^{(m)}(0)\hat{\theta}}{2m!})\otimes\hat{I}}e^{-i(\frac{\gamma}{2})\otimes\hat{\sigma}_z}e^{-i(\frac{\eta\hat{\theta}}{2})\otimes\hat{\sigma}_z}\hat{I}\otimes\hat{I}|\psi\rangle\otimes|D\rangle && (1.47)
\end{aligned}$$

$$= e^{-i(\frac{\mu}{2})} e^{-i(\frac{v\hat{\theta}}{2})\otimes\hat{I}} \prod_{m>1}^{\infty} e^{-i(\frac{\alpha^{(m)}(0)\hat{\theta}}{2m!})\otimes\hat{I}} e^{-i(\frac{\gamma}{2})\otimes\hat{\sigma}_z} \sum_{n=0}^{\infty} \frac{\left(-i(\frac{\eta\hat{\theta}}{2})\otimes\hat{\sigma}_z\right)^n}{n!} |\psi\rangle\otimes|D\rangle \tag{1.48}$$

$$\approx e^{-i(\frac{\mu}{2})} e^{-i(\frac{v\hat{\theta}}{2})\otimes\hat{I}} \prod_{m>1}^{\infty} e^{-i(\frac{\alpha^{(m)}(0)\hat{\theta}}{2m!})\otimes\hat{I}} \left(\cos\left(\frac{\gamma}{2}\right) - i\sin\left(\frac{\gamma}{2}\right)\sigma_z\right) \left(|\psi\rangle\otimes|D\rangle - i\frac{\eta\hat{\theta}}{2}|\psi\rangle\otimes|A\rangle\right) \tag{1.49}$$

$$= e^{-i(\frac{\mu}{2})} e^{-i(\frac{v\hat{\theta}}{2})\otimes\hat{I}} \prod_{m>1}^{\infty} e^{-i(\frac{\alpha^{(m)}(0)\hat{\theta}}{2m!})\otimes\hat{I}} \ldots$$
$$\left(\cos\left(\frac{\gamma}{2}\right)|\psi\rangle\otimes|D\rangle - i\frac{\cos\left(\frac{\gamma}{2}\right)\eta\hat{\theta}}{2}|\psi\rangle\otimes|A\rangle - i\sin\left(\frac{\gamma}{2}\right)|\psi\rangle\otimes|A\rangle - \frac{\sin\left(\frac{\gamma}{2}\right)\eta\hat{\theta}}{2}|\psi\rangle\otimes|D\rangle\right) \tag{1.50}$$

$$= e^{-i(\frac{\mu}{2})} e^{-i(\frac{v\hat{\theta}}{2})\otimes\hat{I}} \prod_{m>1}^{\infty} \sum_{n=0}^{\infty} \frac{\left(-i(\frac{\alpha^{(m)}(0)\hat{\theta}}{2m!}\otimes\hat{I})\right)^n}{n!} \ldots$$
$$\left(\cos\left(\frac{\gamma}{2}\right)|\psi\rangle\otimes|D\rangle - i\frac{\cos\left(\frac{\gamma}{2}\right)\eta\hat{\theta}}{2}|\psi\rangle\otimes|A\rangle - i\sin\left(\frac{\gamma}{2}\right)|\psi\rangle\otimes|A\rangle - \frac{\sin\left(\frac{\gamma}{2}\right)\eta\hat{\theta}}{2}|\psi\rangle\otimes|D\rangle\right) \tag{1.51}$$

utilizing the paraxial approximation and the relation found earlier (see the calculation starting at 1.39)

$$\approx e^{-i(\frac{\mu}{2})} e^{-i(\frac{v\hat{\theta}}{2})\otimes\hat{I}} \prod_{m>1}^{\infty} \left(\hat{I}\otimes\hat{I} + 0 + \ldots + 0 + \ldots\right) \cdots$$
$$\left(\cos\left(\frac{\gamma}{2}\right)|\psi\rangle\otimes|D\rangle - i\frac{\cos\left(\frac{\gamma}{2}\right)\eta\hat{\theta}}{2}|\psi\rangle\otimes|A\rangle - i\sin\left(\frac{\gamma}{2}\right)|\psi\rangle\otimes|A\rangle - \frac{\sin\left(\frac{\gamma}{2}\right)\eta\hat{\theta}}{2}|\psi\rangle\otimes|D\rangle\right) \tag{1.52}$$

$$= e^{-i(\frac{\mu}{2})} e^{-i(\frac{v\hat{\theta}}{2})\otimes\hat{I}} \ldots$$
$$\left(\cos\left(\frac{\gamma}{2}\right)|\psi\rangle\otimes|D\rangle - i\frac{\cos\left(\frac{\gamma}{2}\right)\eta\hat{\theta}}{2}|\psi\rangle\otimes|A\rangle - i\sin\left(\frac{\gamma}{2}\right)|\psi\rangle\otimes|A\rangle - \frac{\sin\left(\frac{\gamma}{2}\right)\eta\hat{\theta}}{2}|\psi\rangle\otimes|D\rangle\right) \tag{1.53}$$

$$= e^{-i(\frac{\mu}{2})} \sum_{n=0}^{\infty} \frac{\left(-i(\frac{\upsilon\hat{\theta}}{2}) \otimes \hat{I}\right)^n}{n!} \cdot ..$$
$$\left(\cos\Big(\frac{\gamma}{2}\Big)|\psi\rangle \otimes |D\rangle - i\frac{\cos\big(\frac{\gamma}{2}\big)\eta\hat{\theta}}{2}|\psi\rangle \otimes |A\rangle - i\sin\Big(\frac{\gamma}{2}\Big)|\psi\rangle \otimes |A\rangle - \frac{\sin\big(\frac{\gamma}{2}\big)\eta\hat{\theta}}{2}|\psi\rangle \otimes |D\rangle\right) \tag{1.54}$$

$$\approx e^{-i(\frac{\mu}{2})} \left(\hat{I} \otimes \hat{I} - i(\frac{\upsilon\hat{\theta}}{2}) \otimes \hat{I}\right) \cdot ..$$
$$\left(\cos\Big(\frac{\gamma}{2}\Big)|\psi\rangle \otimes |D\rangle - i\frac{\cos\big(\frac{\gamma}{2}\big)\eta\hat{\theta}}{2}|\psi\rangle \otimes |A\rangle - i\sin\Big(\frac{\gamma}{2}\Big)|\psi\rangle \otimes |A\rangle - \frac{\sin\big(\frac{\gamma}{2}\big)\eta\hat{\theta}}{2}|\psi\rangle \otimes |D\rangle\right) \tag{1.55}$$

$$\approx e^{-i(\frac{\mu}{2})}\Big[\left(\cos\Big(\frac{\gamma}{2}\Big)|\psi\rangle \otimes |D\rangle - i\frac{\cos\big(\frac{\gamma}{2}\big)\eta\hat{\theta}}{2}|\psi\rangle \otimes |A\rangle - i\sin\Big(\frac{\gamma}{2}\Big)|\psi\rangle \otimes |A\rangle - \frac{\sin\big(\frac{\gamma}{2}\big)\eta\hat{\theta}}{2}|\psi\rangle \otimes |D\rangle\right) +$$
$$\left(-i\frac{\upsilon\hat{\theta}}{2}\cos\Big(\frac{\gamma}{2}\Big)|\psi\rangle \otimes |D\rangle - 0 - \frac{\upsilon\hat{\theta}}{2}\sin\Big(\frac{\gamma}{2}\Big)|\psi\rangle \otimes |A\rangle - 0\right)\Big] \tag{1.56}$$

$$= e^{-i(\frac{\mu}{2})}\Big(\cos\Big(\frac{\gamma}{2}\Big)|\psi\rangle \otimes |D\rangle - i\frac{\cos\big(\frac{\gamma}{2}\big)\eta\hat{\theta}}{2}|\psi\rangle \otimes |A\rangle - i\sin\Big(\frac{\gamma}{2}\Big)|\psi\rangle \otimes |A\rangle - \frac{\sin\big(\frac{\gamma}{2}\big)\eta\hat{\theta}}{2}|\psi\rangle \otimes |A\rangle +$$
$$- i\frac{\upsilon\hat{\theta}}{2}\cos\Big(\frac{\gamma}{2}\Big)|\psi\rangle \otimes |D\rangle - \frac{\upsilon\hat{\theta}}{2}\sin\Big(\frac{\gamma}{2}\Big)|\psi\rangle \otimes |A\rangle\Big) \tag{1.57}$$

$$= e^{-i(\frac{\mu}{2})}\Big(\cos\Big(\frac{\gamma}{2}\Big)|\psi\rangle \otimes |D\rangle - i\frac{\cos\big(\frac{\gamma}{2}\big)\eta\hat{k}_x}{2|k|}|\psi\rangle \otimes |A\rangle - i\sin\Big(\frac{\gamma}{2}\Big)|\psi\rangle \otimes |A\rangle - \frac{\sin\big(\frac{\gamma}{2}\big)\eta\hat{k}_x}{2|k|}|\psi\rangle \otimes |A\rangle +$$
$$- i\frac{\upsilon\hat{k}_x}{2|k|}\cos\Big(\frac{\gamma}{2}\Big)|\psi\rangle \otimes |D\rangle - \frac{\upsilon\hat{k}_x}{2|k|}\sin\Big(\frac{\gamma}{2}\Big)|\psi\rangle \otimes |A\rangle\Big) \tag{1.58}$$

by then taking the definition of the weak value of an operator, $\hat{Q}$, as $\frac{\langle\Psi|\hat{Q}|\Phi\rangle}{\langle\Psi|\Phi\rangle}$. This allows for us to define $\langle k_x\rangle^w = \frac{\langle x|\hat{k}_x|\psi\rangle}{\langle x|\psi\rangle}$ which allows us to simplify our statement above significantly by using this definition as well as post-selecting on the position:

$$= \frac{\langle x|\psi\rangle}{2}e^{-i(\frac{\mu}{2})}\Big(\cos\Big(\frac{\gamma}{2}\Big)|D\rangle - i\frac{\cos\big(\frac{\gamma}{2}\big)\eta}{2|k|}\langle k_x\rangle^w|A\rangle - i\sin\Big(\frac{\gamma}{2}\Big)|A\rangle - \frac{\sin\big(\frac{\gamma}{2}\big)\eta}{2|k|}\langle k_x\rangle^w|A\rangle +$$
$$- i\frac{\upsilon}{2|k|}\cos\Big(\frac{\gamma}{2}\Big)\langle k_x\rangle^w|D\rangle - \frac{\upsilon}{2|k|}\sin\Big(\frac{\gamma}{2}\Big)\langle k_x\rangle^w|A\rangle\Big) \tag{1.59}$$

$$= \frac{\langle x|\psi\rangle}{2} e^{-i(\frac{\mu}{2})} \left(e^{\frac{-i\gamma}{2}} \frac{(2|k| - i\langle k_x\rangle^w(\upsilon+\eta))}{2|k|} |H\rangle + e^{\frac{i\gamma}{2}} \frac{(2|k| + i\langle k_x\rangle^w(\upsilon-\eta))}{2|k|} |V\rangle \right) \quad (1.60)$$

$$\approx \frac{\langle x|\psi\rangle}{2} e^{-i(\frac{\mu}{2})} \left(e^{\frac{-i\gamma}{2}} e^{-i\frac{\langle k_x\rangle^w(\eta+\upsilon)}{2|k|}} |H\rangle + e^{\frac{i\gamma}{2}} e^{i\frac{\langle k_x\rangle^w(\eta-\upsilon)}{2|k|}} |V\rangle \right) \quad (1.61)$$

Now, by post-selecting on the right and left polarizations, we find

$$|\langle R|\Phi\rangle|^2 = \frac{|\psi(x)|^2}{2} \left(1 + \sin\left(\gamma + \frac{\eta}{|k|}\langle k_x\rangle^w \right) \right) \quad (1.62)$$

$$|\langle L|\Phi\rangle|^2 = \frac{|\psi(x)|^2}{2} \left(1 - \sin\left(\gamma + \frac{\eta}{|k|}\langle k_x\rangle^w \right) \right) \quad (1.63)$$

which is of the same form that we expected in the previous treatment. However, there are a few things to note. First, using a slight abuse of notation we can change the form to something with a bit more physical meaning. Let's look just at the R-polarization post-selection

$$|\langle R|\Phi\rangle|^2 = \frac{|\psi(x)|^2}{2} \left(1 + \sin\left(\gamma + \frac{\eta}{|k|}\langle k_x\rangle^w \right) \right) \quad (1.64)$$

$$= \frac{|\psi(x)|^2}{2} \left(1 + \sin\left(\gamma + \eta\langle \frac{k_x}{|k|}\rangle^w \right) \right) \quad (1.65)$$

$$= \frac{|\psi(x)|^2}{2} \left(1 + \sin(\gamma + \eta\langle\theta\rangle^w) \right) \quad (1.66)$$

Now, if we rotate the crystal's normal in the x-z plane, then technically we find the angle will be changed by δ (so the total angle is now $\theta + \delta$); thus, we find

$$|\langle R|\Phi\rangle|^2 = \frac{|\psi(x)|^2}{2} \left(1 + \sin\left(\gamma + \eta\langle(\theta+\delta)\rangle^w \right) \right) \quad (1.67)$$

$$= \frac{|\psi(x)|^2}{2} \left(1 + \sin\left(\gamma + \eta(\langle\theta\rangle^w + \langle\delta\rangle^w) \right) \right) \quad (1.68)$$

$$= \frac{|\psi(x)|^2}{2} \left(1 + \sin\left(\gamma + \eta\langle\theta\rangle^w + \eta\langle\delta\rangle^w \right) \right) \quad (1.69)$$

Therefore, there exists such a δ such that $\eta\delta = -\gamma$. This allows for the intensities of the left and right polarizations to be equal when $\frac{\langle k_x \rangle^w}{|k|} = 0$ (note: the same δ also works for the L-polarization post-selection). Next, we note that the solution above does not include terms from the identity part of the half of the first operator (see 1.17). Thus, we could replace the full operator with only the terms with $\hat{\sigma}_z$ in 1.17. Then, we can make the identification of the simple operator interaction operator that is defined/weakly explained in [19] and the operator that we defined from the crystal properties of birefringence and the angle of the incoming light. In this identification, η is the interaction strength in weak measurement theory. The last thing to do now that the identification of the pure theory to the actual measurement conditions are talked about, is to actually calculate the theoretical values of η and γ.

To do this, we remember that $\gamma = L|k|(\frac{n_o}{\cos\theta'} + \frac{n_e(\theta'')}{\cos\theta''})[0]$ and $\eta = L|k|(\frac{n_o}{\cos\theta'} + \frac{n_e(\theta'')}{\cos\theta''})^{(1)}[0]$ as per our definition in equation 1.33. The $[0]$ is to imply that since θ' and θ'' are functions of θ and here we set $\theta = 0$. Now, for $\theta'(\theta) = \arcsin\left(\frac{\theta}{n_o}\right)$ since the H-polarization component is the original relation from Snells law. The other component is not quite a straight forward calculation unfortunately. However, it turns out that since the incoming angles are small due to the paraxial approximation, the angles interior to the material (derived from $\theta = n_e(\theta'')\sin\theta'' = \frac{\sin(\theta'')}{\sqrt{\frac{\cos^2(\theta''+\theta_{opt})}{n_o^2} + \frac{\sin^2(\theta''+\theta_{opt})}{n_e^2}}}$ where θ_{opt} is the angle of the optical axis in the material) are also small and is linear by use of numerical methods. Using the interpolated line as the function for $\theta''(\theta)$ is well defined and can be used for the calculation. Thus, we have all required definitions to find the numerical values for the interaction parameter, η, as well as the offset, γ. In our case, using the numbers of our experimental setup and calcite crystal $L = .5mm$, $|k| = \frac{2\pi}{808*10^{-9}}\frac{1}{m}$, $\theta_{opt} = \frac{\pi}{4}$, $n_o = 1.6486$, and $n_e = 1.4818$ which leaves with the solution of $\eta = -413.17$. As will be noted later, by slightly decreasing the angle and increasing the length slightly to in the interval of $.503mm$ to $.507mm$, there are solutions for $\eta = 419.555$ which means nothing at the moment, but will become important as it matches the measured value of our interaction parameter in our experiment.

Chapter 2

Experiment

2.1 Theory

In this section, the theory of the specific parts of the experiment will be described. Specifically, it will go through the intricacies of how the experiment works. The first subsection details how the quantum potential is calculated from the trajectories them selves. The last subsection, details how to then create fake propagation using a lens system and how the lens system should work.

2.1.1 The Quantum Potential

Before the process of taking data, it is good practice to simulate the measurements that will take place. We first assume that we have two Gaussian beams flowing down a table, but with no lens system. In this case, to find the trajectories of the photons, we first need to find the Bohmian velocity as a function of distance and transverse position. To do this, we remember that the Bohmian velocity is given by ∇S where $S(x_i, t)$ is the phase function of the wave function $\psi = R(x_i, t)e^{\frac{i}{\hbar}S(x_i,t)}$. In this case, by naively taking the momentum operator to the wave function, we see that

$$\begin{aligned}\hat{p_x}\psi &= -i\hbar\frac{\partial}{\partial x}R(x_i,t)e^{\frac{i}{\hbar}S(x_i,t)} \\ &= -i\hbar\frac{\partial R(x_i,t)}{\partial x}e^{\frac{i}{\hbar}S(x_i,t)} + R(x_i,t)e^{\frac{i}{\hbar}S(x_i,t)}\frac{\partial S(x_i,t)}{\partial x} \\ &= -i\hbar\frac{\partial R(x_i,t)}{\partial x}e^{\frac{i}{\hbar}S(x_i,t)} + \psi\frac{\partial S(x_i,t)}{\partial x}\end{aligned}$$

and, hence

$$\begin{aligned}Re(\frac{\hat{p_x}\psi}{\psi}) &= Re(\frac{-i\hbar}{\psi}\frac{\partial R(x_i,t)}{\partial x}e^{\frac{i}{\hbar}S(x_i,t)} + \frac{\partial S(x_i,t)}{\partial x}) \\ &= Re(\frac{-i\hbar}{R(x_i,t)}\frac{\partial R(x_i,t)}{\partial x} + \frac{\partial S(x_i,t)}{\partial x}) \\ &= \frac{\partial S(x_i,t)}{\partial x} \qquad (2.1)\end{aligned}$$

(2.2)

which follows because $S(x_i,t)$ and $R(x_i,t)$ are defined as a real-valued functions.

This can be used to find the momentum of the particles and, since they are photons, the velocity in a specific direction can be found by dividing by the effective mass. Thus, the velocity of the photons can be found given that we have the initial state of the system for every point in the transverse and flow directions. Now, there are two transverse parts to the beam in our physical system, which we will label the one parallel to the table as x and the one perpendicular, y. In this experiment, the weak measurement couples only one of the directions of the field, in our case the x-direction, projecting only on the x component on the velocity field. In this case, the optic axis is in the x-z plane and we integrate over the y-direction at the end of the experiment to remove this dependence from the system. Thus, the system is now a function over the coordinate double (x,z). In section 1.2.4, we covered that the direction of propagation and time were related. This relation is between our physical system and the system where we can talk about Bohmian mechanics. Thus, our pair in the Sch$\acute{}$odinger space must be (x,t). This is the appropriate space to do all of our trajectory related related work. The majority of results will not be talked about in the analogous space, but in the measurement space instead. We chose to use the z-coordinate in this case since: a) the Gaussian beam is typically written in this way already and b) the experiment will be labeled in the same way so it will keep the presentation easier to understand. Thus, we only have a single direction for the velocity

to go, the x-direction, as the derivative with respect to z is now the same as the temporal derivative and more correctly labeled an energy. So, everything in the simulation will be labeled by the coordinate pair (x, z).

The state can be thought of as a pair of Gaussian beams propagating in the z-direction and having extent in the x-direction. The Gaussian beam is given by the formula

$$E(x,z,w,\lambda,E_o) = \frac{E_o}{\sqrt{1+\frac{z^2\lambda^2}{\pi^2 w^4}}} e^{\frac{-x^2}{w^2(1+\frac{z^2\lambda^2}{\pi^2 w^4})}} e^{\frac{-i2\pi z}{\lambda} - \frac{i\pi x^2}{z\lambda(1+\frac{\pi^2 w^4}{z^2\lambda^2})} + i\arctan(\frac{z\lambda}{\pi w^2})} \tag{2.3}$$

which has the interesting property of having a linear Bohmian-velocity profile. To see this, we recognize that the only part of the phase that is imaginary and contains a term that depends on x is $-\frac{i\pi x^2}{z\lambda(1+\frac{\pi^2 w^4}{z^2\lambda^2})}$. Taking the x-derivative and multiplying by the prefactors of this term should then yield the weak velocity which is clearly linear in x and the velocity is 0 when $x = 0$ (which is the center of the Gaussian). Note: for $z = 0$, the velocity is identically 0 since at the waist, the beam has no phase. The slope will be positive as a function of time and the beam will diverge in the x-direction, but the point in the center will always stay still. Thus, the points where $x < 0$ must travel in the $-x$ direction and those points in the opposite side of $x = 0$ must have positive velocities to satisfy the intuitive picture. The case, for two Gaussians is similar, but care must be taken. Supposing the Gaussians are the same distance, a, from $x = 0$ and that the waist of the beams are small enough that each beam is distinct (i.e. the overlap of the beams is small), then the state is given by $\frac{1}{\sqrt{2}}(E(x-a,z,w,\lambda,E_o) + E(x+a,z,w,\lambda,E_o)$. Since the overlap is small a crude approximation can be used so where the same function can be thought of before as $-\frac{i\pi(x-a)^2}{z\lambda(1+\frac{\pi^2 w^4}{z^2\lambda^2})}$ over the region near $x = a$ and $-\frac{i\pi(x+a)^2}{z\lambda(1+\frac{\pi^2 w^4}{z^2\lambda^2})}$ over the region near $x = -a$. In this way, using the same methodology of taking the derivative of this phase term yields two linear functions which are both zero at their respective peaks (for $z > 0$, but small enough that the beams have not overlapped). However, as x gets closer to 0, the only way to know the value of the Bohmian velocity is to actually calculate the velocity. It is intuitive that the velocity should be 0 at 0, however, because the function that we have described is continuous and the respective wave function is complex, but never 0. Thus, by the intermediate value theorem and that points to the right of $x = -a$ and points to the left of $x = a$ have velocities that are positive and negative respectfully, the velocity must attain 0 at $x = 0$.

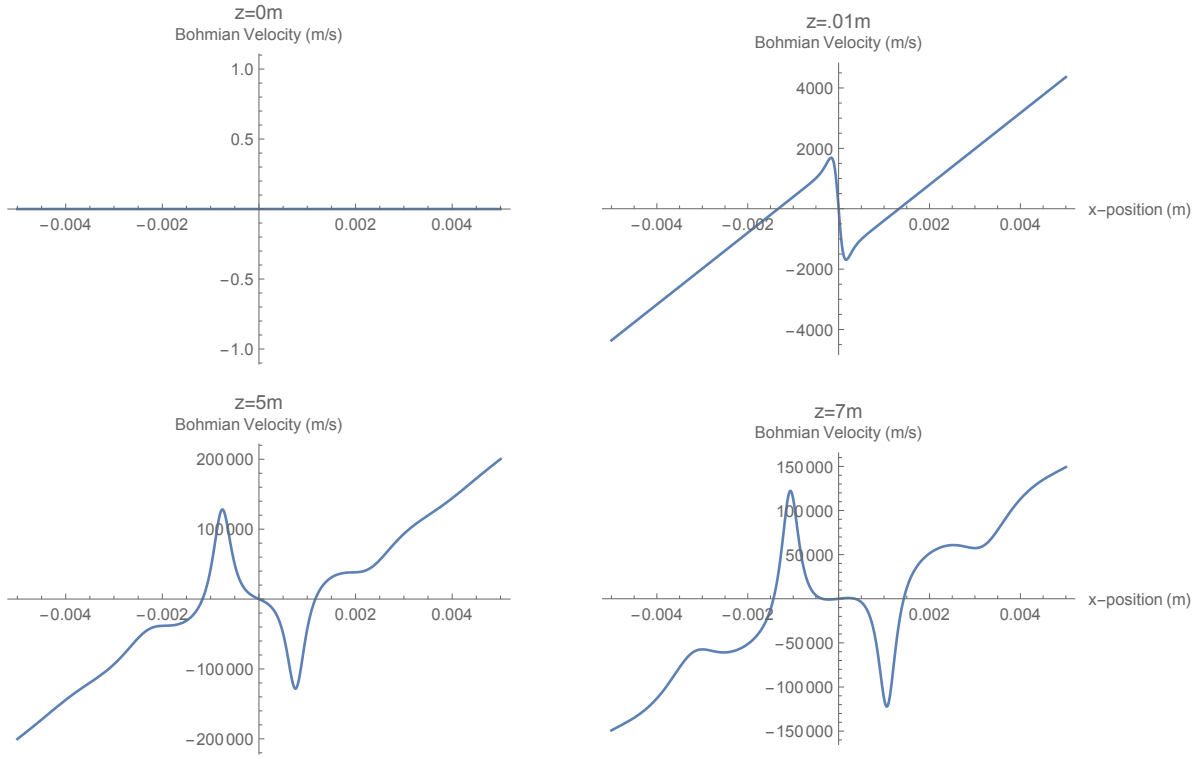

Figure 2.1: The calculated weak velocity for various z-planes

It should be noted that the weak velocity is found from equally spaced x starting points, rather than the equally probable trajectories used below. These velocity curves are calculated using two Guassians each centered at $\pm 1.33mm$ and a waist of $0.64mm$ as well as equation 2.1.

Knowing the velocity field at all points allows the trajectories to be calculated by taking an initial seed point and then applying equation 1.7. This formula gives the new approximate x-position of the particle in question at the new z-position. In the limit of $z_{new} - z_{old} \to 0$, the path of the trajectory should be exactly that of a particle as given by de Broglie or Bohm (this is easy to show in de Broglie's case since it was the velocity that was fundamental and not the quantum potential; thus, the particle's path must be exactly given by the infinite sum described here and since Bohm's trajectories agree with de Broglie's; we are done). The trajectories are shown in figure 2.2.

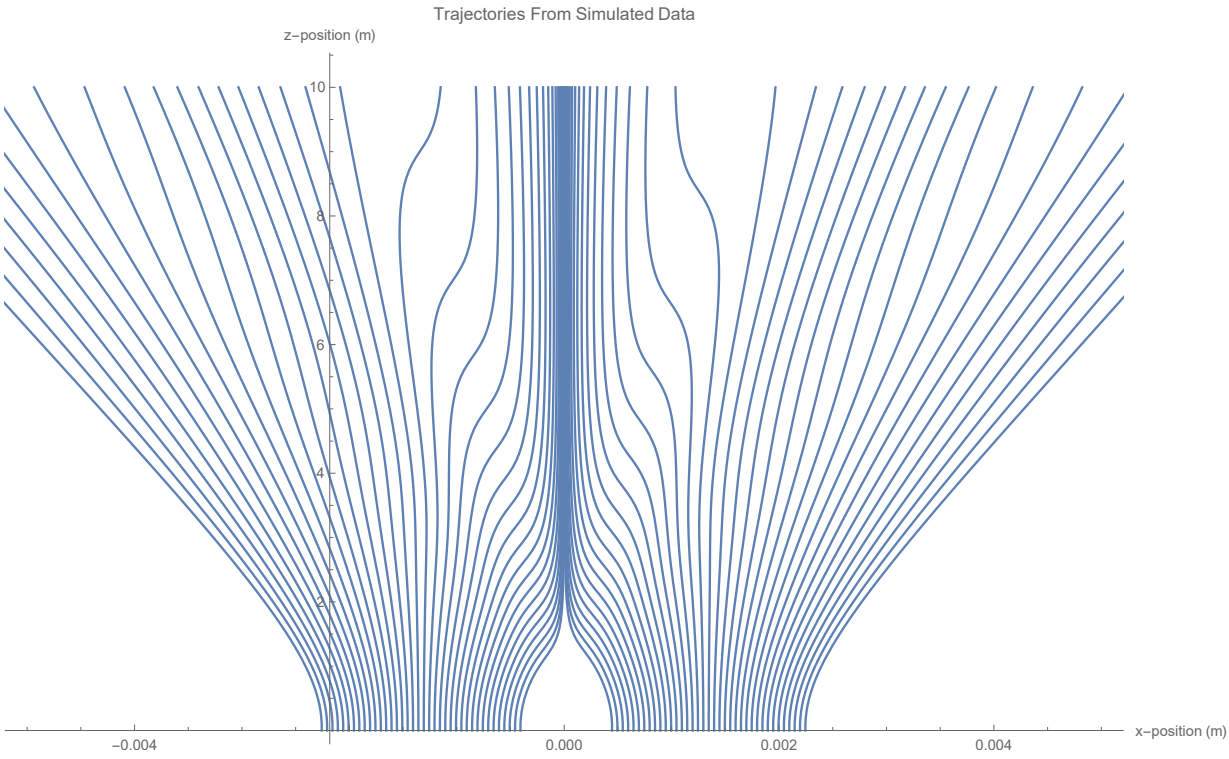

Figure 2.2: The simulated trajectories

It should be noted that these trajectories are found from equally spaced x starting points, rather than the equally probable trajectories.

The trajectories are found using an even distribution of the particles; however, we must be careful. By definition, the state must start in quantum equilibrium meaning that the state of the system had to have started so that the initial probability distribution is the same if one were to calculate from the trajectories. Now, in principle it is possible to start with any initial state as long as you count the probability of the system to be carried by the single particle moving on the trajectory as a separate value. The probability is the usual one where

$$P = \int_a^b \psi^\star \psi dx \tag{2.4}$$

and the limits of integration (a and b) are given by the mid points between the previous/the next particle and the current particle under test (assuming the seeds were chosen with the

typical ordering on $\mathbf{R}$). Assuming that the probability is then kept constant (which is a good approximation because of the probability conservation equation (1.2), we can find the new probability density for that particle after it has undergone its motion, by again finding the midpoints to its partners on either side and dividing the probability by the length of that new interval. It is this that brings up a good point; in the experiment, the camera is not infinitely sensitive and has to deal with outside sources. Thus, there will exist points where the image is washed out by noise or the camera cannot resolve the signal. Since this is the case, we can truly define the beams as separate until the beams start interacting on the camera. So, when we seed the initial starting points of the trajectories, there is no point in seeding a place which will have just contributions from the noise. Thus, the points to start the trajectories must also have a large enough contribution in probability density, that they would make a contribution to the image being seen by the camera. This leaves us with the two plots below:

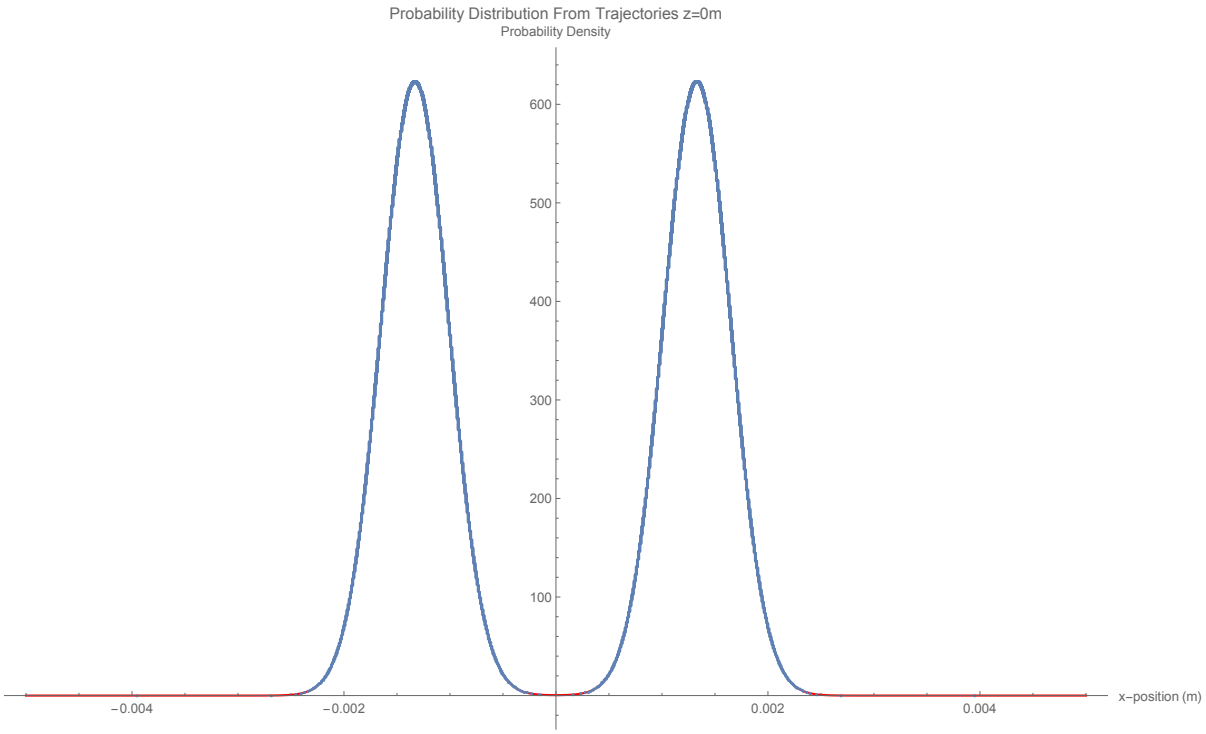

Figure 2.3: Probability Density Comparison at $z = 0$

The probability density distribution found at $z = 0$ where the red line is the normalized distribution from the two Gaussians, and where the blue points are the probability densities for each trajectory.

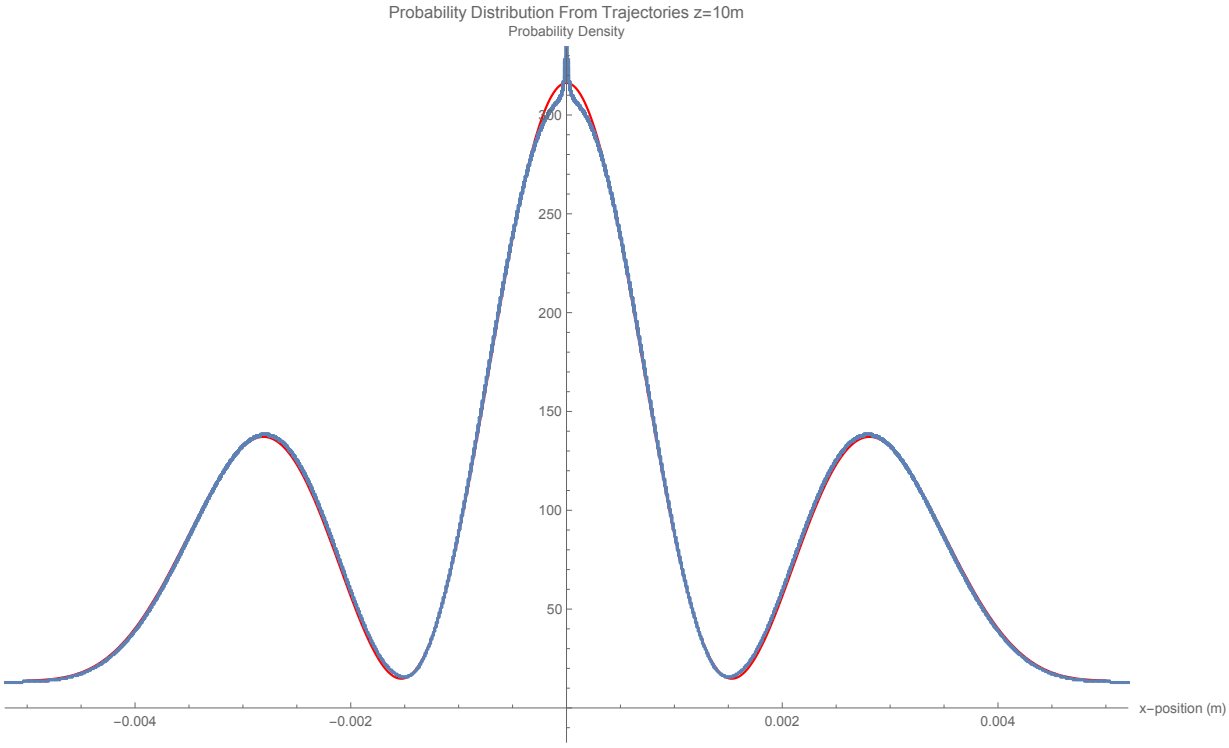

Figure 2.4: The simulated probability density at $z = 10$

The probability density distribution found at $z = 10$ where the red line is the normalized distribution from the two Gaussians, and where the blue points are the probability densities for each trajectory. Note: it is not a perfect comparison. This is from the approximation of how we defined probability in this case as well as that we only have finitely many points and z-slices taken to build up the trajectories.

in this case, the points were selected to have the same probability of 0.0001. Which shows that the trajectories are the correct trajectories as we have fairly good matches to the probability density distribution as expected. For the remaining graphics, the point distribution was taken to be equally spaced points on the x-axis. Since the trajectories above show that the probability distribution is available to be taken, then any other selection of points will work as long as the probability of each trajectory is kept track of as a separate property of each particle that exists.

The quantum potential can then be calculated (see Figure 2.5), by taking the velocity at each point along the trajectory, fitting to it a spline and taking the time derivative of that

spline at each of the projected points. However, all of the trajectories have been plotted as functions of x and z. We have to remind ourselves that we measure in the z dimension. This is in the physical space, but in our analogy, our true photon trajectories are functions of time. The solution to this issue is to remember that the z and t are related. This regains the quantum force for each points along the trajectory. By then fitting the quantum force at a common z-positions with a spline and integrating from 0 to the point one would like to probe yields the quantum potential up to a constant that depends on time or in our physical space, the z-direction. In this case, the error increase typically found by taking the derivative or integral is lessened; however, in the future a better technique may be found to reduce this error. It should be noted that in this case, there is an added difficulty. Since the quantum force is defined as a conservative field by the very definition of the existence of the quantum potential. This means that it is not good enough to integrate only along the x-direction alone as this does not give information about how to stitch the planes at different z-slices of the inferred quantum potential together again. See, Figures 2.5 and 2.6 for a comparison of the quantum potential found from the simulation and from its definition.

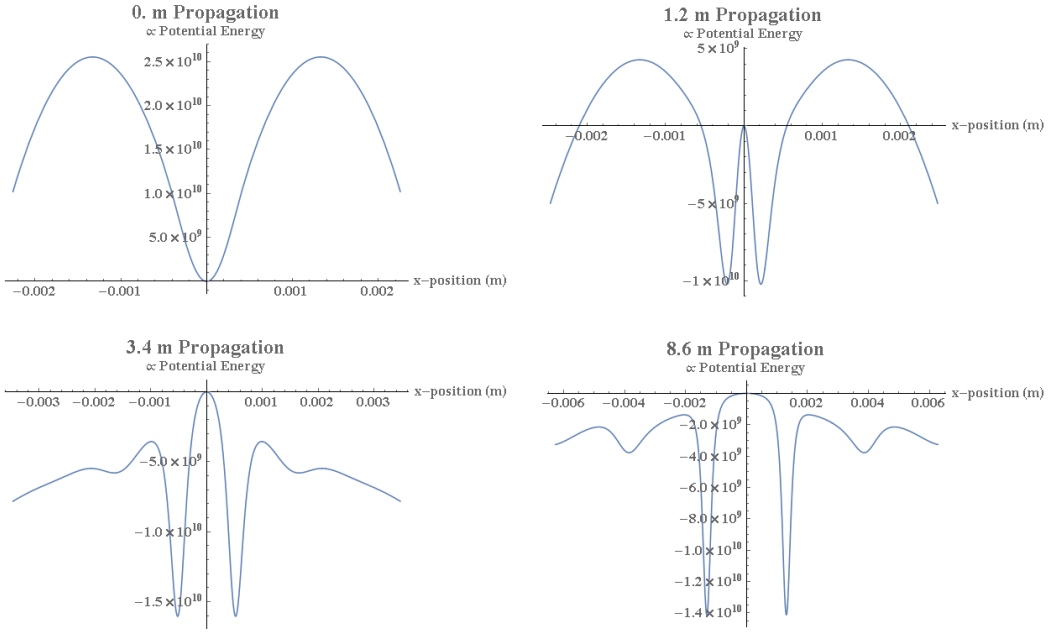

Figure 2.5: The quantum potential: from the simulated trajectories

The quantum potential at various z planes. They are built from approximately 37000 trajectories and distance skips of 0.1m in the $\hat{z}$-direction.

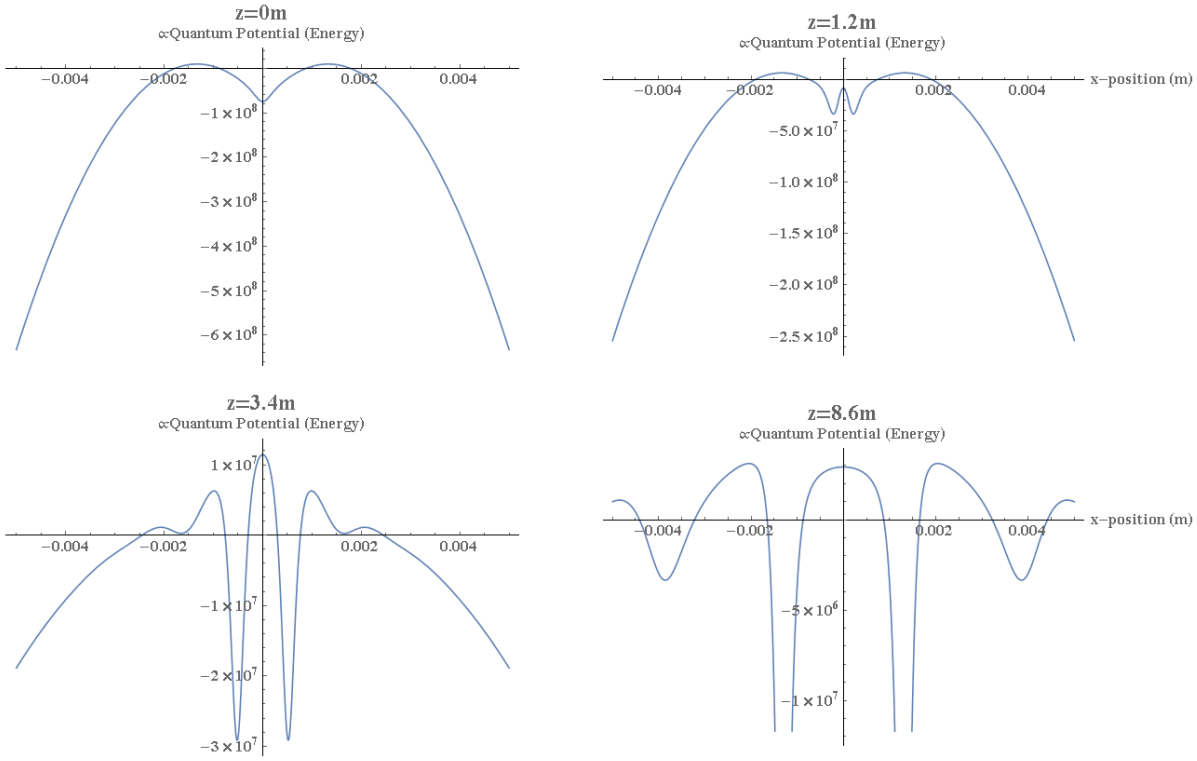

Figure 2.6: The quantum potential

The quantum potential as expected in the experiment given the relevant parameters in the experiment. This was calculated using the relation $Q \propto \frac{\nabla^2 R}{R}$.

In this way, one would naively apply the classical algorithm:

1. Integrate the force in direction one to get a potential that is off by some constant depending on direction two
2. Taking the derivative in direction two and comparing this with the force in direction two yields the derivative of the constant function with respect to direction two
3. Finally integrating this constant function with respect to direction two and adding it to the integration of the force, we find the potential

Realizing that we have already integrated the force for our inference, we now need to find the constant of integration for the z direction (i.e. the force on the particle in the z-direction) and compare that with $-\frac{\partial Q_x}{\partial z}$ where Q_x is the quantum potential that is inferred

from integrating in the x-direction– for some strip given at a single x-coordinate (perhaps repeating the process for a few x-positions in order to make sure the answer is roughly independent of x). This will find the derivative of the constant that varies in the z-direction. Then taking that function, integrating it with respect to z and and adding it to our inferred version (Q_x), will yield the quantum potential (at least up to a global constant). Unfortunately, this does not work. The main issue with that entire description is that the z-direction is not a spatial direction, rather it is one of time in the Schrödinger system where our Bohmian particles lie. In this case, a new approach would have to be taken to account for this discrepancy. One possible approach follows below:

1. First, start by realizing that $\frac{\partial}{\partial z} = \frac{\partial}{\partial (ct)} = \frac{1}{c}\frac{\partial}{\partial t}$.
2. Next, notice that since there are only two directions, that $c^2 = v_x^2 + v_z^2 \rightarrow v_z = \sqrt{c^2 - v_x^2}$.
3. Realizing that if we were to keep with the analogy, $v_z = \frac{\partial S}{\partial z} = \frac{1}{c}\frac{\partial S}{\partial t} \rightarrow \frac{\partial S}{\partial t} = cv_z$.
4. Finally, by taking 1.1, plugging in the values of the calculated $\frac{\partial S}{\partial t}$, $\frac{(\nabla S)^2}{2m}$, and the found quantum potential, we should be able to back out the time dependent constant that will allow us to stitch together the different z-slices. Written out, $-\frac{\partial S(x,t)}{\partial t} = Q_x(x,t) + C(t) + \frac{1}{2m}\left[\frac{\partial S(x,t)}{\partial x}\right]^2$, where $Q_x(x,t)$ is the quantum potential at a specific z-plane and $C(t)$ is the constant function that we are trying to solve for.

While, the plot has the same shape (see Figures 2.7 and 2.8), there are some features that the plot is also missing. This could be related to the fact that we have taken a square root, or perhaps something more esoteric. In any case, at this point we will have to console ourselves with only being able to solve for the Bohmian quantum potential without this constant of integration in the z-direction. Something to note that is not evident from this analysis is that the system must be fed with many, many individual starting points. These points can be chosen in any fashion; however, if the particles are not started with the quantum equilibrium condition in mind, then we must note that the density of trajectories will not give the correct probability density.

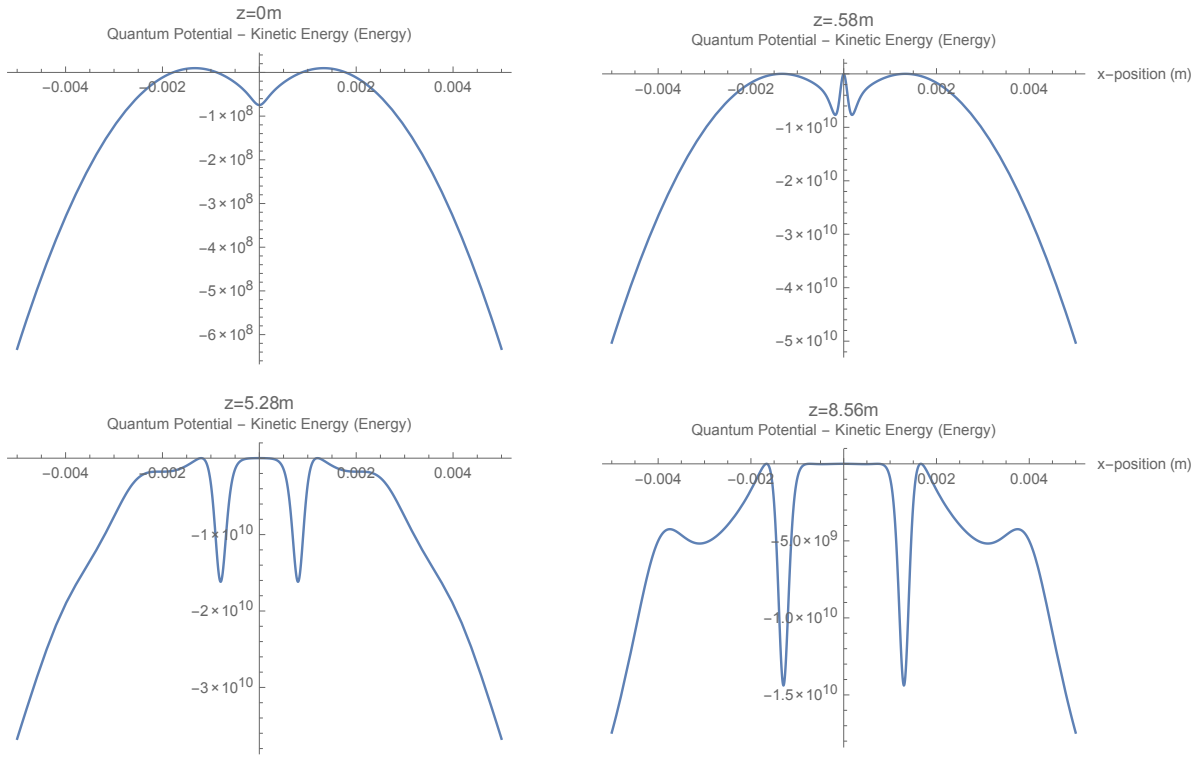

Figure 2.7: Simulating $\frac{\partial S}{\partial t}$ from the quantum potential (found from $Q \propto \frac{\nabla^2 R}{R}$) minus the kinetic energy.

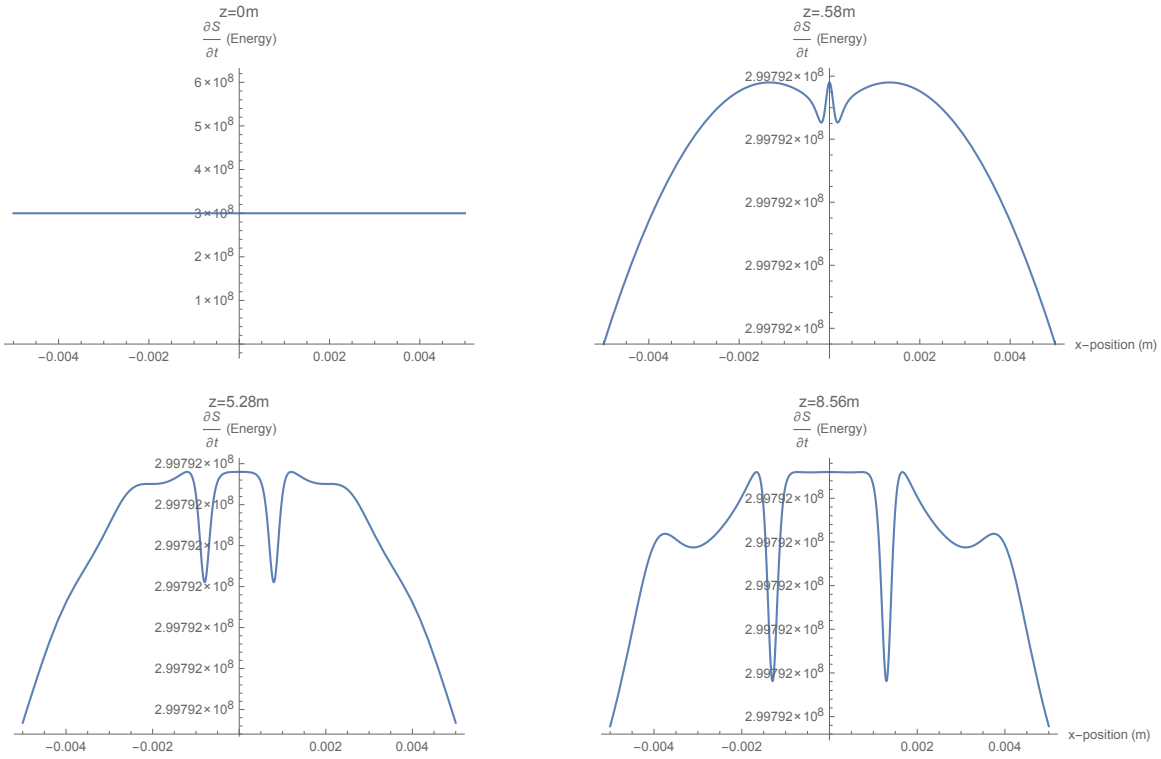

Figure 2.8: $\frac{\partial S}{\partial t}$ as evaluated from the simulated weak velocity curves.

There are some requirements that are necessary for the quantum potential to be numerically stable. It is absolutely necessary to make as many z-position points as it allows for smoother trajectories and increases the numerical stability of quantum forces and thus the potential along with it. This is especially true for interference patterns with more fringes. Intuitively, it should make sense that there would be a greater quantum force in the wells of the quantum potential as the particles are being forced into the smaller area of the fringes in a smaller amount of time. Which means, that the particles will spend less time in the wells and, thus, need more time precision in order to fully see these trajectories. Secondly, there was a minimum number of seed points that were necessary in order to reconstruct the potential. The reasoning behind this fact is that there are now more points of the distribution being sampled which will induce larger numerical stability during the process of finding the potential and they are important to making sure that the features in the potential are well represented. It should be noted that there is a minimum for which the amount of return decreases for the number of points included. For the plots shown here,

the number of initial seed points needed to be roughly 15000 to make up each beam, with a sampling of $0.1m$ of the propagation distance seems to reproduce the majority of the quantum potential.

2.1.2 The Lens System

In order for a double slit to work in this case, there are two options: move the camera back $10m$ and allow the beams to interfere "naturally" or move to a linear optical system so that it artificially creates the distance the beam needs to move down the table. The second choice was preferable in this case. The requirements for this system would be that the beams should "move" in some way together and that their waist at the same point should also change in some way (either decrease or increase). One such system that we could use consists of two overlapping telescopes [19, 21, 31] as shown in the figure 2.9.

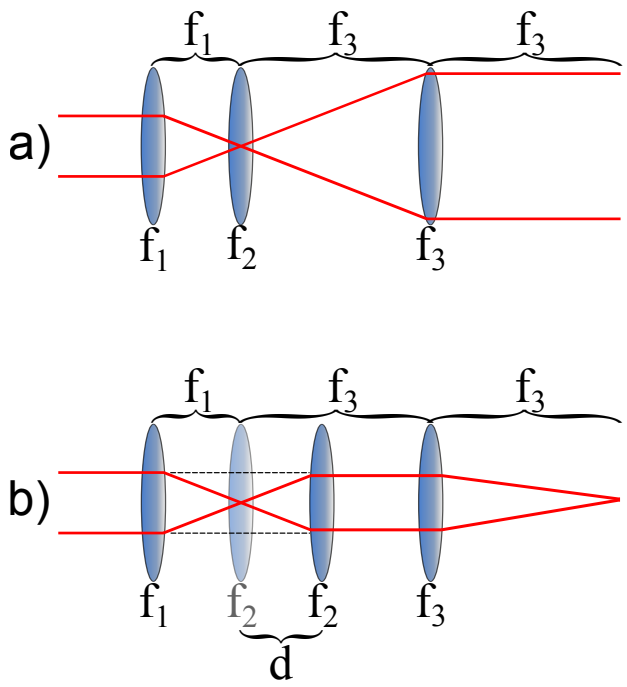

Figure 2.9: A diagram of the lens system at the first and last lens positions

A break down of the suggested lens system to the two extreme cases where a) shows the middle lens at the focal point of f_1 so that f_1 and f_3 make a telescope, and b) shows the middle lens at its furthest position where it has moved a distance f_2 closer to f_3 in order to make a new telescope between f_1 and f_2 and the two separated beams end up overlapping at the focal point of f_3.

As can be seen, the beams start apart and then move together as the second lens is moved forward. The next question is how will the beam shapes change as a function of the lens position? In this case, it is easier to think about a single beam at the center of the lenses. There are two distinct lens systems. One with a telescope made with the two exterior lenses (see Figure 2.9.a) and the other where the first two lenses make a telescope and the last lens serves to focus the beam (see Figure 2.9.b). Assuming perfect alignment, we expect that the first case should have an effective magnification of $|M| = |\frac{f_3}{f_1}|$ and the second case should have an effective magnification of $|M| = |\frac{f_2}{f_1}|$ (which comes out colinear due to the fact that the lens system makes a Galilean telescope) and into the last lens, f_3, to be focused down at its focal length. Thus, the beam should be smaller than in the first case; in other words, solving the second requirement. Unfortunately, this simple

physical picture does not allow for a full understanding of the magnification as a function of position. Now that we know that the system does its job, we can focus on actually understanding this system in a more fundamental level, with the main goal of finding the effective distance the beam would have traveled.

The intuition is a little easier to explain before we fully go through the final solution. As explained above, there is at least a system where the beams come together and if a beam were placed in the center, its waist would decrease (though we do not necessarily know if either of these are linear phenomena). The question is how should the "effective" distance the beam has traveled be determined? It is well known that the Gaussian beams' waist diverge as $w(z) = w_0\sqrt{1 + (\frac{z}{z_R})^2}$. Given this, there is a measure of the distance the beam has traveled by determining the beam size at different imaging planes. But, how does one then define magnification of the lens system? The magnification of an unknown lens system can be found by placing some object and shining a light on that object; by dividing the length of the shadow that the object casts after the lens system and before, this is the magnification. However, how does one think about it for laser beams? In this case, usually taking waist of a beam (or the beam diameters) measurement counts as such an object (shadow or not) as it would be a measure of an object from the center of the lens and just like the shadow it will measure the apparent increase (or decrease) in it yielding the absolute value of the magnification. Formulating this idea, the magnification of the beam should be given by $\frac{w_f}{w_i}$. While this is easy to see and is probably known by most in the experimental optics community, there is an inherent problem in this definition. It becomes circular when we try to use this to solve for the effective distance the beam has propagated. For example, let's take w_f to be the beam waist found after the lens system at a configuration defined by the parameter d, which controls in some way the magnification of the system (i.e. $w_f(d)$). However, it is not possible to strictly compare $w_f(d)$ with the original beam propagation as they, by definition, need to operate in the same manner. To alleviate this problem, take the final configuration and try to map it back to the original beam by dividing by the magnification ($\frac{w_{after}(d)}{M}$). Using the definition of the magnification, the beam waist to compare to is given by $\frac{w_{after}(d)\times w_i}{w_f}$, but the w_f in this case is given by the observable of $w_{after}(d)$. Thus, find $w_i = w_i$, which doesn't answer the question of how the parameter in the lens system relates to the propagation distance since no matter which position is used it would result in always returning the initial beam waist. This implies that for every choice of d, the distance would be identically "z." Rather, there needs to be some independent way of defining the magnification. The two beams which should be propagating parallel together to make the double slit will be able to fill this role. Effectively, the distance between these two beams should then give an independent measure (from the beam waist) of the magnification so that the notion of the dependence

of the parameter, d, does not get removed from the measurement. Therefore, to sum up, we want the magnification to be defined as $|M(d)| = |\frac{D_{after}(d)}{D_{before}}|$, where D is the distance between the two beams. Now, note that the magnification still depends on d, which is fine as the only problem was that the previous definition was circular. Now, we have the final definition of how to find the effective distance as a function of the lens system parameter, d. Thus, we have the final set of equations:

$$w_{free} = \frac{w_{after}(d)}{|M(d)|}$$
$$w_o\sqrt{1 + (\frac{z_{eff}\lambda}{\pi w_o^2})^2} = \frac{w_{after}(d)}{|M(d)|}$$

Where, w_{free} is the waist of a freely expanding beam, w_o and λ is the original waist and wavelength of that freely expanding beam, and z_{eff} is the effective travel distance of that beam. And, thus

$$z_{eff} = \sqrt{\frac{\pi((\frac{w_{after}(d)}{|M(d)|})^2 - w_o^2)}{\lambda}}. \tag{2.5}$$

Now that there is a clear understanding of what we need in order to get the effective distance traveled, we should try to model what we expect the magnification of the lens system to be like. To do this, we utilize ***ABCD*** matrices where lenses are functions of the focal length –L(f),– and free space propagation is a function of distance –FS(s). In this case, the lens system as defined above can be modeled as:

$$\begin{aligned} N &= FS(f_3)L(f_3)FS(f_3 - d)L(f_2)FS(f_1 + d)L(f_1) \\ &= \begin{pmatrix} 1 & f_3 \\ 0 & 1 \end{pmatrix} \begin{pmatrix} 1 & 0 \\ -\frac{1}{f_3} & 1 \end{pmatrix} \begin{pmatrix} 1 & f_3 - d \\ 0 & 1 \end{pmatrix} \begin{pmatrix} 1 & 0 \\ -\frac{1}{f_2} & 1 \end{pmatrix} \begin{pmatrix} 1 & f_1 + d \\ 0 & 1 \end{pmatrix} \begin{pmatrix} 1 & 0 \\ -\frac{1}{f_1} & 1 \end{pmatrix} \\ &= \begin{pmatrix} \frac{(d-f_2)f_3}{f_1 f_2} & \frac{-f_1(d+f_1-f_2)f_3}{f_1 f_2} \\ \frac{d^2}{f_1 f_2 f_3} & \frac{-f_1(d(d+f_1)+f_1 f_2)}{f_1 f_2 f_3} \end{pmatrix} \end{aligned}$$

where we note the parameter, d, is the parameter that controls the magnification of the system and takes values from 0 through f_2. Since, we defined above that the magnification would come from distance between each of the beams and we can assume that the beams are parallel to each other and meeting the lens symmetrically about the center of the lens, we can find the amount that the beams diverge from the center after passing the lens

system by letting the beam be assigned to the ray with no angle ($\theta = 0$) and at some distance from the center ω. Thus,

$$\omega_{new} = N \begin{pmatrix} \omega \\ 0 \end{pmatrix} = \begin{pmatrix} \frac{(d-f_2)f_3\omega}{f_1 f_2} \\ \frac{d^2\omega}{f_1 f_2 f_3} \end{pmatrix}$$

Since the first element of the vector is defined to be the distance to the center, the magnification of the lens system is found by dividing by the original distance to the center of that given ray. Therefore, the magnification is given by

$$|M| = |\frac{(d - f_2)f_3}{f_1 f_2}| \tag{2.6}$$

The absolute values are included because at the end of the day, it does not matter if the beams invert since ideally the beams would be identical; however, only the distance between them matters. Now that the magnification of the system is quantified, the effective distance that the beams have "traveled" due to the lens system given that the beam waist is sampled for enough distances.

2.2 Experiment

In this section, we will take an extended look into how to build the experiment. This experiment can be broken into five separate parts: the source, Bob's tomography section, the setup of the double slits, the weak measurement, the lens system and strong measurement, and the single photon camera.

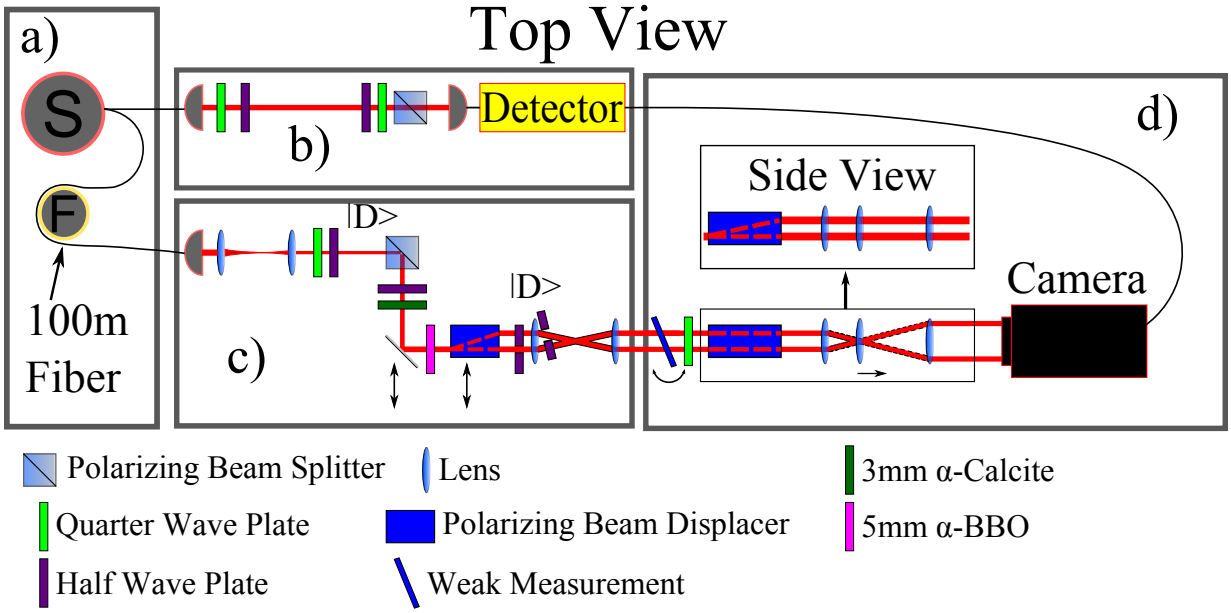

Figure 2.10: System diagram

A break down of the experiment. In section a) we have our source that sends out two photons (polarization entanglement is possible). Section b) contains a polarization tomography station for Bob's photon. c) contains the setup for creating the double slits, polarization and timing compensation, and beam compensation. d) contains the weak measurement crystal, strong measurement and the single photon camera who heralds off of a measurement of a photon from the tomography station.

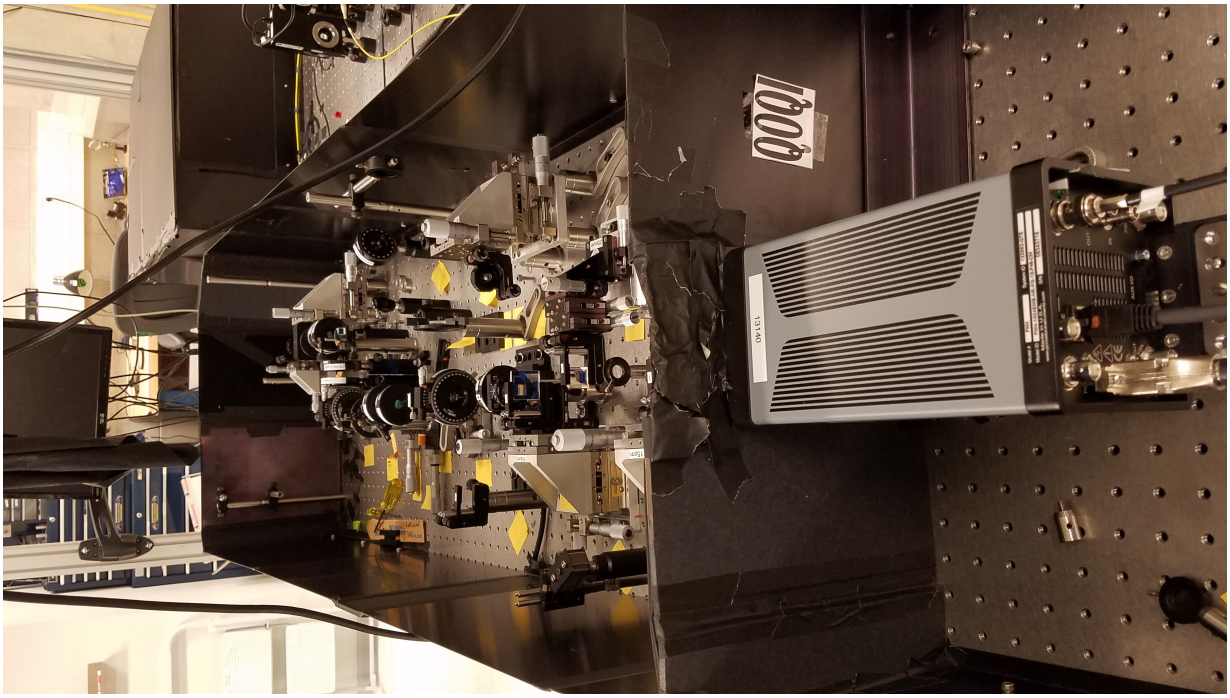

Figure 2.11: An angled top view of the experimental sections c) and d) found in Figure 2.10

2.2.1 The Source

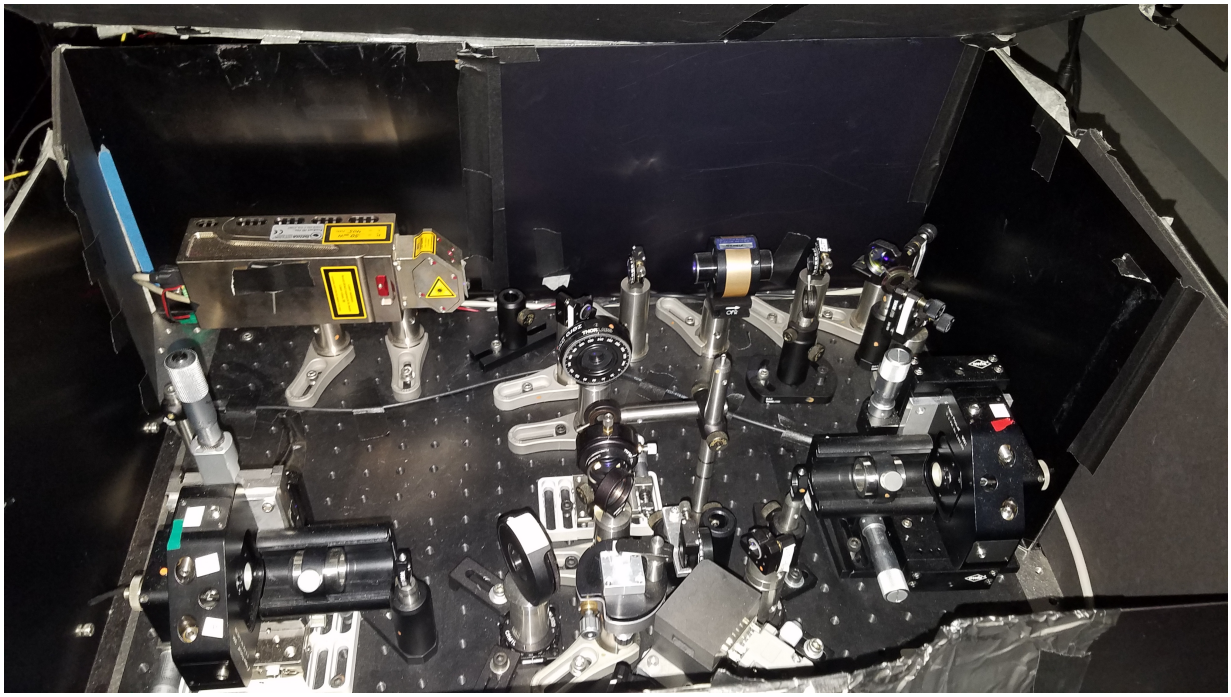

Figure 2.12: A picture of the entanglement generating SPDC source used in section a) of Figure 2.10

The source chosen for this experiment was a Sagnac polarization source [28]. Using a continuous wave laser, single photons are created going through a crystal of periodically polled Potassium Titanyl Phosphate (PPKTP). In this case, the source is a type two spontaneous parametric down-conversion (SPDC) process, where the final states of the photons leaving are phase matched to have the same momentum, but opposite polarization and having the same frequency (remember, energy conservation makes $\omega = \omega_i + \omega_s$ and in this case $\omega_i = \omega_f$). In this case, an 405nm continuous wave laser set to enter the PPKTP crystal with polarization in the $|H\rangle$ direction, would go through the crystal and become two photons: one of polarization $|V\rangle$ and the other of polarization $|H\rangle$; and each of the photons will leave with a wavelength of 810nm as well as the same momentum. However, the source does not necessarily produce only two photons at a time. Due to the fact that it is related to the displacement field within the crystal and that displacement field is really given as an infinite sum of the electric field tensor. Typically, the constants (given as χ^i) are related to

the probability of the number of photons occurring orders happening. The source is then tuned to make sure that the photons are given in the bell state $|HH\rangle + |VV\rangle$. Each of these photons are then coupled into separate single mode fibers and sent to either Alice's side with the double slit or to Bob's side with tomography. Furthermore, we produce a the Bell state $|H\rangle|H\rangle + |V\rangle|V\rangle$ with about 100,000 coincidences a second as well as a CHSH inequality violation of 2.57 ± 0.017. Hence, we know that we have two entangled photons and that the photons are in the state that we want. See Figure 2.12 for a picture of the source.

2.2.2 Bob's Tomography

From the source, Bob's photon emerges from the fiber via a fiber collimator only to immediately go through a quarter wave plate and a half wave plate tuned so that the polarization of the photon ensures that if $|H\rangle$ is sent through that $|H\rangle$ also emerges. The cause for the polarization shift is due to the stress acting on the single mode fiber. This stress (such as coiling the fiber) causes just enough of a change in the index of refraction in the fiber, that the polarization can rotate; however, we can always undo the rotation since it is a unitary assuming the fiber stays still. Next, the photon then goes through another set of quarter and half wave plates and finally through a polarizing beam splitter. The quarter and half waveplates allow for any polarization we want to be rotated to $|H\rangle$ and then selected. The reason for this is that polarizing beam splitters typically have higher efficiencies compared to their thin film brothers and sisters. Once the state has been selected, the photon will then be collected into a single mode fiber and be sent (assuming it made the previous selection) to be a herald for the camera. Refer to figure 2.10b.

2.2.3 The Double Slits

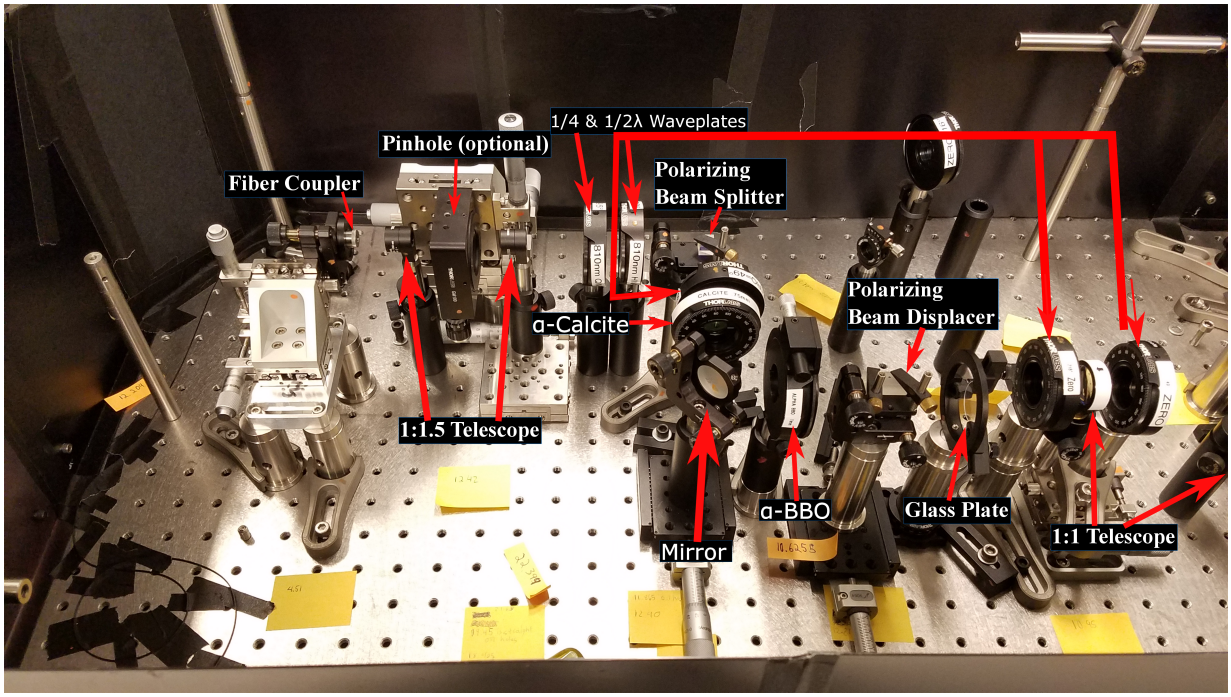

Figure 2.13: The Double Slit Apparatus shown in c) of Figure 2.10

The other photon then passes through a quarter and half waveplates (to compensate for any polarization drift through the fiber from the source to the collimator). The photon then hits two mirrors to change the direction and then hits a quarter wave plate to change the polarization of the photons to $|D\rangle$ or $|A\rangle$. The photon then goes through a long piece of calcite. This splits the photon into two beams. However, these beams are distinguishable by their polarization. To get rid of this problem, each beam passes through a half wave plate to switch the polarization to $|D\rangle$ in each beam. Thus, now two separate beams exist with a separation of $2.66mm$ and widths of $0.00064mm$. If these beams propagated forever, eventually, the beams would subsume each other and, if measured on a camera, then the image would have interference on it just like a double slit experiment. However, this is impractical as the length of the optical table would need to be 5-7 meters long with submillimeter precision on placing the camera. For a picture of this setup, refer to Figures 2.13 and 2.10c). Finally, the beams pass through a 1:1 telescope to reduce the amount of effective space the beams pass through. This is due to the fact that without it, the beams

were too large in diameter to get three fringes on the camera by the time they entered the telescope system.

2.2.4 The Weak Measurement

Given that each beam now has separate polarizations, one $|H\rangle$ and one $|V\rangle$, they must be switched to $|D\rangle$. To do this, two half wave plates (each with a hole in the center) in each are placed so that the hole of one wave plate is lined up with exactly one beam, but it will then pass through the other wave plate. This way, only one wave plate acts on a beam at a time. Hence, even though the beams are not the same polarization, they can be made to be. The next thing needed in the weak measurement is the weak measurement crystal. For this, we used a thin piece of calcite that was $0.5mm$ thick, an optical axis of $\frac{\pi}{4}$ and with an interaction parameter of $\eta = 419.6 \pm 0.9$ which is in correspondence to our theoretical value with some concessions to the length and optical axis angle. See Figures 2.10c) and 2.14 below.

2.2.5 The Lens System and the Strong Measurement

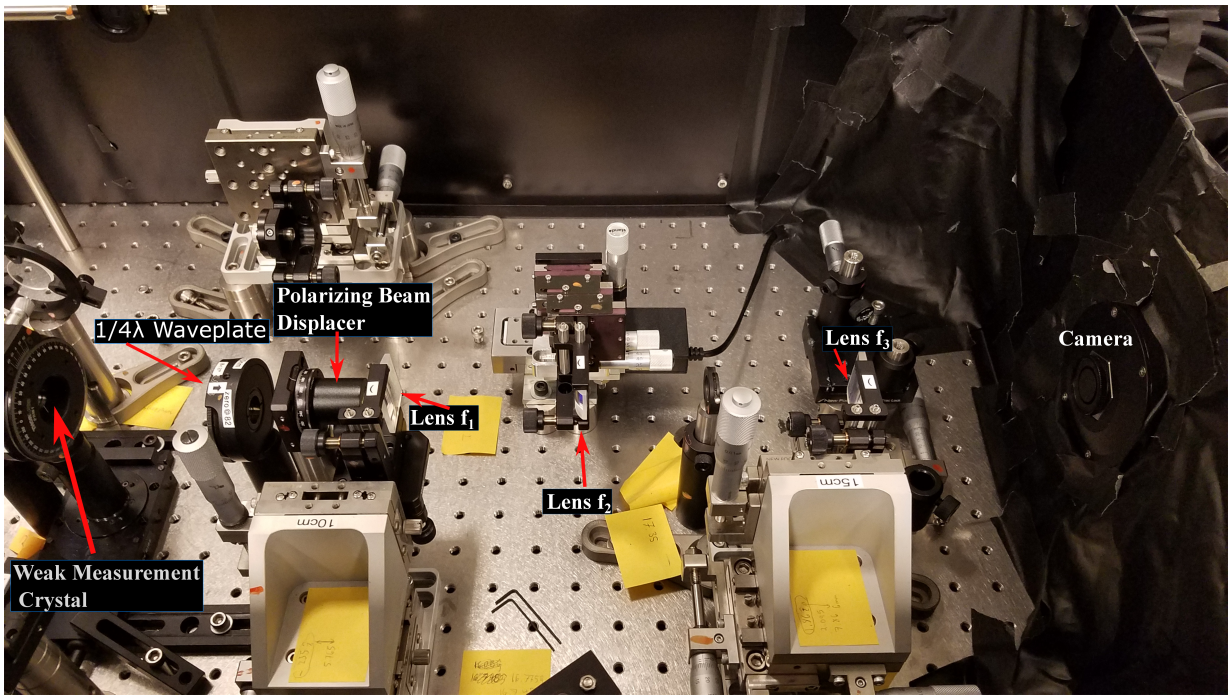

Figure 2.14: A picture of the weak measurement crystal followed by the strong measurement and lens system as drawn in Figure 2.10d)

Finally, the photon going through the double slit side of the measurement impinges upon a quarter waveplate and a long piece of calcite. In this case the quarter wave plate is set so the final polarization measurement (and also the strong measurement in this case) is for the $|L\rangle$ and $|R\rangle$ basis. In this case, the $|L\rangle$ polarized light beams are $3mm$ lower than the $|R\rangle$ beams and thus can be seen on the camera at the same time. The beams will then hit three cylindrical lenses, which are placed in succession, with focal lengths given respective of the order that the light hits them $f_1 = 10cm$, $f_2 = 2.5cm$ and $f_3 = 15cm$. The middle lens can travel by a motorized stage and it is what allows for the apparent change in the propagation distance to the camera. Once the photon has traversed through the polarization measurements and the lenses, the photon is then measured on the camera in coincidence with the herald photon from Bob's tomography side. This entire process is then repeated for numerous amounts of photons in order to obtain a spatial pattern and the image is finally read out. For reference please see Figures 2.10d and 2.14

2.2.6 Alignment

In this case, most of the alignment techniques needed to make this setup can be done with back reflections. However, there are a few parts that are a bit more nuanced. For example, aligning the source requires maximum overlap of the two separate paths. In this case, the secret to aligning the source is given in [28]. Another example is the lens system with the camera. This was, and probably is, the most difficult part of the entire project to align; so, understanding how to align it is extremely important. First, each lens was placed into their approximate distance down the table from the strong polarization measurement. In this case, we chose to make sure that the size of the 808nm diode laser was approximately 1mm in diameter. Then the most difficult part of the entire alignment (making sure that the second lens' travel is straight with respect to the table) needs to be done. Now, unfortunately due to the way the table is setup (in imperial units) and that the translation mount is in metric units; therefore, a converting piece is required. However, the converting piece has a significant amount of clearance around the screws causing the ability to attach the converting piece in a way so that the motorized translation stage moves only in the $\hat{z}$ direction is difficult. Therefore, a procedure is needed to make it move only in the $\hat{z}$ direction which includes:

1. Place two iris' on a straight line in the direction of $\hat{z}$
2. Using the $\hat{x}$ translation, center the beam on the lens (meaning put the laser beam through the two iris' and close the iris' to just see the beam)
3. Now that the beam is centered, use the translation in the $\hat{z}$ direction and move to the end of its motion and note which side of the hole the beam lands on (note always start from closest position to the source for every iteration):
    - If the beam stayed centered on both of the iris' then it is centered and done
    - Otherwise, the beam will have moved to one side of the hole in the iris or the other
4. Using the $\hat{x}$ translation move the beam to approximately the opposite side of the hole in the iris and translate the lens to the starting position
5. Undoing three of the screws of the converting piece, lightly tap the converting piece to move the light beam back to the center

6. If done correctly, as the lens travels forward again, the beam should be closer to the middle of the iris and repeat. If the beam appears on the other side of the iris, it has gone to far.

Now that the middle lens can be translated without fear of the beam wandering off axis, the lens system in total can be aligned, which is the second hardest alignment of the setup. The best way to align the system is to start with lens three (the lens closest to the camera) and the camera placement.

1. Back reflect the lens (which includes the centering the lens) using a single beam centered between the two beams that will be used there
2. Back reflect the camera using the same single beam making sure that the beam is visible on the camera
3. Note the location of the center of the single beam; this will be the center of the setup
4. Using two beams that are separated and parallel to each other and centered around the single beams above, move the camera along the $\hat{z}$ direction until the center of the each beam (using on camera software) is the same and equal to the center of the single beam (using the $\hat{x}$ translation on the first lens)

Now, placing lens one (the lens closest to the source) into the path, the alignment is given.

1. Using the single beam again (in the center) back reflect the lens
2. Then, adjust the $\hat{z}$ translation on lens one so that the two beams' expansion is given by the magnification equation $x' = \frac{f_3}{f_1}x$ where x is the distance from the center of one beam to the center of the other, f_1 and f_3 are the focal lengths for the lenses, and x' is the distance of the center of one beam to the center of the other
3. The average of the two beam centers should also be the center point found in the previous steps; if it is not, then use the $\hat{x}$ translations on lens one to make it so

Once lens one is in place, continue by placing lens two. The second lens is placed so that at one point of its motion the lens does not affect the beams (to relatively first order; unfortunately depending on the lenses thickness this approximation, may not be valid). The alignment method, for this lens is below:

1. Begin by noting the position of lens three's $\hat{x}$ direction translation and move the third lens out of the way so that the beams pass by it, but do not interact with the lens

2. Move the second lens to its furthest position away from the first lens in the $\hat{z}$ direction, a telescope should have been created between lens one and lens two

3. Using this telescope, adjust the $\hat{z}$ translation on lens two so that the two beams' expansion is given by the magnification equation $x' = \frac{f_2}{f_1}x$ where x is the distance from the center of one beam to the center of the other, f_1 and f_2 are the focal lengths for the lenses, and x' is the distance of the center of one beam to the center of the other

4. The average of the center of the two beams will be the center that was found in the beginning with lens three and the camera, adjusting the $\hat{x}$ translation if it is not.

This procedure is finished by placing lens three back into the lens array and checking two things:

1. That as lens two is moved, the average center of the two beams is as close to the calculated center of the single beam found at the very beginning (in practice, it is enough to check three spots: the beginning, middle and end).

2. As lens two moves from the position closest to lens one to the position closest to lens three, the beams impinge upon each other and, finally, the center of each beam will be as close to being the same number as possible and should follow the magnification $x' = \frac{f_3}{f_1}x$ (given when lens one was put into place) when lens 2 is as close to lens one as possible.

If the average of the beam centers moves more than is required, then it is possible that $\hat{x}$ translation of one of the lenses is off or that the $\hat{z}$ translation of the middle lens is not enough. As long as step 2 above is true, one can take out the lenses and start from the beginning, but only correcting the $\hat{x}$ translations of the lenses. If that did not fix the problem, then lens two $\hat{z}$ is not perfectly square with the beam direction and everything must be realigned.

If the second step is incorrect, then one of the steps was not followed correctly. To compensate, it is best to first quickly measure the distances between the lenses so that they follow the correct formulas: lens three to the camera is roughly f_3, lens one to lens

three is roughly $f_1 + f_3$, and lens two at its minimal state is f_1 away from lens one while it is $f_1 + f_2$ away from lens one at its maximal state. Note that there might be some discrepancy as the lenses may not have focal lengths that was specified on the box due to machining error, etc. Once the calculations are done, it is best determine which lens is the problem and address it for each individual case.

2.2.7 The Single Photon Camera

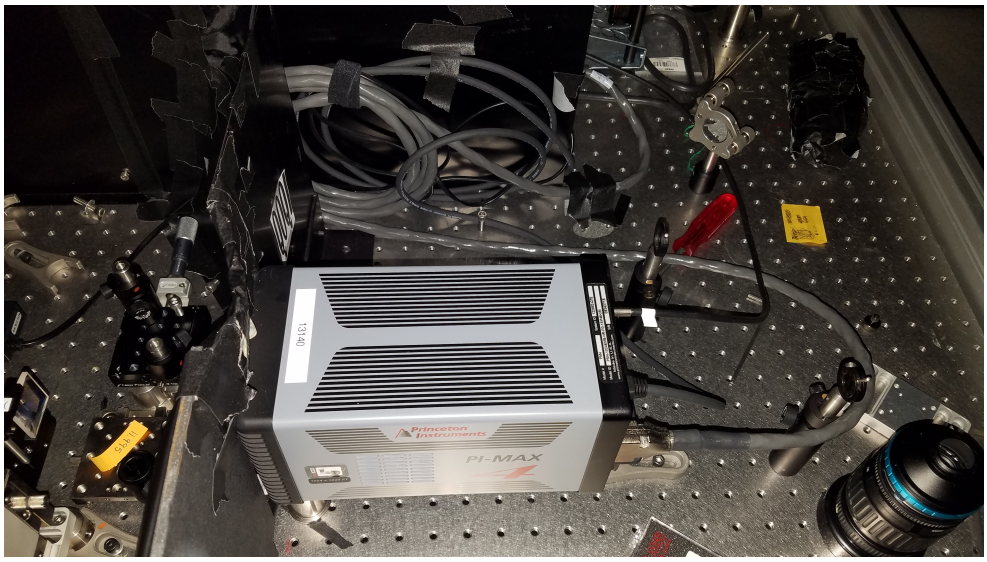

Figure 2.15: The PI-MAX4 camera

One of the most important pieces of equipment used in this experiment was the single photon detecting camera, a Princeton Instruments' PI-MAX 4 Electron-Multiplied Intensified Charge-Coupled Device (EMICCD) (Princeton, NJ) and its controlling software (Lightfield v6.5). In this camera (as seen in Figures 2.15 and 2.10), there are multiple properties that make it ideal for this application. First, the camera has an electrical fast shutter, allowing it to take pictures spanning approximately $3ns$ as well as heralding on an outside detection such as the detection of the second photon from an SPDC source. The camera also is able to electronically delay its shutter opening after is has received an electrical signal from the separate detector. The camera has a high quantum efficiency around the photon wavelength in this experiment ($408nm$ and $409nm$). Lastly, the camera consists of both a EMCCD and an ICCD in a combination known as an EMICCD. This combination allows

for the resolution of single photon events. All of these features allow for the detection of the spatial modes of single photons in coincidence from an SPDC source.

Intensifier Gain

One way to view low-intensity light using a camera is to use an intensified CCD. The amplification of the light in this case, is a multistep process. The process starts when the photon hits a photocathode and the releases an electron. That electron is then attracted via a high voltage induced electric field to the Microchannel plate which is filled with glass channels. Since a high voltage is applied to the Microchannel plate, when the electron enters one of the glass channels, the electron accelerates through it causing additional electrons to be released from the walls, which are also accelerated to the end of the plate. The electrons then slam into a phosphor screen where light is released due to the properties of phosphor and then emitted into a fiber optic piece. The fiber optic is coupled to the CCD and the intensified image is then read out to a computer [16].

EMCCD Gain

Another way to illuminate low-light conditions is to use an EMCCD. Typically, the camera works by creating "photoelectrons" or electrons created by the photo-electric effect during exposure on the pixel in the CCD; these electrons are then moved to a storage area at the back of the CCD to allow for fast capturing and imaging. The storage area is then readout through several electrodes where there is a small chance of creating more electrons. The charges then reach an amplifier, which creates an electric signal that can interpreted by the computer and creates the image. If the images are required to be read out quickly, the higher voltages and signals within the timing chips end up contaminating the signal and are one of the greatest noise inducing effects in EMCCDs [5].

On CCD-Accumulations and Frames

This is a confusing and perhaps less well-documented feature in Lightfield where there are two seemingly similar features, but are not usually distinguished. On CCD-Accumulations are defined as when the camera opens up its electronic shutter and closes it, however, rather than the signal getting read directly to the computer, the signal is stored in the storage area in the EMCCD. This happens regardless of whether or not the camera is using the EMCCD or the ICCD or some combination above. A frame on the other hand,

is whenever the data is transferred from the storage area in the camera to the computer (i.e. taking the analog data in the camera and then digitizing it). In this sense, if the program has 100,000 on CCD-Accumulations and requires 50 frames, then the camera will open its shutter 100,000 times per frame, the frames will then be added together digitally. This means that the camera was exposed $50 \times 100,000 = 5,000,000$ times in a single picture. As stated earlier, the more times the camera converts the analog data into digital, the more noise will be injected into the system. On the other hand, the camera should not over-saturated by overflowing the electron wells (where the electrons are stored before digitization). Therefore, it becomes a compromising procedure between injecting more noise into the system, but also making sure not to over-saturate the camera.

Single Photon Detection- Thresholding & Clipping

The last important setting in Lightfield to understand for single photon experiments is the "single photon detection" mode and the two options that exist: thresholding and clipping. They are, for the most part, very similar. Essentially, they both take an input value that is set by the user before the experiment, and anything that is readout below that value is automatically set to zero by the program. However, the difference between the modes is what happens afterward the detection. In the clipping mode, the value is readout like there was no photon detection, while in the thresholding mode any pixel which is over the user's value is automatically set to 1 (i.e. a single photon event happened at this point).

Controlling the Camera Using Lightfield Parameters

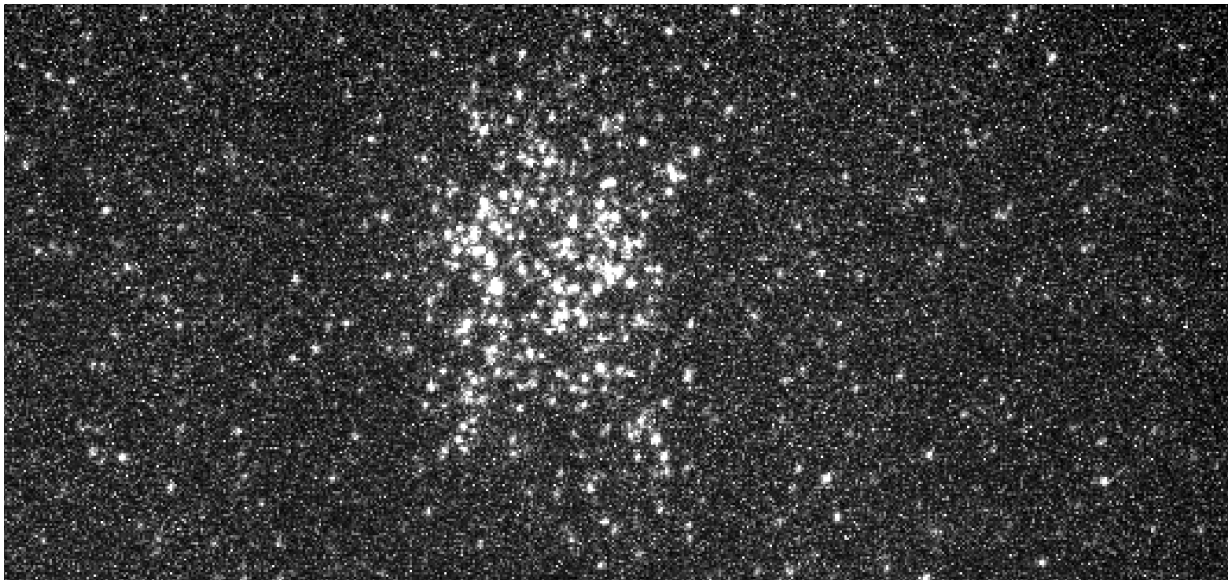

Figure 2.16: Single photons with minimal thresholding

Note that the obvious particle strikes are large blots with very distinct extent. This means that the effective pixel size is larger than the physical size of a pixel implying that smaller features are harder to see.

Figure 2.17: Single photons appropriately thresholded

Note that the obvious particle strikes are small blots on the order of one to three pixels wide.

With the explanation of each of the parameters available through Lightfield, the next important process is to learn how to set them and how they are to be used together in order to get the best image possible. First, unless the CCD is cooled, trying to see single photons using just the electron-multiplying gain (em-gain) is not possible on the PI-MAX 4. That is unless the PI-MAX 4 is cooled to liquid nitrogen temperatures like other EMCCDs; however, it is a large risk to the internal electronics due to condensation issues that could short out the electronics. Thus, in order to see a single photon at the relatively high temperature the CCD utilizes the intensifier gain in order to detect these events. However, this gain should be used in a relatively limited manner in order to reduce smearing or blurring of the photons on the image as explained in the above subsection. The best way to use this is to allow the photon to be imaged on the CCD using the intensifier and then amplify that signal by using the em-gain in order to raise the signal above the background noise; thus, allowing the thresholding to be effective. Blurring of the

photons over multiple pixels will occur due to the intensifier. To fix this, the thresholding should be relatively high so that only the peaks of the individual impacts are selected and reducing the blurring at the price of also reducing the number of successfully imaged photons. Finally, the number of on CCD-Accumulations should be used to make sure that the photons do not hit the same place twice, since using the thresholding photon detection mode does not reward multiple strikes in the same place. Instead, multiple frames should be used. As the gating time becomes shorter, some pixels will become "hot," meaning that they are more likely to register false events due to the high voltages being applied and possible defects in the individual pixels. Since these pixels should be relatively constant, taking an image with the same settings, but with the cap on could reduce/remove these defects in the images.

Proposed Sequence to Image Single Photons

It is possible to take pictures of single photons using this setup; however, it is a difficult task. In order to make the setup function effectively, a set procedure was developed in order to measure single photons. This sequence allows the camera's user to go from needing to measure multiple photons to get an image down to single photons being imaged on the single photon camera. There are possible improvements which could be made to this sequence and there are some limitations to the camera as described above. This sequence requires that the user has sufficient knowledge of the Lightfield software and that they have successfully done the first light instructions which have been supplied by the Princeton Instruments PI-MAX 4 manual. Note: because the intensifier and CCD chip are wavelength dependent, some of these parameters should be changed/thought about given the information above while these steps are taking place. The sequence described below was specifically outlined for the source defined in 2.2.1.

1. First, it is best to put a regular CCD camera in front of the beam(s) to make sure the size of the beam will be able to fit on the PI-Max 4 using a classical laser with about 20μW of power.

2. The timing window for the single photons should be approximated by removing the classical camera and placing a coupler (which couple free space light to single mode fiber) and running a fiber to a single photon detector and coincidence logic device. Using the single photon histogram program (which varies the relative delay between two signals to find the largest amount of coincidence counts between two photons as in an SPDC source), and finding the relative delay between the two photons.

3. Once the relative delay between the photons is found, any variances between the setup with the coupler and the camera needs to be accounted for such as differing coax-cable lengths (signals run at $\frac{2}{3}c$ in that case) as well as any differences in how far the camera is placed compared to where the coupler was placed, and that you have removed a length of fiber (which also has light move at roughly $\frac{2}{3}c$). Using this, one can find the new relative delay taking these things into account.

4. After creating a marker for the delay, the next step is to find the signal on the camera. Making sure the camera is placed down the optical line (which can be done by making sure to cap the camera and check with a classical beam that the beam will hit the CCD via visual inspection), ensure that the camera will have the beam(s) placed in an appropriate location on the camera by placing the photons down the line and reduce the em-gain and intensifier gain set to 1. Then changing the coincidence window to somewehere between 1s and 5s (your milage may vary/being careful to not overexpose) and placing the camera under internal trigger (set to approximately 1kHz) and with a single frame (on CCD accumulations also set to 1) and hit play. This will allow the user to see the beam on the camera. If the beam is not seen, then the gains need to be increased being careful to not over saturate the camera. If the beam does not show up, even after increasing the gain to 21 on the intensifier and 53 on the em-gain, then the beam(s) must not be on the camera. Readjust the beam and try again.

5. The next step is to find the timing window for single photon sensitivity. Start by taking the beam used in step three and taking the BNC cable connected to the port where the heralding photon is detected and connect the free end to the Trigger In port on the back of the PI-MAX 4. Beginning with a coincidence window of 200ns and setting the delay starting at the relative delay found above minus $300ns$. Take images with a gain setting (assuming the photons are at 808-810nm wavelengths as it changes the quantum efficiency of the camera, and a heralding rate of around 130000 photons/second) of em-gain to 58 and intensifier gain to 21, and with on-CCD accumulations around 10^6 and about 3 frames so that the with each image the delay setting is increased by 100ns. Once an image is formed, record the delay number.

6. Starting with the delay found in the previous step and using the same gain settings, start by varying these following settings: decrease the number of heralding photons by either decreasing the pump laser power or by some other method (one method of achieving this is to purposely misalign the polarization analyzer in Bob's side) to get the total number of heralding photons to around 10,000 detections/second as the reprate of the camera decreases as the gate width decreases; and increase the

number of frames to approximately 10, while decreasing the on-CCD accumulations to 100,000. Now, by changing the width of the gate to 100ns, increase the delay from the number found in the previous step by around 20ns watching for the delays where the signal disappears entirely. Then starting just outside of those delays found above (i.e. using the delay minus the new coincidence window), repeat the process by adding to the delay half of the gate width setting until you get to 3ns of gate width. Making sure to record/save each of the files so that if a clear photo is produced, the camera settings from that photo can be retrieved by using the convert data to experiment feature in Lightfield.

These steps allow the user to obtain images of single photons using a PI-MAX 4 camera.

2.3 Analysis & Results

2.3.1 Calibration

Lens System

Now that the system is set up and aligned, we need to be able to calibrate the individual systems in the experiment. First, the distance between the two beams after the first polarizing beam displacer from the source seen in Figure 2.10. To do this an $808nm$ diode laser was allowed through the system, a Coherent LaserCam-HR II camera (Santa Clara, CA) was placed in the beam, and a movable iris was placed so that the iris allowed only one beam through at a given time. By aligning the iris to each of the beams, the iris can then by moved along via micrometer and stage. When the image of the beam looks as circular as possible, the beam is centered on the iris. The two readings for the beam are subtracted and the beams are found to be $2.66mm$ apart.

The beams Gaussian nature must be found, by taking the classical laser and the same camera as above, the beam was allowed to freely expand down the table. Using the Coherent HRII camera's diameter measurement, the beams diameter as a function of propagation distance is measured and shown below:

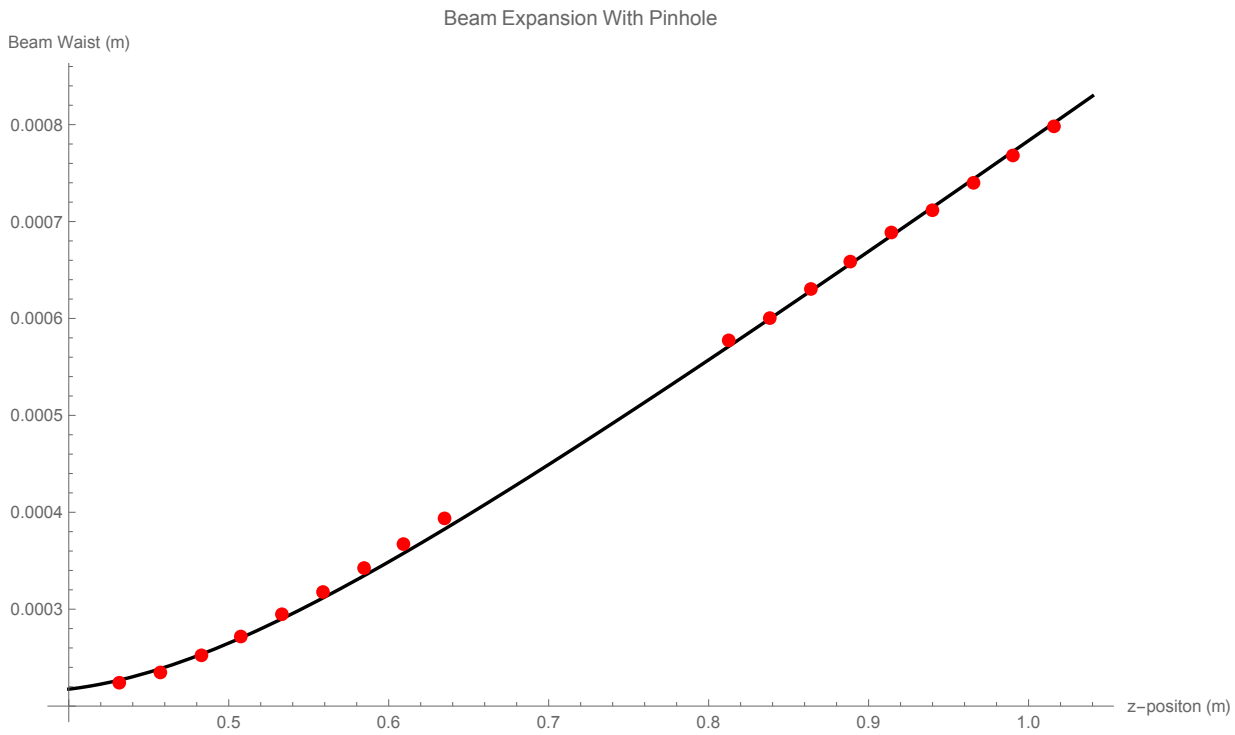

Figure 2.18: A graph of the beam width data for the beam after the pinhole and its fit as a function of propagation

The beam diameter as a function of the lens displacement when using the pinhole. Note that it follows a Guassian well with a waist of $0.2145mm$.

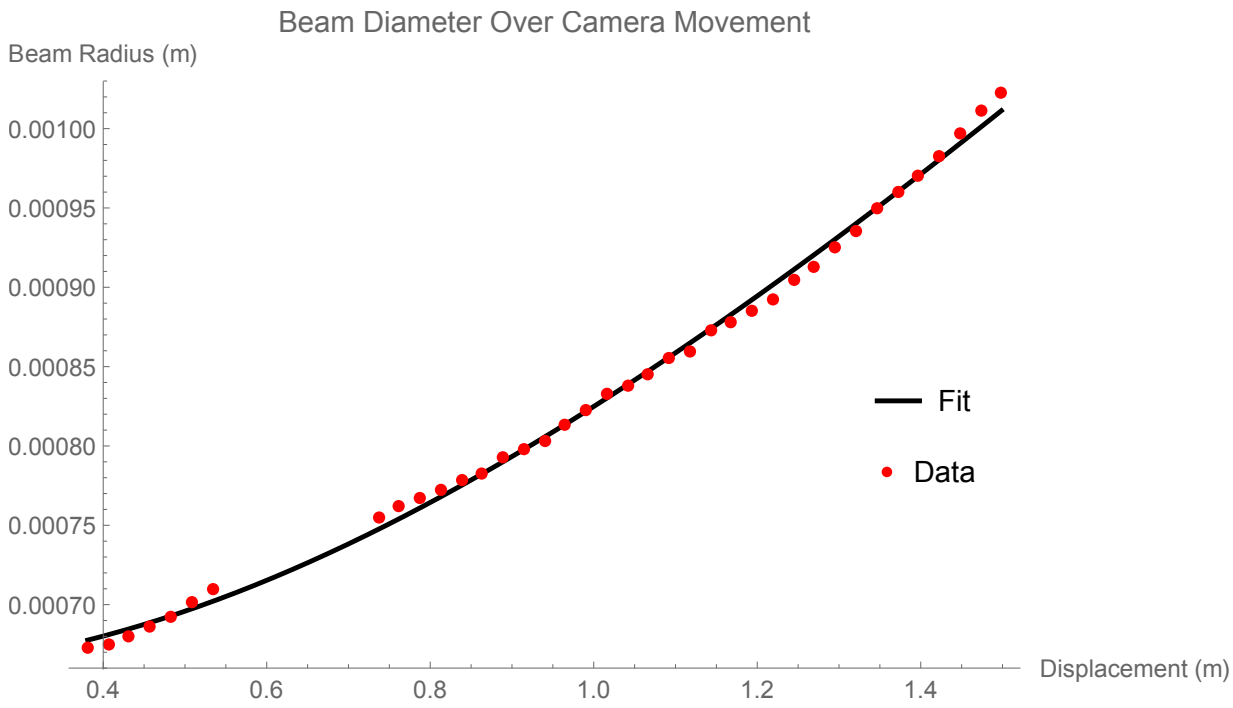

Figure 2.19: A graph of the beam width data for the beam without the pinhole and its fit as a function of propagation

The beam diameter as a function of the middle lens displacement. While it was unable to be fitted by a Gaussian beam, it was able to be fitted with a general hyperbolic equation.

After numerous attempts at fitting the data using the typical Gaussian propagation equation, the data was able to be fit using a modified hyperbolic implying that the beam in question is not a pure Gaussian and in fact made up of multiple modes. Since the number of pixels being illuminated is over 10 (ranging from just under 60 to over 200) the error in the measurement is only a few percent [14]. Thus, the fitted curve will be used as the theoretical beam expansion when compared with the beam waists after the dividing by the magnification.

The lens system also needs to be calibrated. In this case, each of the lenses are given in section 2.2.5. Plugging these values into equation 2.6, the line to compare the system to is given by $|M| = 1.5 - 60d$ and if the results are a line similar in nature the alignment of the lens system is ensured. By using the HRII camera instead of the single photon

camera at the end of the lens system as described in the alignment section and reusing the selection of the individual beams by using the iris above, the centers of both beams can be determined by using the camera's center function. By subtracting the x-coordinate of the right beams center from the left beams center, the new distance between the beams can be calculated for a given position of the middle lens. Further, by dividing this new distance by the distance between the two beams right out of the polarizing beam displacer, the magnification is found and shown below:

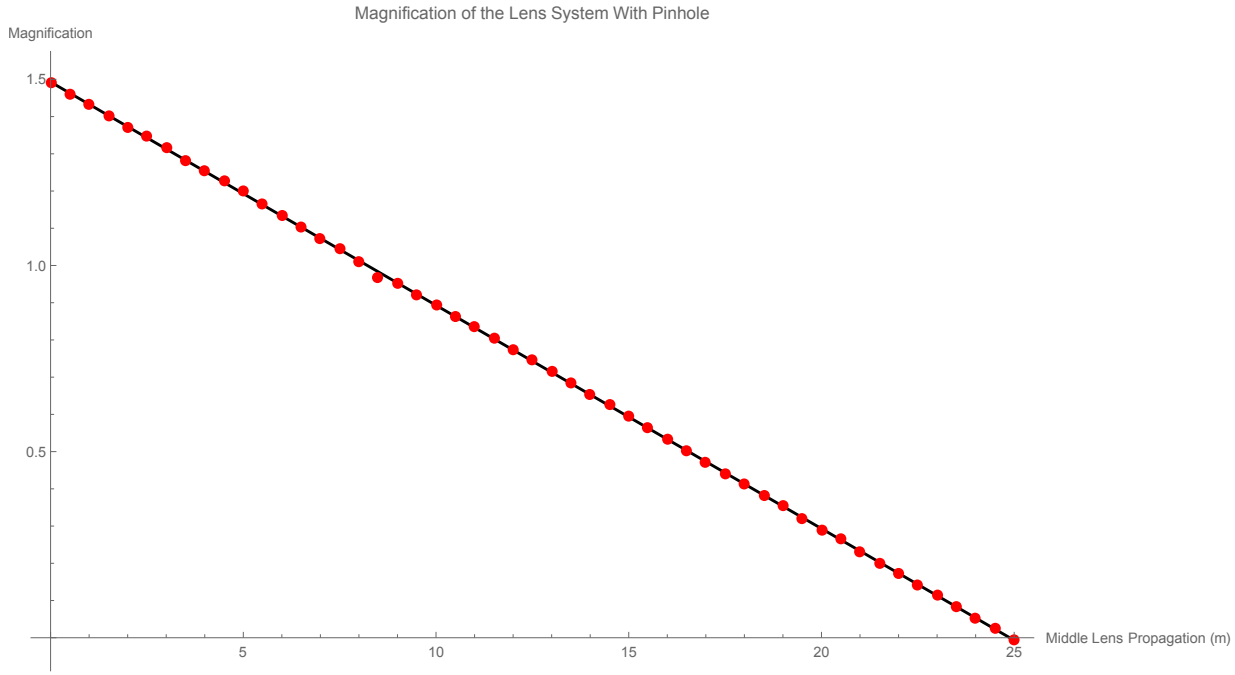

Figure 2.20: The magnification from the distance between the two beams when the pinhole is included

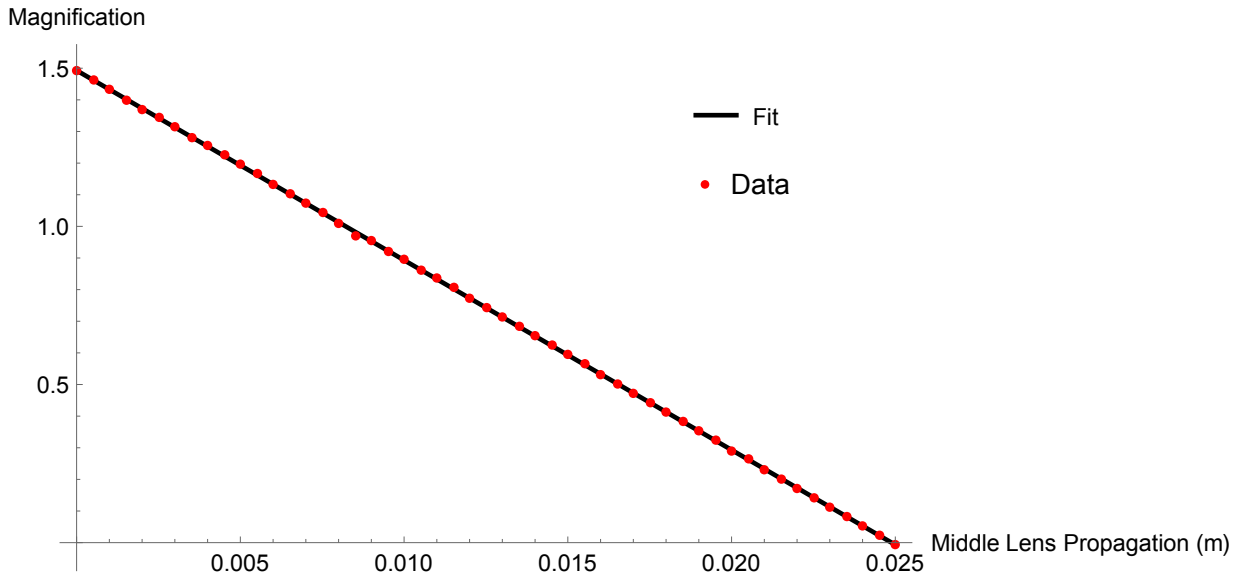

Figure 2.21: The magnification from the distance between the two beams when the pinhole is not included

The fit is found to be given by

$$y = 1.49301(\pm 0.00078)x - 59.99343(\pm 0.05374) \tag{2.7}$$

which is in good standing with the expected results of $1.49301 - 59.99343x$ as found from equation 2.6 being careful to match units.

Next, the beam waists after the lens system must also be found. In order to do this, one of the output beams must be placed straight in the middle of the lens system. This is done, by once again closing the iris so that just a bit of light is going through and then moving both the iris and the back mirror by half of the amount that the beams are displaced by the polarizing beam displacer. Using the iris to allow the center beam through, but completely blocking the off-center beam, allows the beam diameter measurement to be done by the Coherent HR-II. There is an issue of making sure the beam has the same intensity from one lens position to the next. However, because this is as the camera sees, there is no other way to make sure this intensity stays the same with out knowing more about the beam. Thus, there can be a lot of variation in the measurement. In order to counter act this, one must decrease the intensity of the light from when the camera was saturated to the point where the beam became just unsaturated allowing us to standardize the measurement.

The waist is then recorded for each lens displacement from values ranging from $0mm$ to $25mm$ displacement as plotted below.

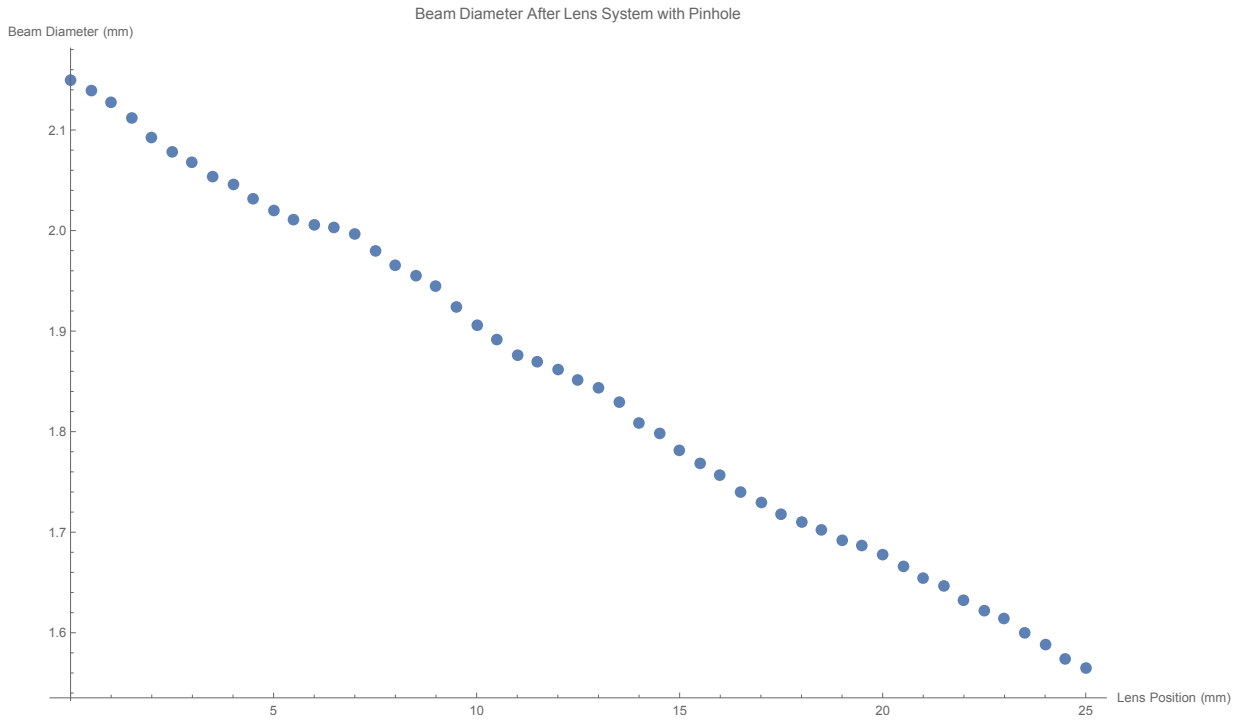

Figure 2.22: The beam diameters measured after the lens system with the pinhole

Note: that the beam diameter is not quite a straight line as we would expect. This is mainly due to user error in setting up the intensity on the camera correctly. However, because it is continually decreasing, the values can be used for our effective propagation distance.

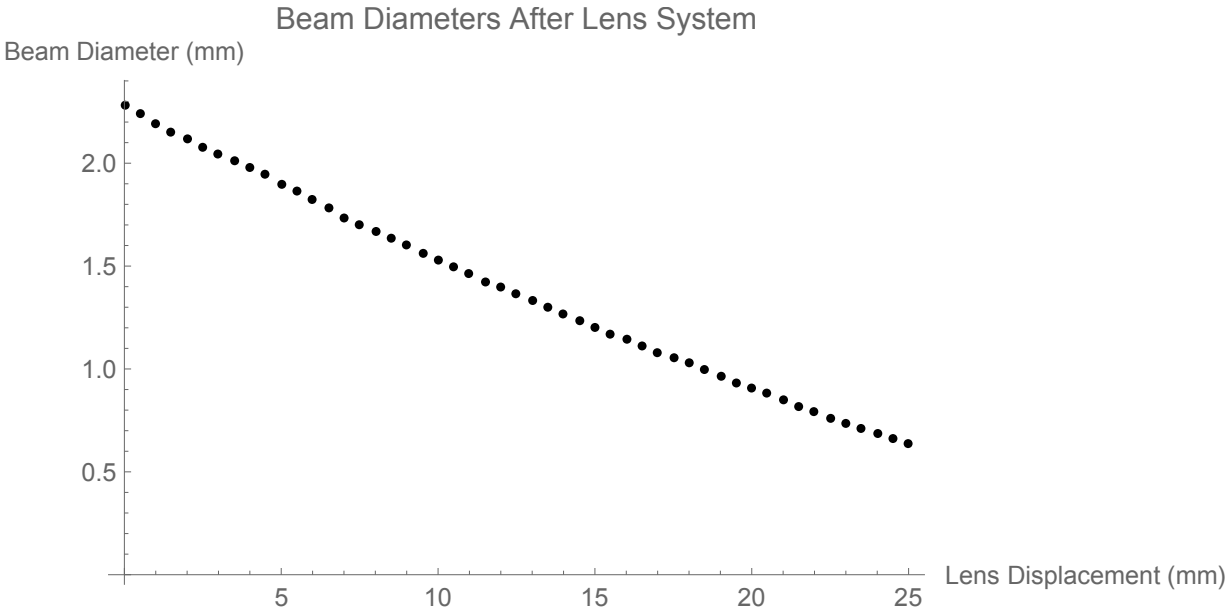

Figure 2.23: The beam diameters measured after the lens system without the pinhole

With all three of the measurements taken, the effective propagation distance can be found. To do this, we follow the steps outlined in section 2.1.2. Shown below is the plot of the effective propagation as found from these steps.

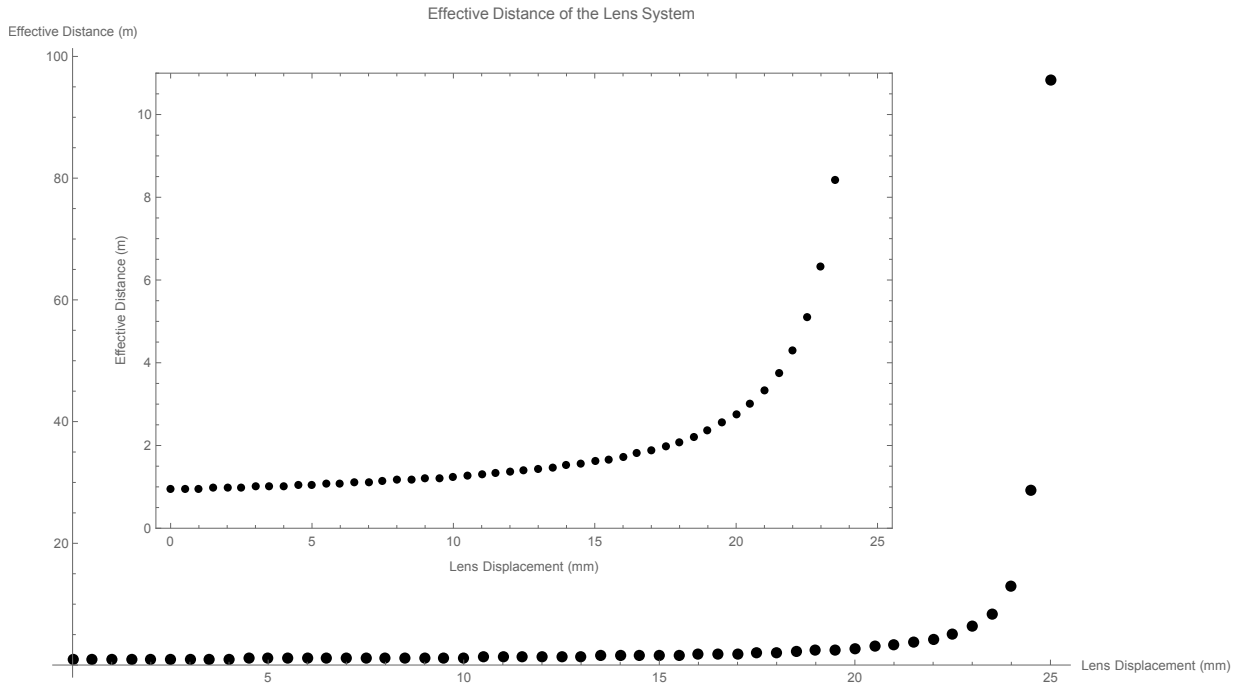

Figure 2.24: The Effective Distance the Lens System Produces With Pinhole

The plot shows the effective distance the particles go as the middle lens moves when the pinhole was in place. The inset shows that the scale of change compared with the bigger graph as it only stops at the target of $10m$.

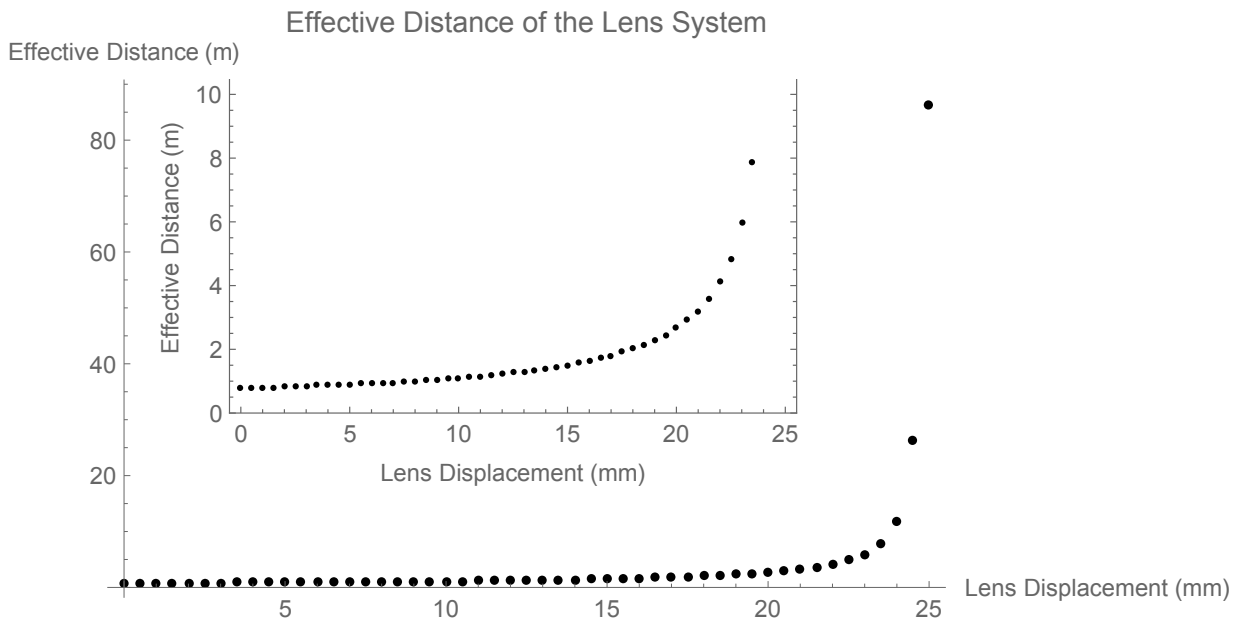

Figure 2.25: The Effective Distance the Lens System Produces

The plot shows effective distance that the particles go to when the middle lens of the lens system is moved. The inset shows the same graph, but only looking at points that are below the $10m$ mark to give a sense of scaling as the lens moves further away from the first lens.

The Weak Measurement

The calibration of the weak measurement is done by rotating the weak measurement crystal's normal in the x-z plane to change the direction of the optic axis compared to the beam. As explained above in 1.2.4, the weak measurement crystal works by taking the phase difference of the two beams. The phase difference is linear with respect to the incoming angle of light and the difference between the optical path lengths gives the interaction parameter, labeled as η in section 1.2.3. The angle in this case is defined as $\frac{k_x}{|k|}$, so we need to do two things: characterize the total strength of the interaction, η, and find the angle such that the constant term, γ, in the linear equation is 0. From the analysis in section 2.1.1, we find the phase (the weak momentum since the angle is really an operator measure as the momentum is not known) in its linear form is given as $\sin\left(\eta\frac{k_x}{|k|}+\gamma\right)=\frac{I_R-I_L}{I_R-I_L}$. Meaning, that if we collect the total intensity for both the right circularly polarized light and the left circularly polarized light and plug them into the equation above, we can try

to fit the data in order to know for which angle we can effectively make $\gamma = 0$ (using a redefinition of γ) and the slope given by the value of the derivative given at $\gamma = 0$ (or through a fit of the function given enough points).

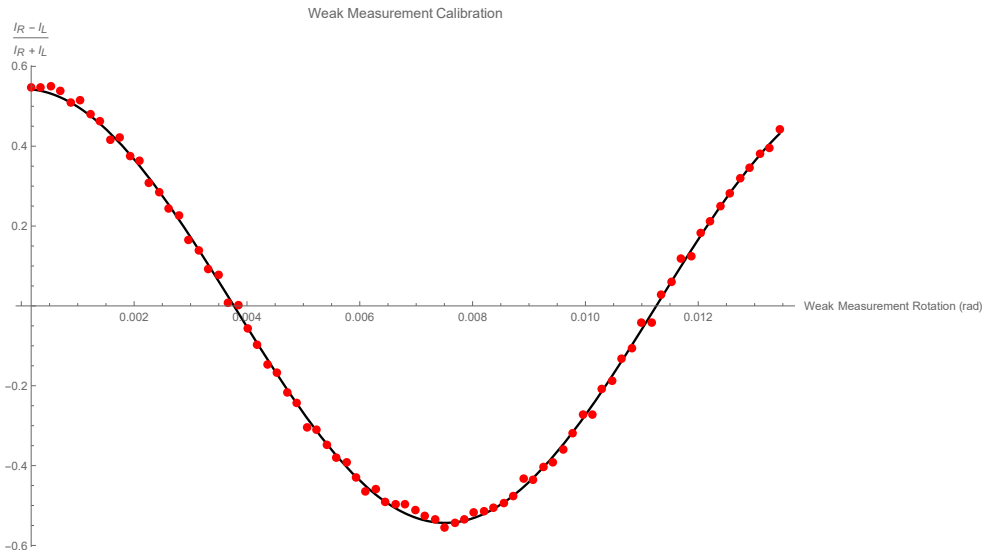

Figure 2.26: The experimental differences in intensities divided by their sum as a function of the rotation of the weak measurement crystal normal in the x-z plane as well as their fit

The plot shows the angular dependence of the weak measurement crystal on the measurement from quantum light without the pinhole. The strength of the measurement is calculated as the derivative of the curve divided by the amplitude or using a fit to estimate the parameters of the function. Typically, the amplitude is 1; however, in this case it was lower than this. This is most likely due to the crystals optic axis not being set correctly in the x-z plane. The fit is given by $-0.5435(\pm 0.0020)\sin(-419.6(\pm 0.8519)x + 4.723(\pm 0.0071))$. It should be noted that the 0 in the x-axis is not guaranteed to have the normal of the crystal fully in the z-direction.

Hence, we find that the optimal point is around $.00375rad$ from our crystals original position and we find that the crystal has an interaction parameter of roughly 419.6 (note: that the sign here is meaningless as the sign can always be brought out of the sine. Using these parameters, we can set our week measurement crystal and use it to produce measurements of the weak velocity at different x-positions.

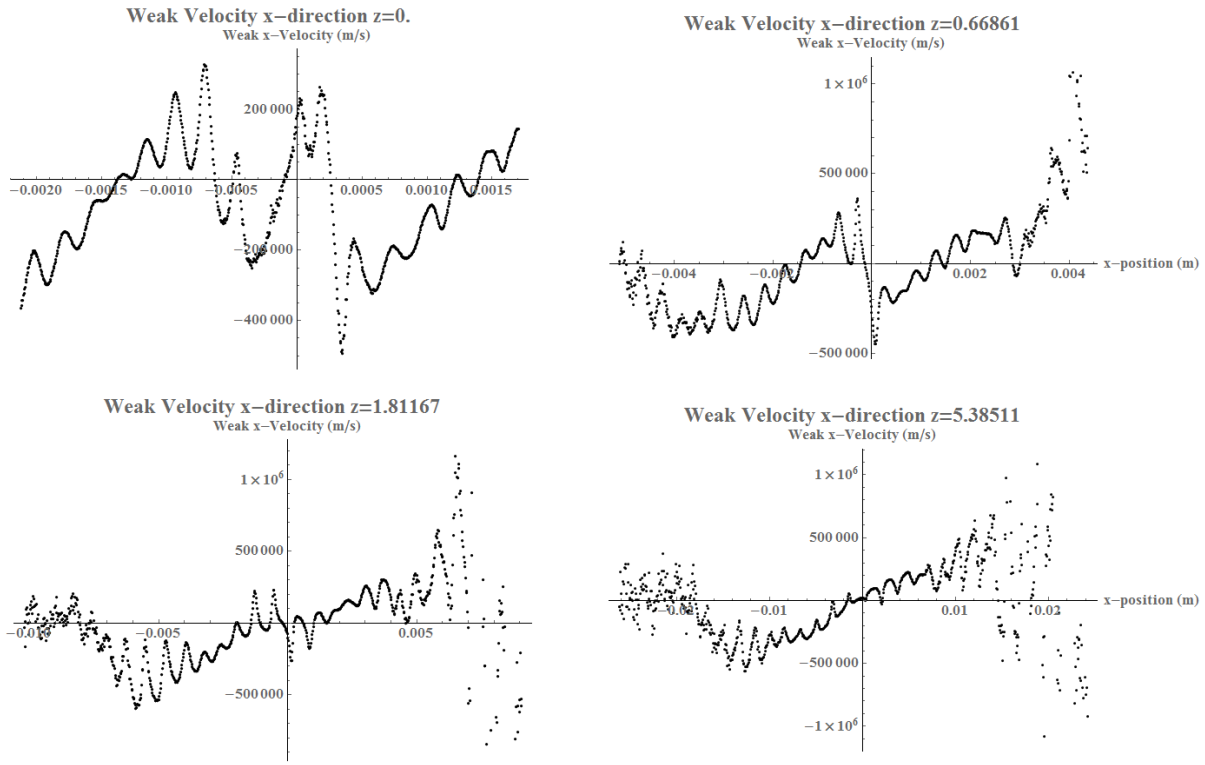

Figure 2.27: A distribution of the weak velocity data over many z-slices

These plots shows the evolution of weak velocity as a function of x-position over many z-slices. This data was take using a classical beam with a pinhole. It is interesting to note that the reason for the velocity to not be in straight lines before the beams overlap is due to the higher order modes that are created from the light going through the pinhole.

Using, these momentum values, seed points were found by taking approximately 10000 points equally spaced out points in each of the Gaussians where the velocity of the separated beams were stable (at $z = 0$). Each of the points were updated to each of the different z-planes creating the trajectories seen in Figure 2.28

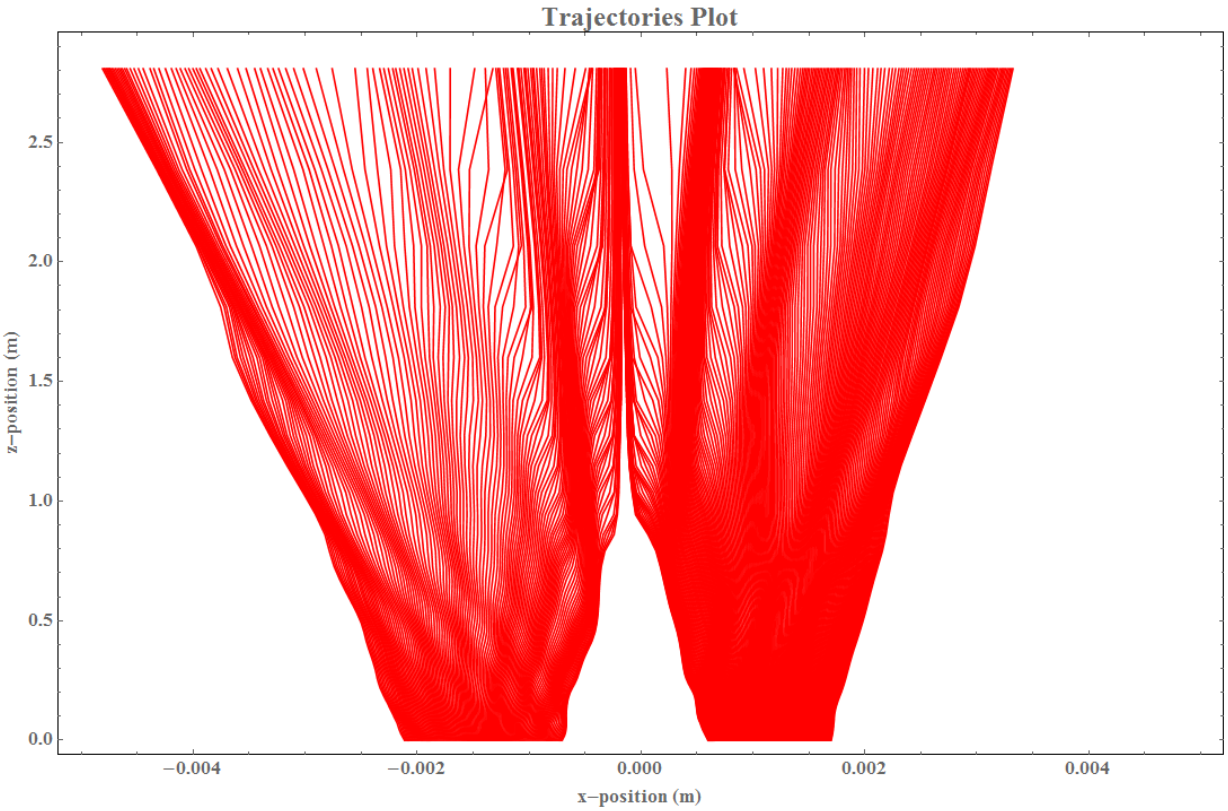

Figure 2.28: Trajectories of the photons moving through the Gaussian beams as a function of both x and z positions using a classical beam.

It should be noted here that it seems like there are more fringing before the beams overlap than would appear in the actual pattern. The reason for this is due to the interference from the overlap of the higher-order modes produced from the pinhole with the opposite Gaussian beam.

Now, given that the classically found weak values and trajectories looked like they had some of the more interesting features correct, but the quantum potential could not be found from the data. Moving on the next step was to try the same experiment using single photons and removing the pinhole. The following pictures were taken:

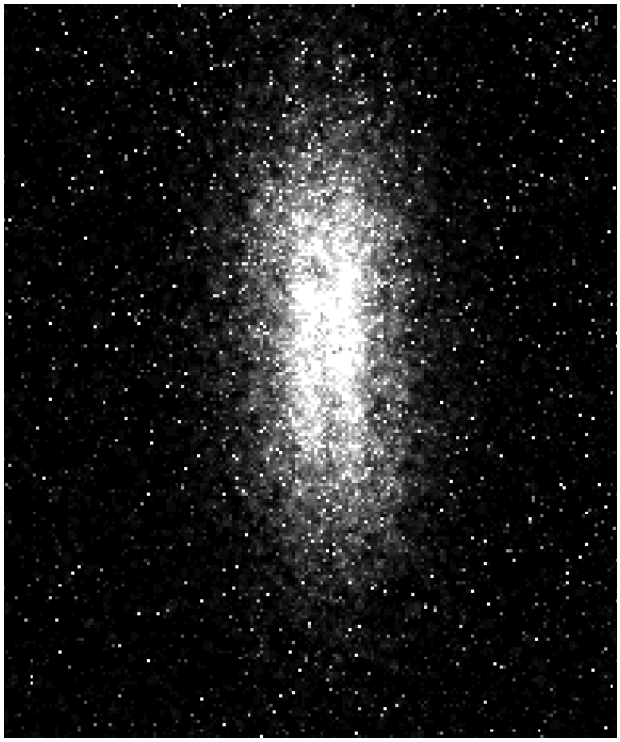

Figure 2.29: The single photon image with the lens at 25mm without any thresholding applied.

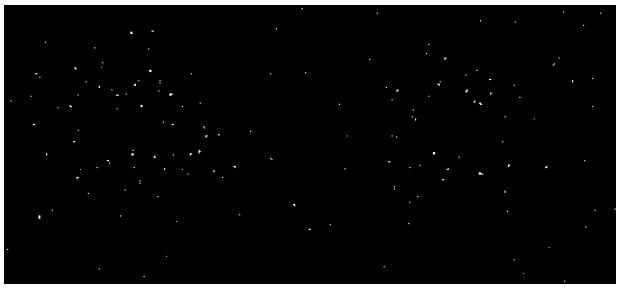

Figure 2.30: The single photon image with the lens at 25mm with thresholding applied.

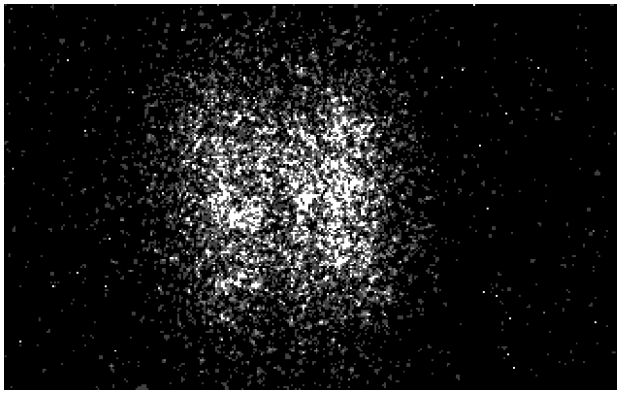

Figure 2.31: The single photon image with the lens at 21mm with thresholding applied.

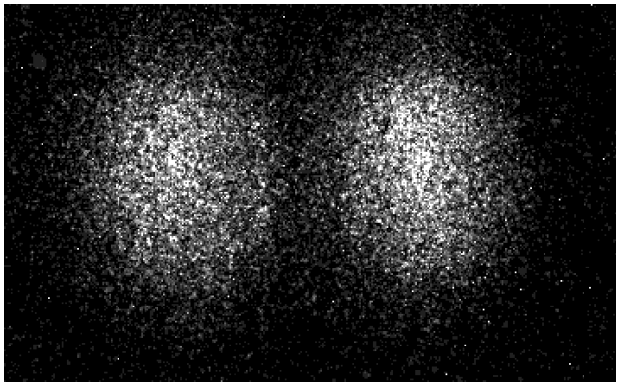

Figure 2.32: The single photon image with the lens at 13.5mm with thresholding applied.

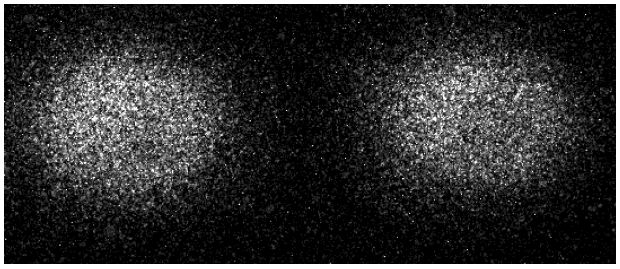

Figure 2.33: The single photon image with the lens at 0mm with thresholding applied.

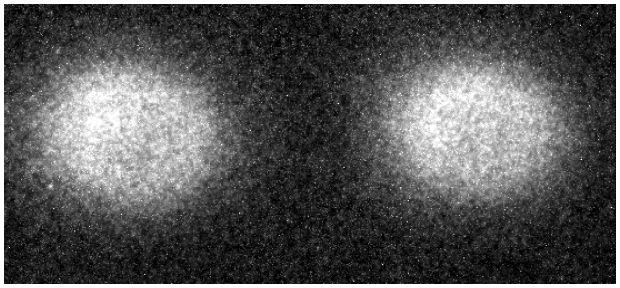

Figure 2.34: The single photon image with the lens at 0mm without any thresholding being applied.

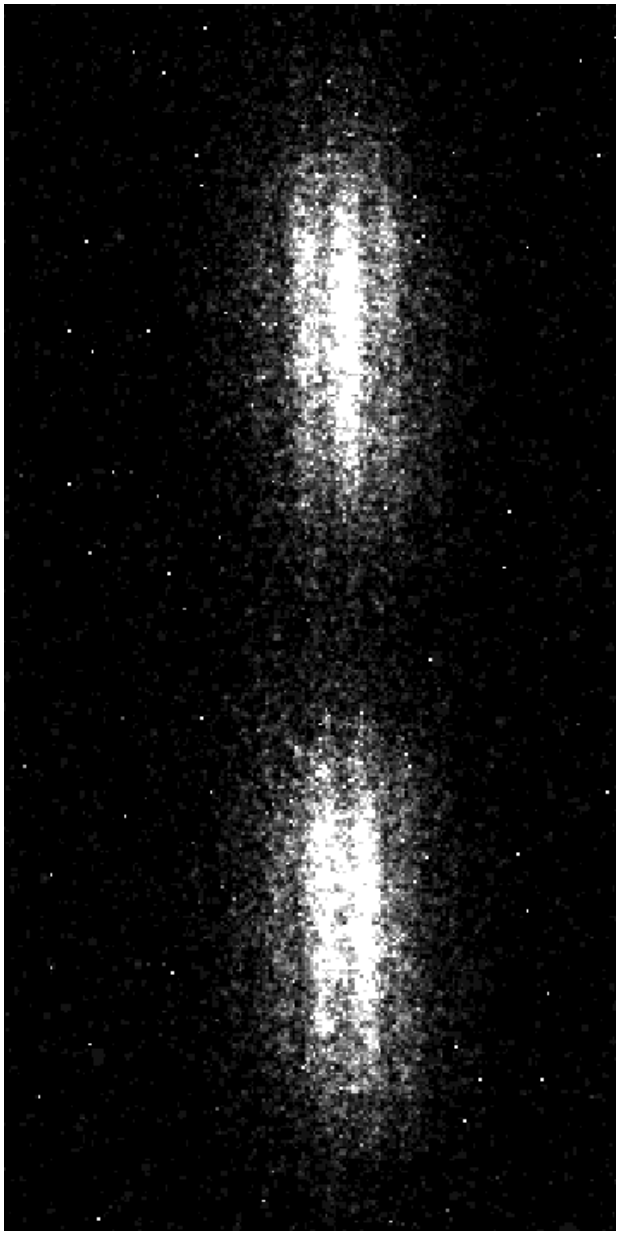

Figure 2.35: A sample of the beams with the weak measurement at 25mm

Note: the white speckle in the background, those are large values of "photons" usually in the 1000's, which is most likely a false reading in those pixels.

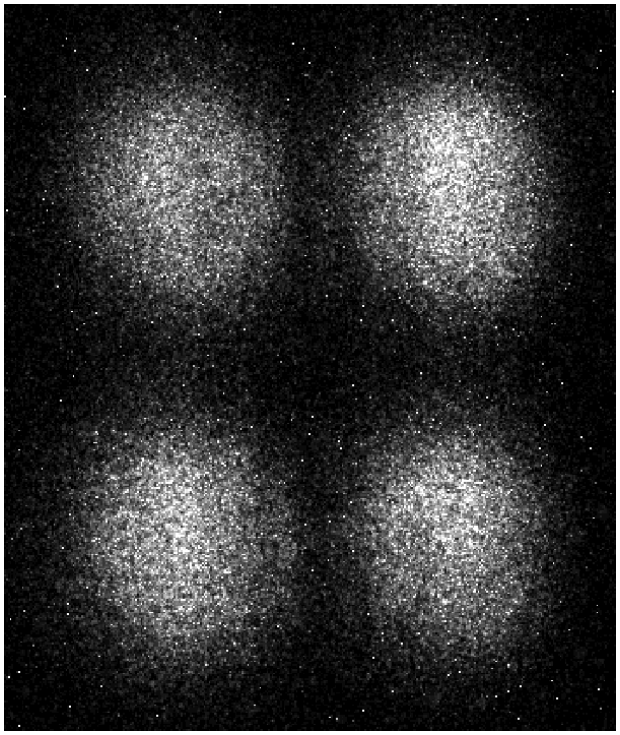

Figure 2.36: A sample of the beams with the weak measurement at 13mm

Due to some concerns about the background noise, a picture was taken with camera cap on and compared to data sets. All of the pictures have been modified so that the lowest value was mapped to 0 and the highest to 1. Using this, we can pick up any background that would be drowned out by the rest of the image so we can compare them on a similar footing.

Figure 2.37: A picture taken with the photon camera capped at an intensifier gain of 21 and an EM gain of 58 for 100,000 On-CCD Accumulations with 500 frames

Figure 2.38: A picture taken with the photon camera not capped while single photons are being imaged at an intensifier gain of 21 and an EM gain of 58 for 100,000 On-CCD Accumulations with 500 frames

Figure 2.39: A picture taken with the photon camera not capped while single photons being imaged at an intensifier gain of 21 and an EM gain of 58 for 100,000 On-CCD Accumulations with 1000 frames captured 3 months before the picture in 2.37

2.4 Discussion

The question, having gotten this far, is what was learned from this experiment? In this case, first a simulation of the data from the trajectories was created using the experimental parameters. The trajectories were created and the quantum potential was calculated from those trajectories just like they would be in the experiment. When that data (Figure 2.5) is compared with the actual calculated quantum potential from the probability density function (Figure 2.6), we should see that the results from the trajectories are of the same order and have similar features. They are not exactly the same, but by increasing the number of points taken in the z-direction and sampled in the x-direction we should see the resemblance get better and better. There is something to be said about the fact that, at the moment, we cannot stitch together the individual z-slices. The cause of this seems to be the fact that we typically think of the trajectories in the measurement space (in x and z coordinates); however, this is not governed by the Schrödinger equation. Thus, when doing calculations for our trajectories, they should be done in the analog space (in x and t coordinates). Once the trajectories and the quantum potential have been calculated in the analog space, we can then return our trajectories and quantum potential to the

measurement space taking advantage of the one-to-one nature of the mapping.

Next, sample data was taken using a classical beam with a pinhole in the setup. We should note that there seems to be some odd features in the x-velocity curve toward (see Figure 2.27) when compared to the thoretical description of the Bohmian velocity in Figure 2.1. These features are actually due to interference that was present in the experiment and were caused by the pinhole that was inserted to make the beam more Gaussian in its evolution as shown in Figure 2.18. However, that is only true of the main peak, if one were to place a camera after the pinhole, there would be a few higher order modes which would be slightly larger in diameter than the main peak, but much less intense. So, once the singular beam is split into the two slits of the double slit experiment, the ringing would also get doubled into both slits as well. Furthermore, since the ringing is larger in diameter than the main mode, the ringing will also interact with the opposite beam and actually gives rise to the jagged appearance in both the velocity and the resulting trajectories as could be seen by replacing the Gaussian beams in the simulation with those of a sinc function. By sacrificing the Gaussian-ness of the beam, the idea was to get back the nice clean features in the velocity and trajectories as seen in Figures 2.1 and 2.2. The quantum potential unfortunately was unable to be reproduced because rather than taking equal steps in the effective z-planes, it was instead equal steps done by the lens meaning that the larger differences will cause the particles with high-velocity to have trajectories that cross with their neighbors.

Finally, what about the single photon camera and measuring the single photon weak value? Unfortunately, as seen in Figures 2.29-2.36, there was too much noise in the pictures than could be dealt with. Part of the noise was due to the low amount of light that was going through the experiment and, in addition to this, there was also the fact that we have to split the beam into fourths and the beams had variable widths that made it difficult to get a good image. There was the possibility of reducing the noise in the images, by taking many background images and subtracting out the average of those in order to remove these large spike features. These, hot spots, can be seen by looking at Figures 2.37-2.39. Looking at the patterns, we see that all of the pictures have many similarly lit pixels. Indicating that the process is not random and seems to be consistent as long as the camera settings are kept the same. There does seem to be some differences between 2.37 and 2.39. This seems to be mainly an issue with aging of the camera as well as the fact that in 2.39 there was two times as many frames as in the background file; however, some of the differences between 2.37 and 2.38 or 2.39 is also due to the fact that there were photons being measured with the camera as well. The last thing to take away from the background is that the best that we can do is remove the information in that pixel. This is because in the thresholding mode, the pixel either fires or does not. In the ones that are firing every time, there is no

distinguishing between if it was a legitimate photon strike or a miss fire, since these hot spots seem to fire nearly every time the camera opens. However, this will get rid of the majority of the spikes that made it impossible to look at the trajectories. It should be noted that this seems to only happen in very dim light such as in this experiment. The more photons that seem to be concentrated in an area there is a reduction in hot spot activation inside of the signal such as in the bright fringes of Figure 2.35.

Chapter 3

Future Work

3.1 Identification of the Beam Waist

One perhaps useful tool that would be of interest to an experimenter would be some simple experiment that would allow for the precise measurement of the beam waist. In this case, the weak velocity of the beam in the x-direction was determined to be 0 everywhere when the weak measurement occurs at the waist. This is because there should be no phase at the waist in a Gaussian beam. In this way, rather than guessing that the waist has been found due to extrapolation, this would give a realistic metric for quantifying how close the current z-plane selected is to the waist based on the slope of the velocity line.

3.2 Momentum Entanglement

Another interesting experiment would be to see how the measurement of the weak momentum compares to the actual momentum operator as measured at the same time. To compare these two, a momentum entangled source such as one that outputs $|p\rangle|-p\rangle+|-p\rangle|p\rangle$ should be built. The first step would be to characterize the momentum measurement. That way it will be possible to know the value of the momentum that was measured. This could be done using first two momentum measurements rather than one of the measurements being the weak momentum as well as test the entanglement. The weak momentum setup created by Kocsis et al. is the one that would be of interest and relevant to this idea; however, there might be other measures that would be more important [19]. Now, two things should happen: 1) the measurement of the momentum as given originally will be

able to be directly compared to the momentum found using the weak value and, ideally, there would be a single column of pixels accessed assuming the beam is a Gaussian since it has a linear momentum curve implying a singular location with a momentum that is equal and opposite of what was measured on the other photon. If they are not Gaussian, it would be interesting to see if the beam has more than one column of pixels lit up. 2) if the measurement of the momentum is then taken by a slightly wider slit (meaning more variance in the momentum), then more columns of pixels should become active since more momentum states are being allowed through on the non-weak measurement side.

3.3 Trajectories of Diffraction

In the 1927 conference proceedings, one of the points that was of interest was the paths the particles would take after there is a partial block in the beam [17]. Now that the trajectories are experimentally accessible it would be interesting to reconstruct the trajectories for these patterns. There are some things to note about this system. First, the beam block should be placed at or a little before halfway into the beam. This allows the experimenter to know exactly which photons should pass just to the side of the beam block (assuming a Gaussian beam input). The rest of the setup is similar to the one built in Kocsis et al., but without the lens system [19]. In fact, the strong measurement should be placed right before the camera in order to do this. Furthermore, the block should be as thin as possible and the space that the strong measurement takes up should be as small as possible (in fact it is the spatial length requirement of both the quarter wave-plate and polarizing beam displacer that discount many experiments one could do with trajectories). In theory, there should be a path created by those photons right before beam block and as well as after it. However, the parts of path beside the beam block will be experimentally untestable. Instead, after the trajectories are found for a few positions before and after the block, the trajectories might be able to be stitched together. However, the longer the weak measurement setup is in space requirements (lengths of crystals etc.), means that more instability in the resulting trajectories. As a bonus, it would also be interesting to see what happens to the photons that would not be able to move around the barrier; so, if the surface was mirrored, then measuring the reflection of the photons would be quite interesting.

Chapter 4

Conclusion

In conclusion, after attempting to measure the quantum potential by using a weak value of the momentum to construct photon trajectories with a single photon camera, it still goes unmeasured. However, in terms of theory, the measurement should work as increasing the number of sampled points gets closer and closer to the actual quantum potential. There is still a problem with trying to get the different z-planes to be stitched together, but there does seem to be a way forward in that regard. Next, we saw that is was possible to extract the weak values and build the trajectories using a classical laser. Further, the quantum potential was not able to be replicated in this case due to the choice of measurement using a pinhole, which deviated from the ideal Gaussian case. Finally, using single photons to recreate the trajectories of the particles was unable to be realized due to the fact that the images, which were obtained with the single photon camera, were too noisy to extract the necessary information to create trajectories. In the future, perhaps a better measurement style will come along to reduce the noise or the noise could be reduced by background subtraction.

References

[1] Y Aharonov, DZ Albert, and L Vaidman. How the result of a measurement of a component of the spin of a spin-1/2 particle can turn out to be 100. *Physics Review Letters*, 60(14):1351–1354, 1988.

[2] G Bacciagaluppi and A Valentini. *Quantum Theory at the Crossroads: Reconsidering the 1927 Solvay Conference*. Cambridge University Press, Cambridge, United Kingdom, 2009.

[3] D Bohm. A suggested interpretation of the quantum theory in terms of "hidden variables" i. *Physical Review*, 85(2):166–179, 1952.

[4] D Bohm. A suggested interpretation of the quantum theory in terms of "hidden variables" ii. *Physical Review*, 85(2):180–193, 1952.

[5] Nuvu Cameras. *EMCCD TUTORIAL*, (accessed December 15, 2017).

[6] R.Y. Chiao, P.G. Kwiat, and A.M. Steinberg. Analogies between electron and photon tunneling: A proposed experiment to measure photon tunneling times. *Physica B: Condensed Matter*, 175(1):257 – 262, 1991. Analogies in Optics and Micro-Electronics.

[7] LV de Broglie. *On the Theory of Quanta*. PhD thesis, Paris, France, 1926.

[8] Ivan H. Deutsch and John C. Garrison. Paraxial quantum propagation. *Phys. Rev. A*, 43:2498–2513, Mar 1991.

[9] D. Dürr, S. Goldstein, and N. Zanghi. Quantum equilibrium and the origin of absolute uncertainty. *Journal of Statistical Physics*, 67:843–907, 1992.

[10] D. Dürr, S. Goldstein, and N. Zanghi. On the weak measurement of velocity of bohmian mechanics. *Journal of Statistical Physics*, 134(5-6):1023–1032, 2009.

[11] A Einstein. Quantentheorie des einatomigen idealen gases. *Sitzungsberichte der Preussischen Akademie der Wissenschaften, Physikalish-mathematische Klasse*, 52:3–14, 1925.

[12] R. Flack and B. J. Hiley. Weak values of momentum of the electromagnetic field. average momentum flow lines, not photons trajectories. *arXiv:1611.06510*.

[13] P Ghose, AS Majumdar, S Guha, and J Sau. Bohmian trajectories for photons. *Physics Letters A*, 290:205–213, 2001.

[14] Lucas Hofer. *Small Beam Width Theoretical and Experimental Error*, March 14, 2016 (accessed December 15, 2017).

[15] PR Holland. The de broglie-bohm theory of motion and quantum field theory. *Physics Reports*, 224(3):97–148, 1993.

[16] Oxford Instruments. *Intensified CCD Cameras*, (accessed December 15, 2017).

[17] Institut international de physique Solvay. *Electrons et photons: rapports et discussions du cinquime Conseil de physique tenu Bruxelles du 24 au 29 octobre 1927*. Gauthier-Villars et cie., Paris, FR, 1928.

[18] Thomas F. Jordan. Simple proof of no position operator for quanta with zero mass and nonzero helicity. *Journal of Mathematical Physics*, 19(6):1382–1385, 1978.

[19] S Kocsis, B Braveman, MJ Stevens, RP Mirin, LK Shalm, and AM Steinberg. Observing the average trajectories of single photons in a two-slit interferometer. *Science*, 332(6034):1170–1173, 2011.

[20] E Madelung. Quantentheorie in hydrodynamischer form. *Zeitschrift fr Physik*, 40(3-4):322–326, 1927.

[21] DH Mahler, L Rozema, K Fisher, L Vermeyden, KJ Resch, HM Wiseman, and A Steinberg. Experimental nonlocal and surreal bohmian trajectories. *Science Advances*, 2:e1501466, 2016.

[22] J Mehra and H Rechenberg. *The Historical Development of Quantum Theory*, volume 5. Springer, New York, NY, 1987.

[23] T. D. Newton and E. P. Wigner. Localized states for elementary systems. *Rev. Mod. Phys.*, 21:400–406, Jul 1949.

[24] C Philippidis, C Dewdney, and BJ Hiley. Quantum interference and the quantum potential. *Il Nuovo Cimento B*, 52(1):15–28, 1979.

[25] JJ Sakurai and J Napolitano. *Modern Quantum Mechanics*, volume (2nd ed.). Pearson, New York NY, 2013.

[26] Bahaa E. A. Saleh and Malvin Carl Teich. *Fundementals of Photonics*, chapter 2, pages 41–79. John Wiley & Sons, Inc., 2001.

[27] R Tsekov. Bohmian mechanics versus madelung quantum hydrodynamics. *Annuaire de l'Universit de Sofia Facult de Physique*, Special Edition:112–119, 2012.

[28] L Vermeyden, M Bonsma, C Noel, JM Donohue, E Wolfe, and KJ Resch. Experimental violation of three families of bell's inequalities. *Phys Rev A*, 87:2105, 2013.

[29] A. S. Wightman. On the Localizability of Quantum Mechanical Systems. *Reviews of Modern Physics*, 34:845–872, October 1962.

[30] HM Wiseman. Grounding bohmian mechanics in weak values and bayesianism. *New Journal of Physics*, 9:165–177, 2007.

[31] Y Xiao, Y Kedem, JS Xu, CF Li, and GC Guo. Experimental nonlocal steering of bohmian trajectories. *Optics Express*, 25(213):14463–14472, 2017.